Methods To Reduce Built-In Residual Stresses in Steel Bridge Diaphragms *(Phase I)*

July, 2000

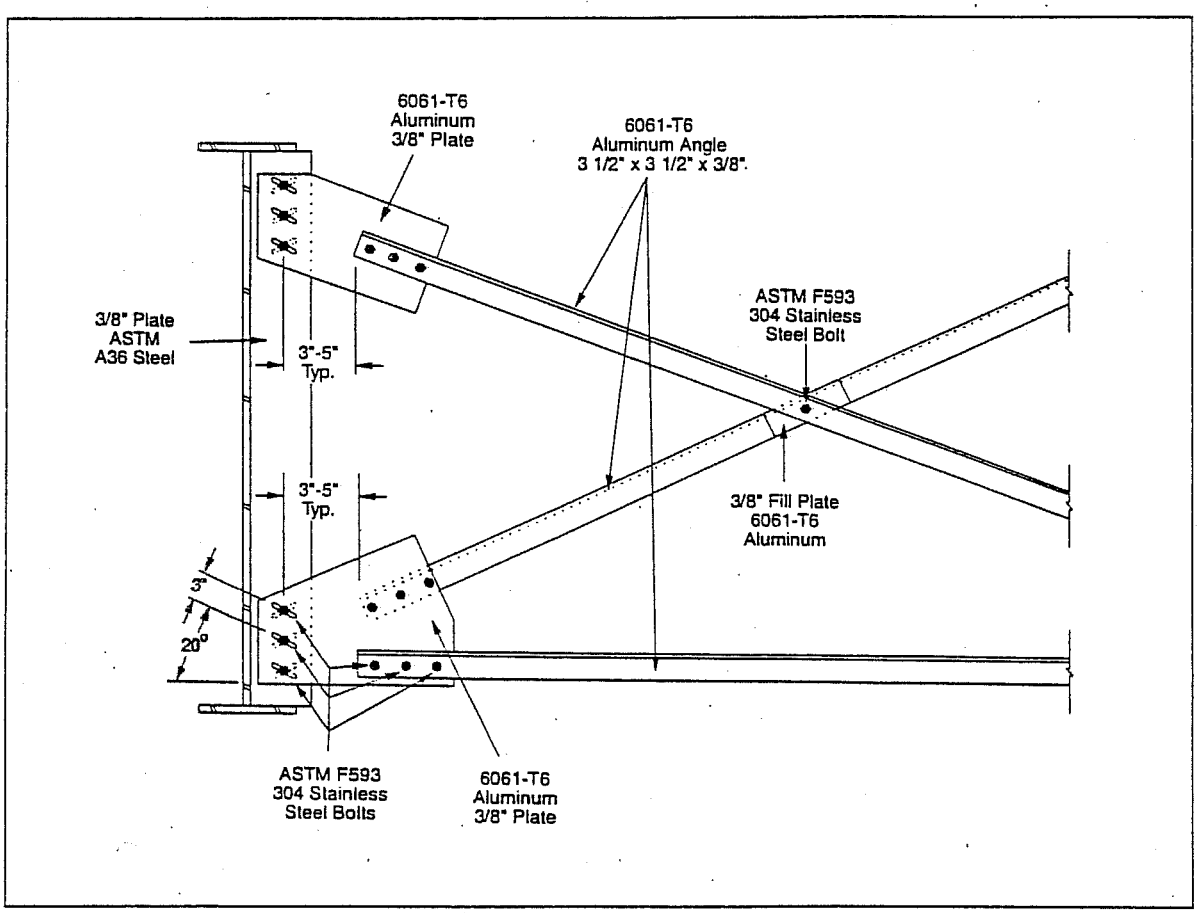

Physical Research Report No.109

Illinois Department of Transportation
Division of Highways / Bureau of Materials and Physical Research
126 East Ash Street / Springfield, Illinois / 62704-4766

Technical Report Documentation Page

1. Report No.	2. Government Accession No.	3. Recipient's Catalog No.
FHWA/IL/PRR-109		

4. Title and Subtitle

METHODS TO REDUCE BUILT-IN RESIDUAL STRESSES IN STEEL BRIDGE DIAPHRAGMS (Phase I)

5. Report Date: July, 2000

6. Performing Organization Code:

8. Performing Organization Report No.: PRR-109

7. Author(s)
Jeffrey M. South, PE and Christopher Hahin, PE

9. Performing Organization Name and Address
Illinois Department of Transportation
Bureau of Materials & Physical Research
126 E. Ash St. Springfield, IL 62704

10. Work Unit (TRAIS):

11. Contract or Grant No.: HR-25-318-97-1

13. Type of Report and Period Covered: Final Report, March 1994 to December, 1999

12. Sponsoring Agency Name and Address
Illinois Department of Transportation
Bureau of Materials & Physical Research
Springfield, IL 62704

14. Sponsoring Agency Code:

15. Supplementary Notes
This report is prepared in cooperation with the Federal Highway Administration, US Department of Transportation.

16. Abstract

EXECUTIVE SUMMARY

This investigation determined the magnitude and origin of residual stresses in plate girders, diaphragms and stiffeners built-in during construction. Residual stresses can contribute to crack formation. Three different steel bridges were studied: (1) a multi-girder bridge anchored at the abutments with no center pier; (2) a 4-span continuous multi-girder bridge with piers; (3) a movable, double-leaf bascule bridge. Bridges were instrumented with strain gages at the fabricator. Changes in reference strains were monitored: (a) after steel erection and bolt-up; (b) after deck placement; and (c) after parapet placement.

Built-in stresses varied widely. Mean tensile stress was 35 MPa [5.1 ksi], with a standard deviation (SD) of 40 MPa [5.8 ksi]. Mean compressive stress was -51 MPa [-7.4 ksi] with an SD of 39 MPa [-5.7 ksi]. Highest tensile stress measured was 146 MPa [21 ksi].

Methods to attenuate the effects of built-in strain were proposed, including: (1) lower-modulus aluminum and zinc alloys for diaphragm components; (2) synthetic rubber used in shear connectors; (3) new designs which accommodate misalignment, distortion and deflection; and (4) retrofit attachments to X and K-brace diaphragms. The study recommends Phase II testing of proposed modifications which could improve constructibility and durability in actual bridges.

17. Key Words	18. Distribution Statement
Bridges; Built-In Stresses; Residual Stresses; Diaphragms; Bascule Bridges; Multi-Plate Girder Steel Bridges; Strain Gages; Strain Relief; Aluminum Alloys; Rubber	*Unlimited.* This document is available through the National Technical Information Service, Springfield, Virginia 22161.

19. Security Classif. (of this report)	20. Security Classif. (of this page)	21. No. of Pages	22. Price
Unclassified	*Unclassifed*	94	

LIST OF FIGURES

LIST OF FIGURES
(cont'd)

LIST OF FIGURES
(cont'd)

LIST OF TABLES

INTRODUCTION

Cracking in steel bridges is caused by the combination of live load stresses, dead load stresses, and residual stresses. Residual stresses are present in the raw materials of construction. They can also result from fabrication and construction, or can be magnified by deficiencies in design. Material deficiencies are usually uncovered by inspection or testing for conformance to specification. Design and construction problems are more difficult to define and address if no construction abnormalities or deviations from codes, specifications or plans are noticed. In many cases involving cracking in bridges, heavy truck traffic can induce damaging stresses into structural details with low fatigue resistance. Built-in residual stresses can result from thermal changes in the structure during construction, from liberal fabrication tolerances, or unreported deficiencies in fit-up. Residual stresses can also result from field modifications by contractors, consultants, or transportation engineers which may not be described in the plans or specifications.

Many bridges develop cracks in areas which are subjected to live load stresses in the range of 4 to 6 ksi (28-41 MPa). Cracks may appear in structural details where longer fatigue lives were expected. Cracks can originate from high stresses that were built-in during fabrication or construction. Floorbeam-to-girder or diaphragm-to-girder connections are common areas of crack initiation and development which can spread to main load-carrying members. The objectives of this report were: (a) to measure the stresses built into various kinds of bridges during construction; (b) to consider the effects of residual stresses on fatigue life; and (c) to recommend methods of attenuating these built-in stresses.

Three different bridges and their component parts were instrumented with strain gages at the fabrication plants before field assembly. Here the intent was to measure built-in stresses from start-to-finish. Static strain data were collected during various phases of construction until the entire bridge was completed. Three different bridges were studied: (1) an anchor tie-back design without a center pier, carrying County Highway 14 over I-39 at Wenona; (2) a three-span, multi-girder river crossing, carrying IL-52 over the DuPage River near Joliet; and (3) a movable, double-leaf bascule bridge, carrying Brandon Road over the Des Plaines River in Joliet.

Built-in mean stresses can be beneficial or detrimental to fatigue life, depending on the nature of that stress. Compressive mean stresses will either increase fatigue life or may be neutral in effect. Tensile mean stresses, on the other hand, will generally reduce fatigue life. Equations are available to predict the effects of mean residual and dead load stresses on fatigue

life of welded details. Factors of safety can be calculated for welded details. The effect of residual, operating, and mean stresses on bridge life can be quantified with reliability theory, which has widespread use in the construction, automotive, shipbuilding, and aerospace industries.

Analytical methods can be used to predict the fatigue life of details affected by residual stresses. The magnitude of built-in stresses can be reduced by making changes (a) in construction practices; (b) in diaphragm and connector design; and (c) in the materials of construction. This report summarizes the magnitude of residual stresses found in steel bridge diaphragms, and proposes improvements to construction procedures, designs, and material specifications which could increase the fatigue life of bridges. By increasing the durability of bridges, the number of future inspections and maintenance problems can be considerably reduced.

EXPERIMENTAL PROCEDURES

The sensors used to measure built-in strains were weldable, 120-ohm resistance strain gages manufactured by MicroMeasurements, Inc. of Raleigh, North Carolina. This type of weldable gage has the strain gage grid bonded to a thin (5 mil, [0.129mm]) metal carrier. The metal carrier is micro-spot welded to the detail of interest. A drawing of this type of strain gage is shown in ***Figure 1.*** Since these strain gages are self-temperature compensating, a three-wire, ¼-bridge circuit configuration was used, allowing the Wheatstone bridge circuit to be completed with precision resistors in the strain gage indicator. The strain gage indicator used was a MicroMeasurements Model P-3500. Surface temperature was noted at each separate time and date of data collection. The apparent strain due to temperature is calculated from surface temperature data and a polynomial expression unique to each lot of strain gages. This apparent strain is subtracted from the indicated strain to get the corrected strain. Leadwire effects were ignored in this study, since losses are minimized with a three wire circuit. Leadwire lengths were less than 30 ft (9.1 m).

This study primarily focused on diaphragms, although other details were instrumented. Strain gages were installed on the top and bottom flanges, near the ends of the diaphragms. Nominal longitudinal strains were measured for the diaphragms. Crossframe details, floor-beams, a trunnion detail, and anchored tiebacks over girders were also instrumented.

Strain gages were installed on the diaphragms and the other elements at the fabrication plants before shipment to the job site, so that construction of the bridges would not be delayed. All mill scale and paint was removed at the details of interest by light grinding to insure proper adherence of the gages to the steel surfaces. The strain gage shims were then attached by welding using a portable microspot welder. The lead wires were soldered to the gages, and waterproofed using a self-adhesive butyl rubber sheet. This rubber sheet also protects the gage from light impact during shipping or assembly of the diaphragms. The initial strain readings of the gages resulting from self-weight of the elements were recorded, and served as baselines for subsequent assembly and dead weight strains. The surface temperatures of the diaphragms were simultaneously recorded for future temperature compensation.

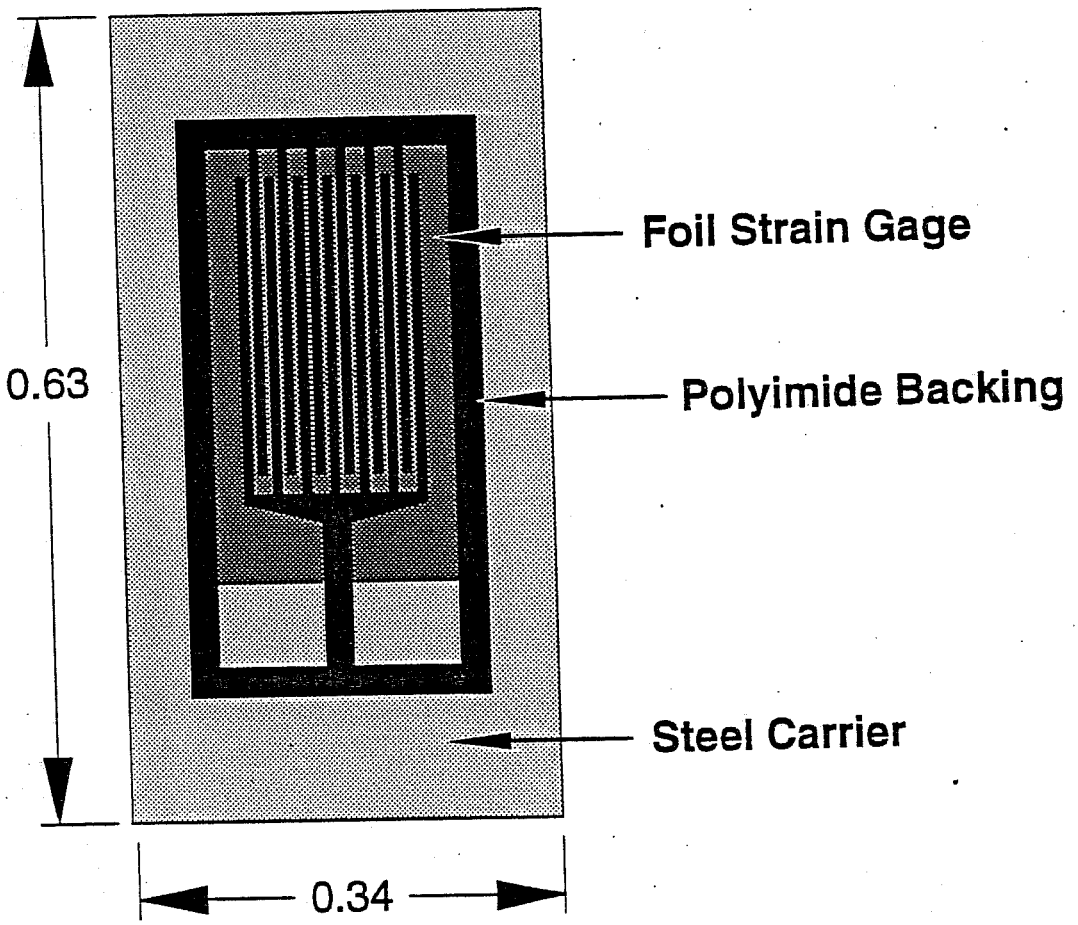

Figure 1. The weldable strain gage used in this study. The steel carrier backing is shim stock of approximately 0.005" thickness, and is micro-spot welded to the detail of interest. Dimensions are in inches (1 inch = 2.54 cm).

MEASURED CONSTRUCTION STRAINS

This chapter presents the strain data collected during the construction of three different bridges in Illinois: (1) a bridge where the girders are anchored at the abutments, and have no center pier; (2) a three-span multi-girder design with piers; and (3) a movable, double-leaf bascule bridge.

County Highway 14 over Interstate-39 at Wenona

The grade separation bridge carrying CH 14 over I-39 at Wenona has no center pier. This design is commonly used on this route between Bloomington and LaSalle-Peru for grade separations. The ends of the girders are held down by tensioned steel bars to provide a fixed moment connection at the ends. Details are shown in ***Figure 2***. The bridge is 234 ft (71.3 m) long between back walls, and accommodates two full width lanes and shoulders. There is no skew. The bridge has five variable-depth girders at 7' - 9" (2.36 m) spacings. Bolted splices are located 64 ft (19.5 m) from the back walls, and 32 ft (9.75 m) from the front walls. ***Figure 3*** shows a plan view of the erection diagram showing the locations of the instrumented sections. The details instrumented on this bridge were conventional diaphragms using W 21x44 wide flanges. Crossframes at the front and back walls of the abutments were actually plates with a large circular hole in the center. The lines of action of the tiedown bars passed through the girders and bearing stiffeners at the tiedown points at the back walls.

Figures 4, 5 and ***6*** show strain gage locations and relevant dimensions for the instrumented details. Strain gages were installed at the fabrication plant before shipment to the job site, so the contractor would not be delayed. Thirty-eight strain gages were installed on this bridge.

a. Strains measured in diaphragms.

Four diaphragms were instrumented. The locations and designations of the instrumented sections were shown in ***Figure 3.*** Each diaphragm had four strain gages installed as shown in ***Figure 4.*** In each case, Gages 1 & 3 are on the top flange; Gages 2 & 4 are on bottom flange.

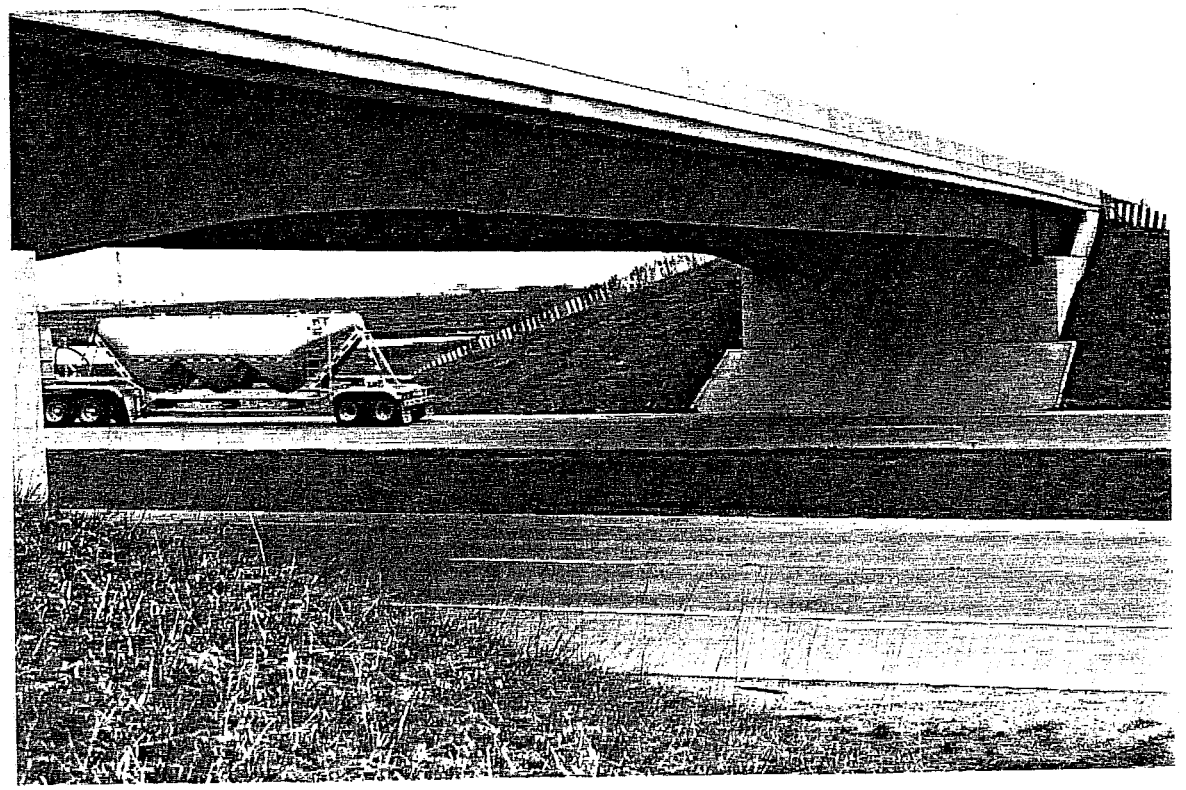

Figure 2. Photograph of the County Highway 14 bridge over Interstate 39 at Wenona, Illinois. This bridge design incorporates steel bar anchors at the end of the abutments and no center pier.

For each diaphragm, gages 3 and 4 are on the north (fascia) side. ***Table 1*** presents corrected strain data for each diaphragm instrumented for the construction phases of: (1) steel erected; (2) deck installed; and (3) parapet installed. The data for these phases were collected on November 9, 1990; May 1, 1991; and October 8, 1991, respectively.

The data in ***Table 1*** is also shown in ***Figures 7*** through ***Figure 10***. Inspection of the data shows that strain values vary between -692 to +694 microstrain, which translates to a stress in steel of -20.8 to +20.8 ksi (-143 to +144 MPa).

The highest construction-induced tensile stress measured were as follows: in diaphragm 411D1-1, 7.6 ksi (53 MPa) at Gage 4; in diaphragm 411D1-2, 7.7 ksi (54 MPa) and occurred at Gage 2; in diaphragm 411D2-1, 20.8 ksi (145 MPa) at Gage 2; in diaphragm 411D2-2, 12.8 ksi (89 MPa) at Gage 3.

Table 1

Microstrain Data For Diaphragms on County Highway (CH)14 Over I-39 at Wenona*

	411D1-1			411D1-2			411D2-1			411D2-2		
	Steel Erected	Deck On	Parapet On	Steel Erected	Deck On	Parapet On	Steel Erected	Deck On	Parapet On	Steel Erected	Deck On	Parapet On
Gage												
1	-26	-9	3.4	147	160	166	-158	-452	194	-39	-41	-387
2	-62	-40	71	164	153	256	-162	-154	694	-85	-108	-692
3	-158	-200	-136	-52	-79	39	49	-117	-177	-28	-47	426
4	42	117	252	-162	-129	-101	-6	-7	465	0	46	-357

*Strain values are given in units of microstrain (10^{-6} in/in). To convert strain data to stress in steel into MPa, multiply strain data by 0.207; for psi, multiply by 30. Positive values indicate tension; negative values indicate compression. See ***Figure 4*** for locations of gage number in each numbered diaphragm in the bridge.

(2). Strains Measured in Girders

The strain gage locations for the instrumented girders are shown in ***Figure 5.*** The locations of the girders in the structure are shown in ***Figure 3.*** Girders were instrumented on this bridge because of the use of the newer abutment tiedown design. Similar bridges were used for grade separations across I-39 between Bloomington and LaSalle-Peru. The areas of interest were the lines of action of the tiedown bars and the bearing stiffness. Corrected strain data for girder 403A1 is given in ***Table 2.***

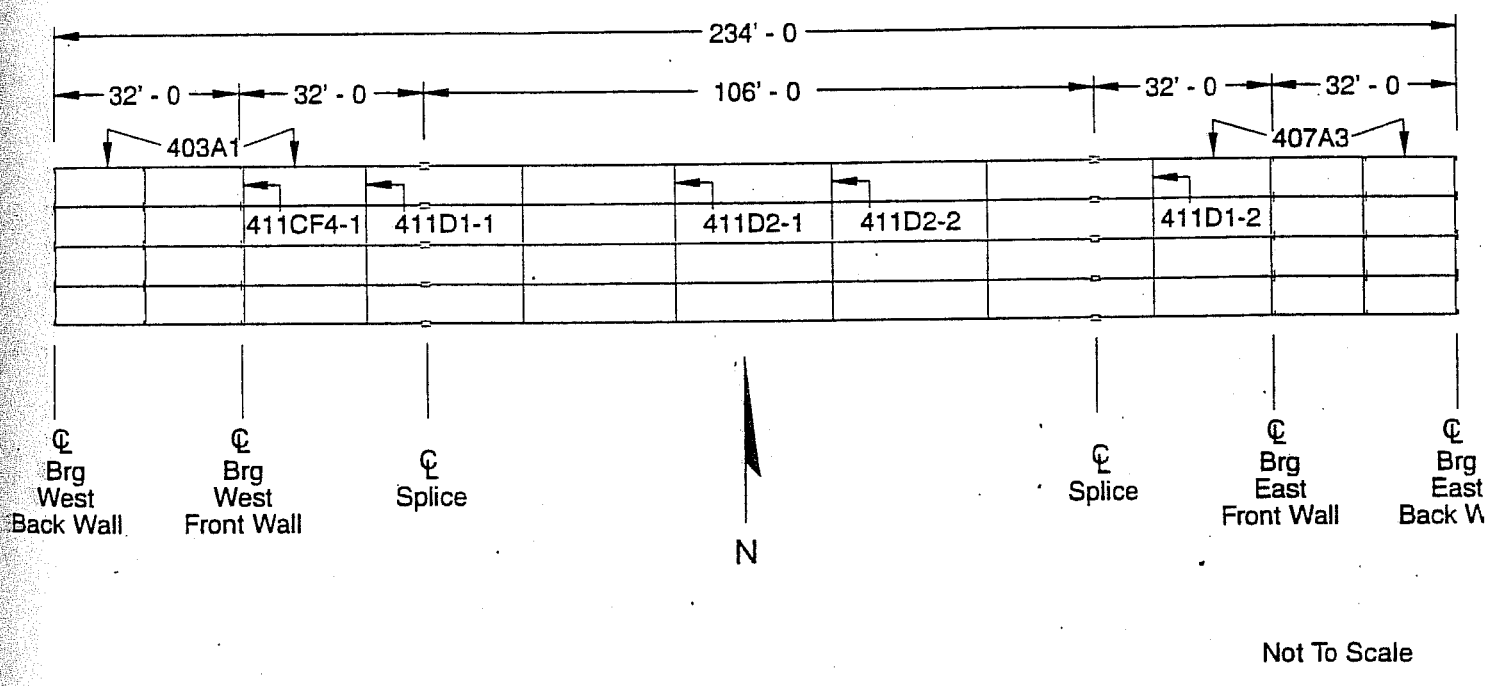

Figure 3. Plan view of erection diagram for CH14 over I-39 at Wenona, showing locations of instrumented components and component designations.

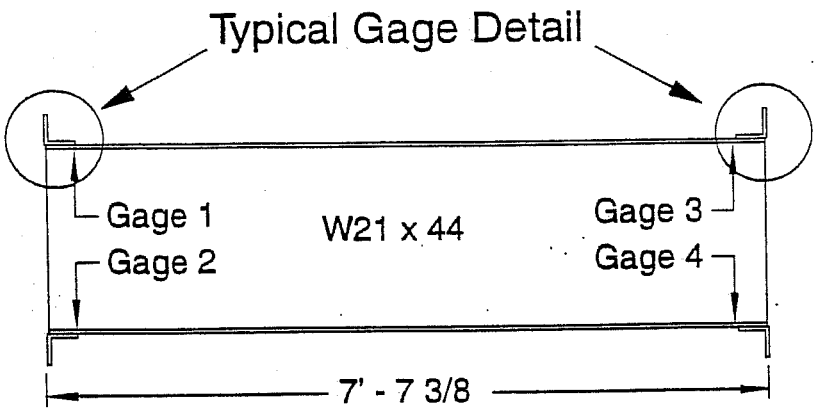

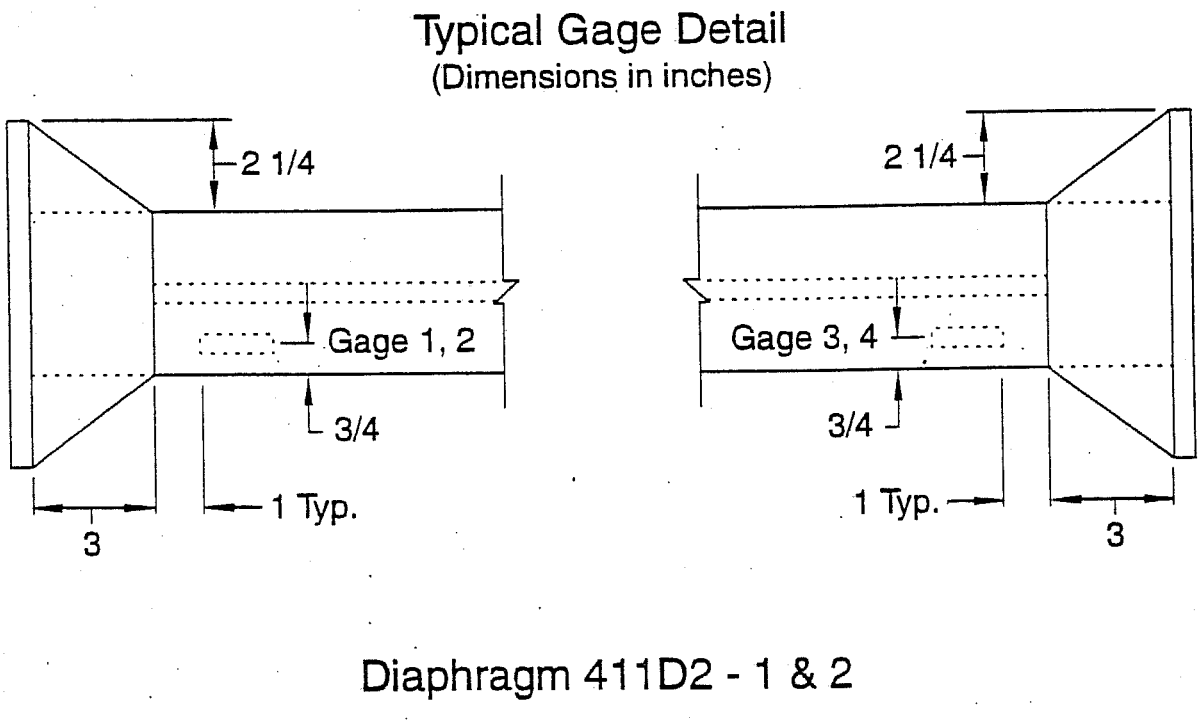

Figure 4. Representative diagram of instrumented diaphragms on CH14 over I-39 at Wenona.

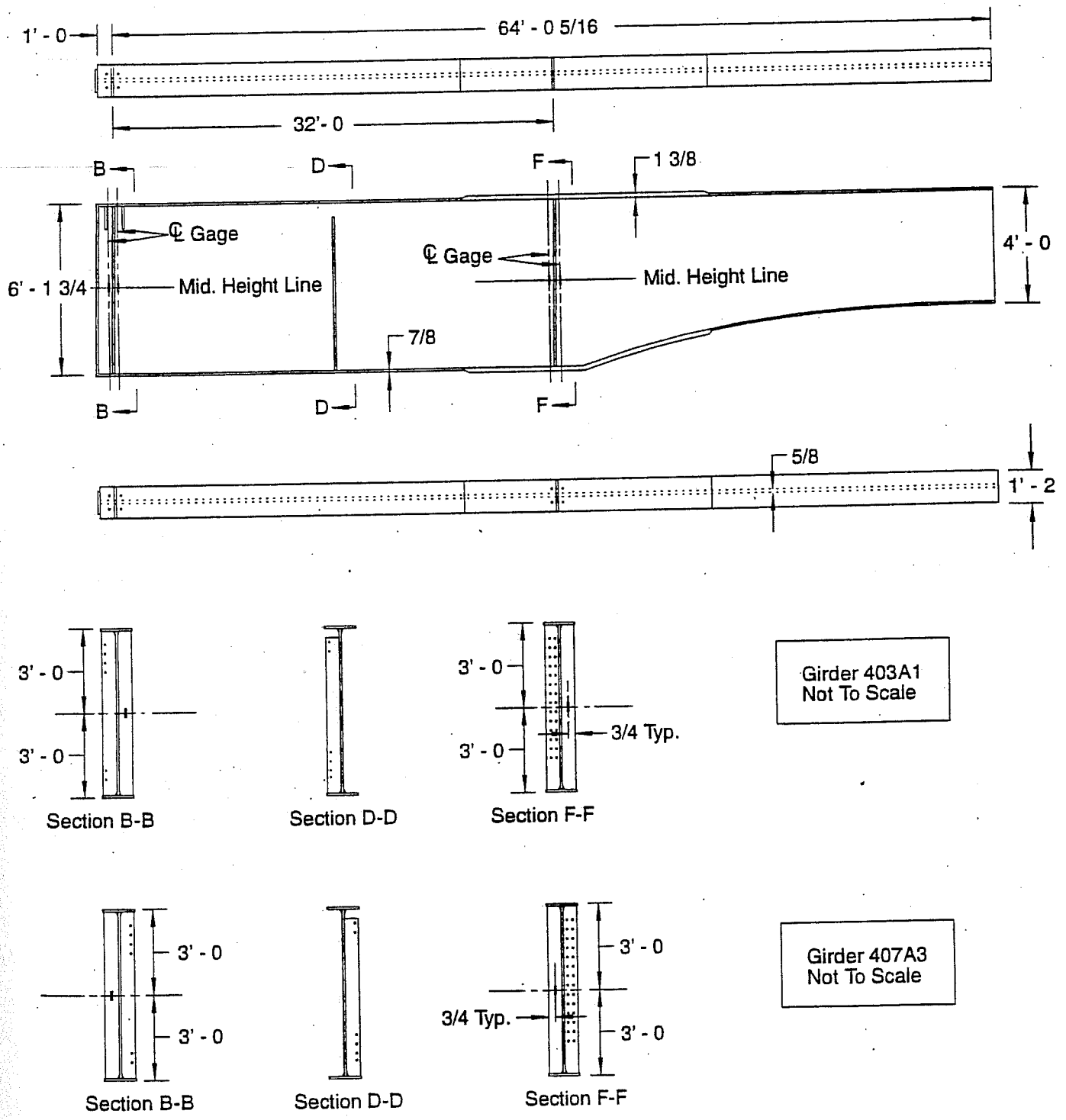

Figure 5. Representative diagram of instrumented bridge girders on CH14 over I-39 at Wenona. Dimensions are in feet and inches (1 foot = 0.305 m; 1 inch = 2.54 cm).

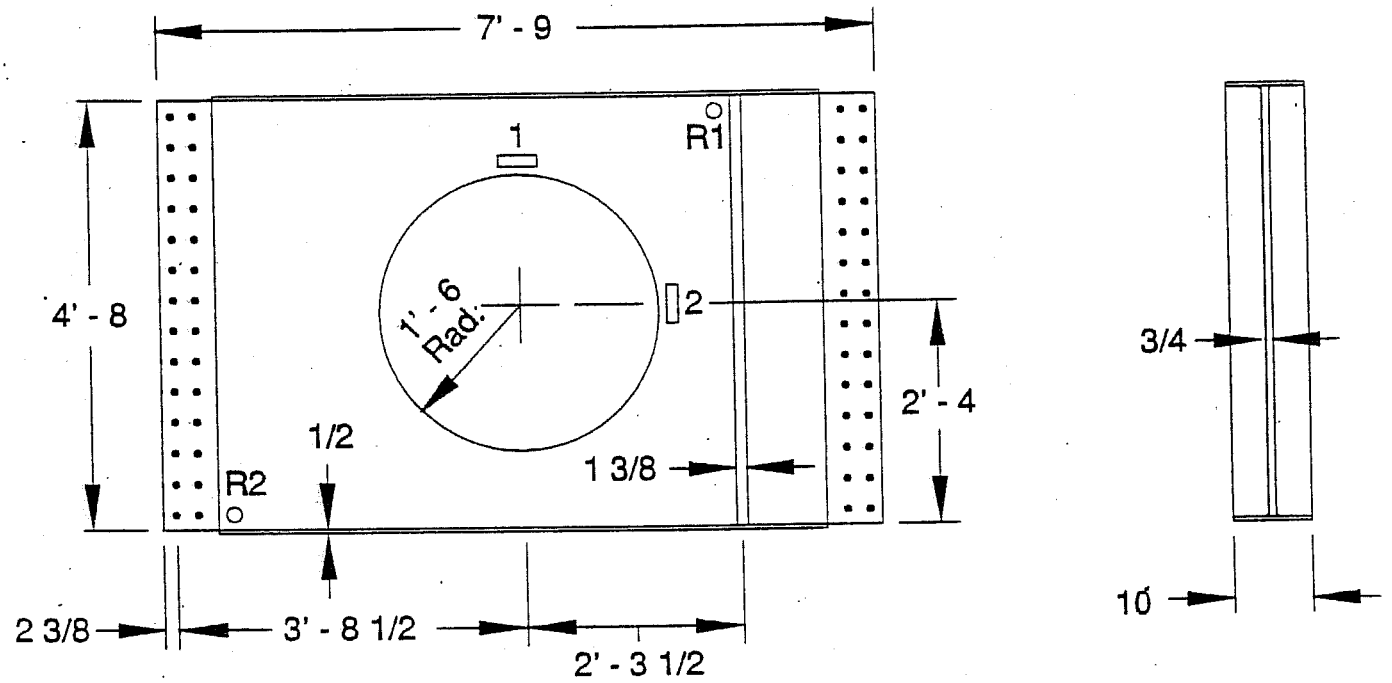

Figure 6. Representative diagram of instrumented crossframe details on CH14 over I-39 at Wenona. Dimensions are in feet and inches (1 foot = 0.305 m; 1 inch = 2.54 cm).

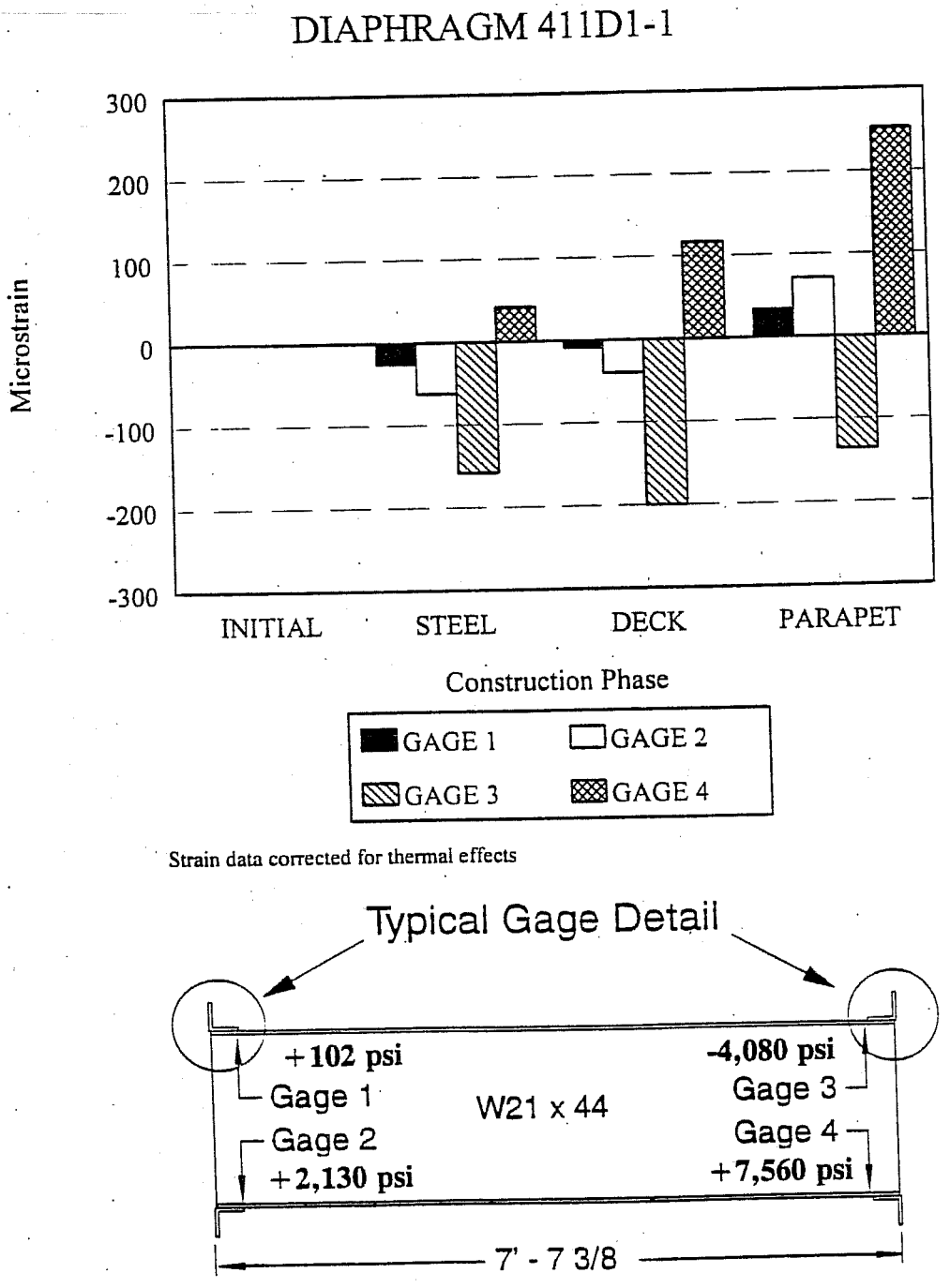

Figure 7. Strain data collected for diaphragm 411D1-1 for the construction phases of steel placement, deck placement, and parapet placement. Final stresses shown are for steel only.

CH14 OVER I-39 AT WENONA

DIAPHRAGM 411D1-2

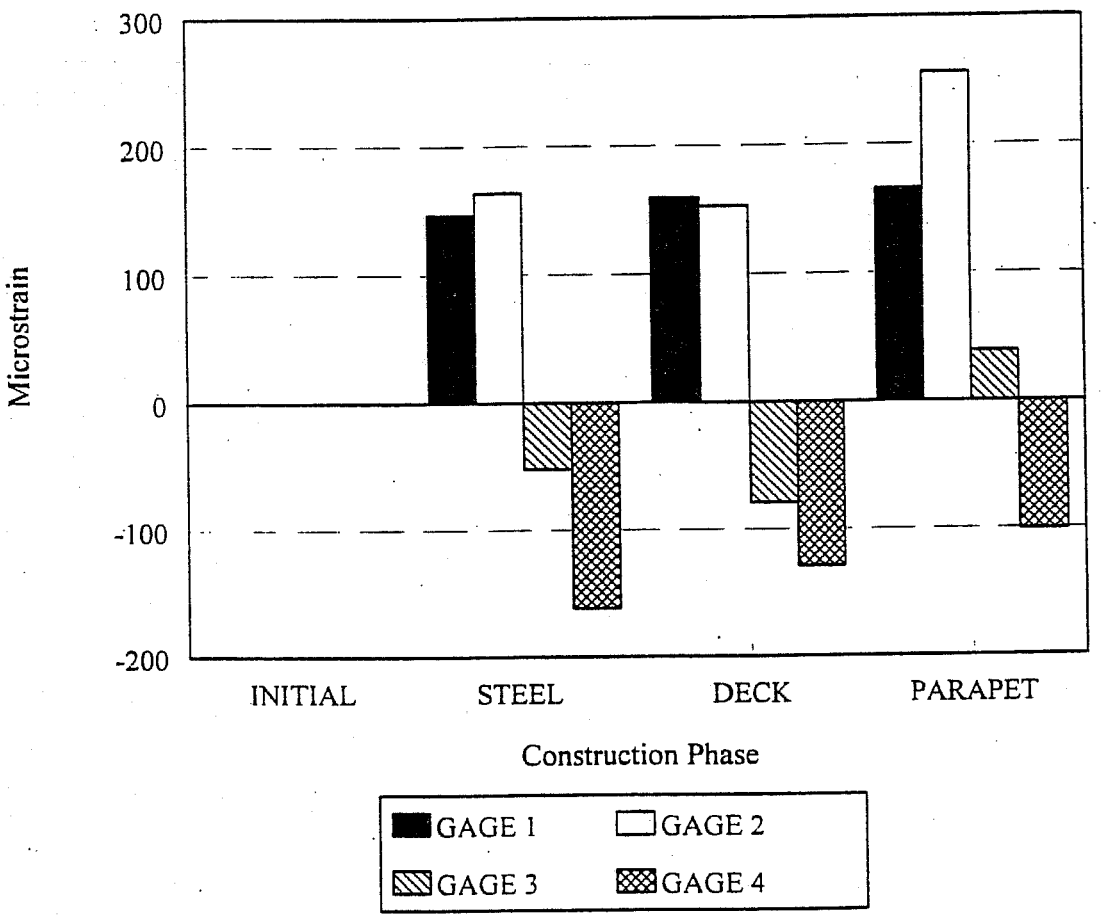

Strain data corrected for thermal effects

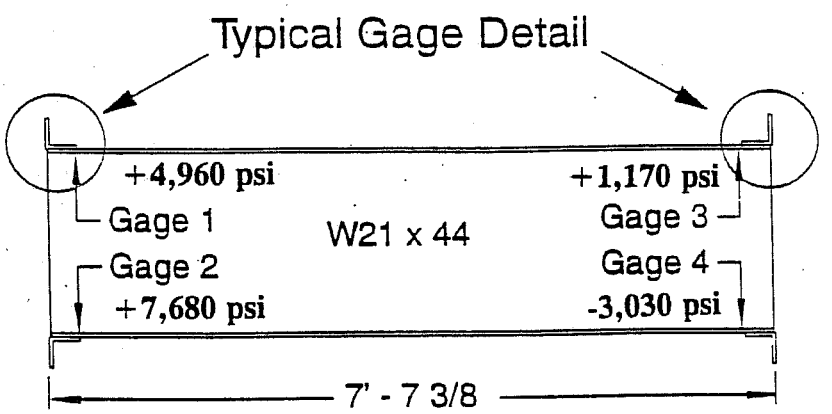

Figure 8. Strain data collected for diaphragm 411D1-2 for the construction phases of steel placement, deck placement, and parapet placement. Final stresses shown are for steel only.

CH 14 OVER I-39 AT WENONA

DIAPHRAGM 411D2-1

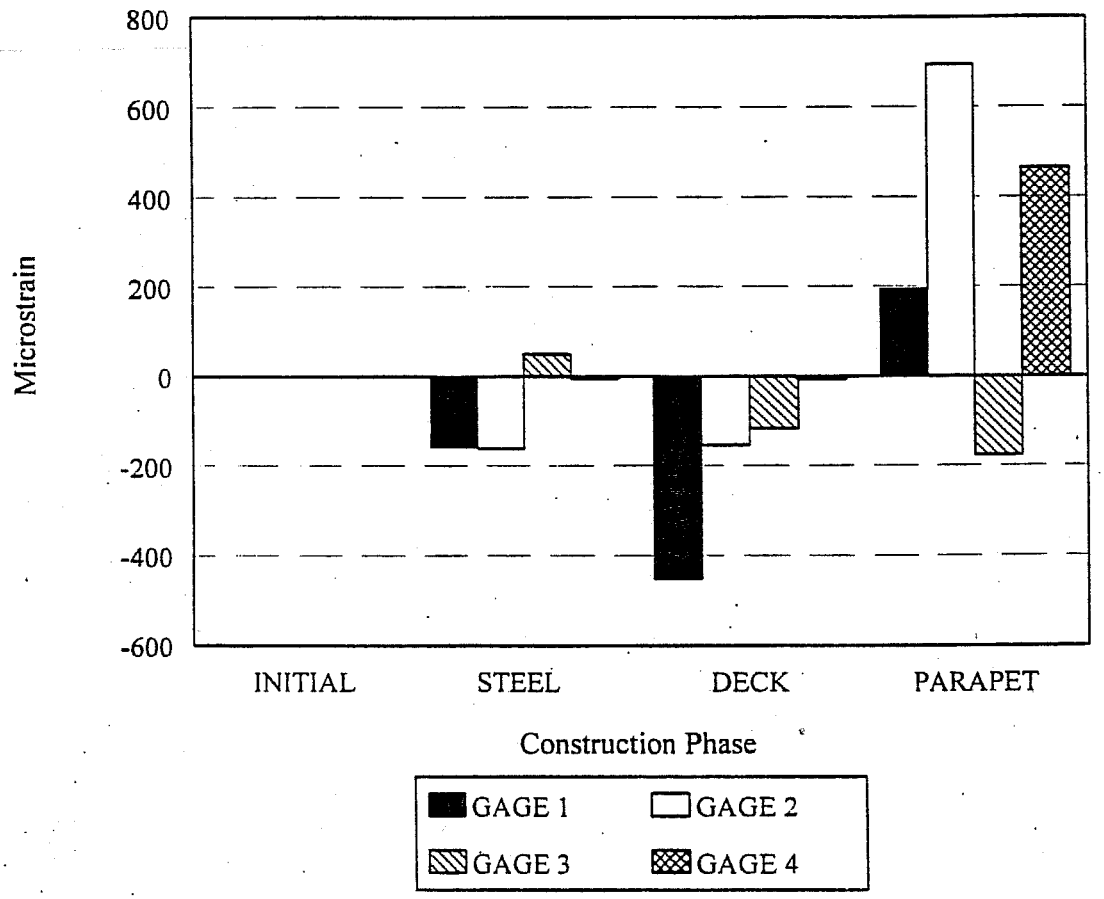

Strain data corrected for thermal effects

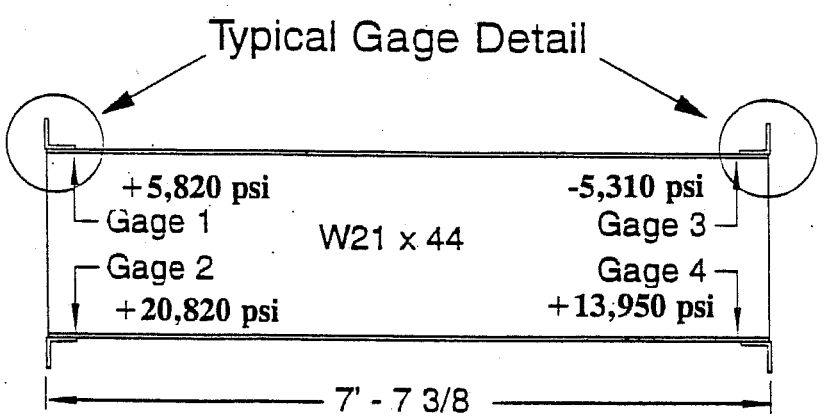

Figure 9. Strain data collected for diaphragm 411D2-1 for the construction phases of steel placement, deck placement, and parapet placement. Final stresses shown are for steel only.

CH 14 OVER I-39 AT WENONA

DIAPHRAGM 411D2-2

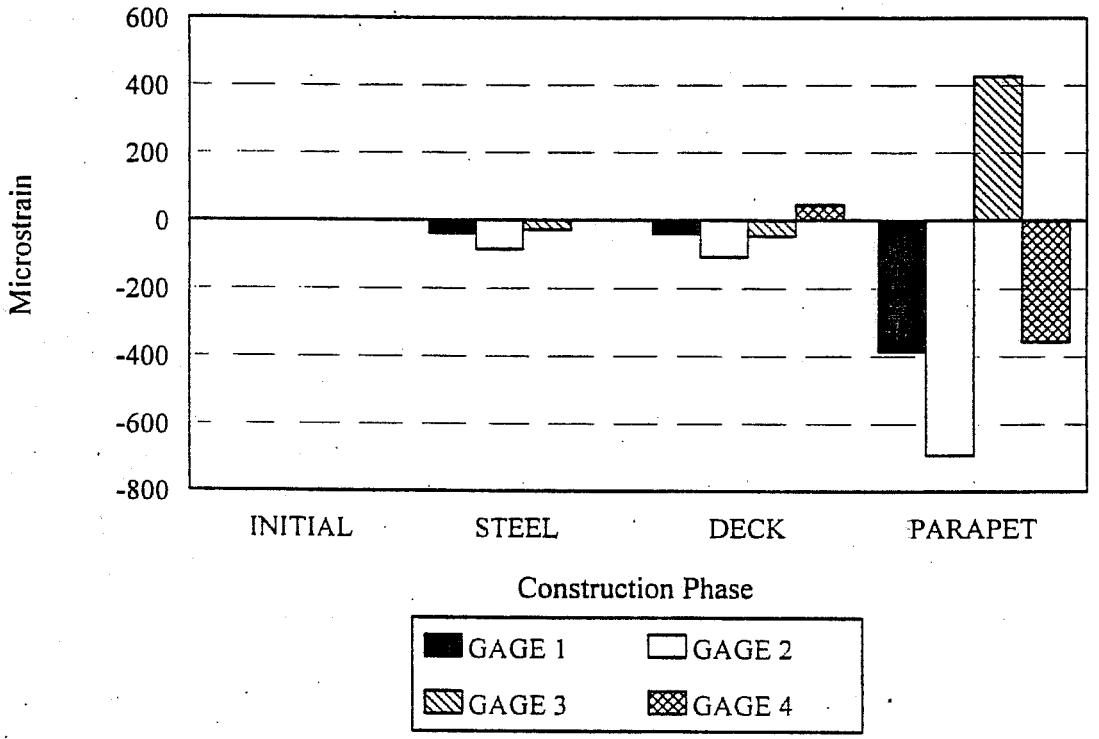

Strain data corrected for thermal effects

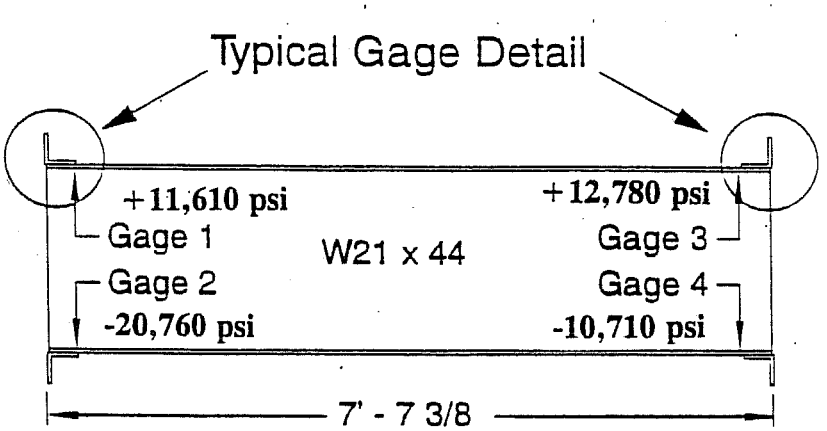

Figure 10. Strain data collected for diaphragm 411D2-2 for the construction phases of steel placement, deck placement, and parapet placement. Final stresses shown are for steel only.

Corrected strain data for girder 403A1 are graphed in ***Figures 11 and 12*** for the back and front walls, respectively. In ***Figures 11 and 12,*** Gages 1 and 4 are on the girder web, Gages 2 and 3 are on the bearing stiffener. For this particular tiedown detail, built-in stresses were either compressive, as expected, or slightly tensile. The highest measured tensile stress remaining in the instrumented frontwall detail of girder 403A1 was 1.4 ksi (10.7 MPa) at Gage 2.

Girder 407A3 is in a position symmetrical to that of girder 403A1. Corrected strain data for girder 403A7 are presented in ***Table 3.***

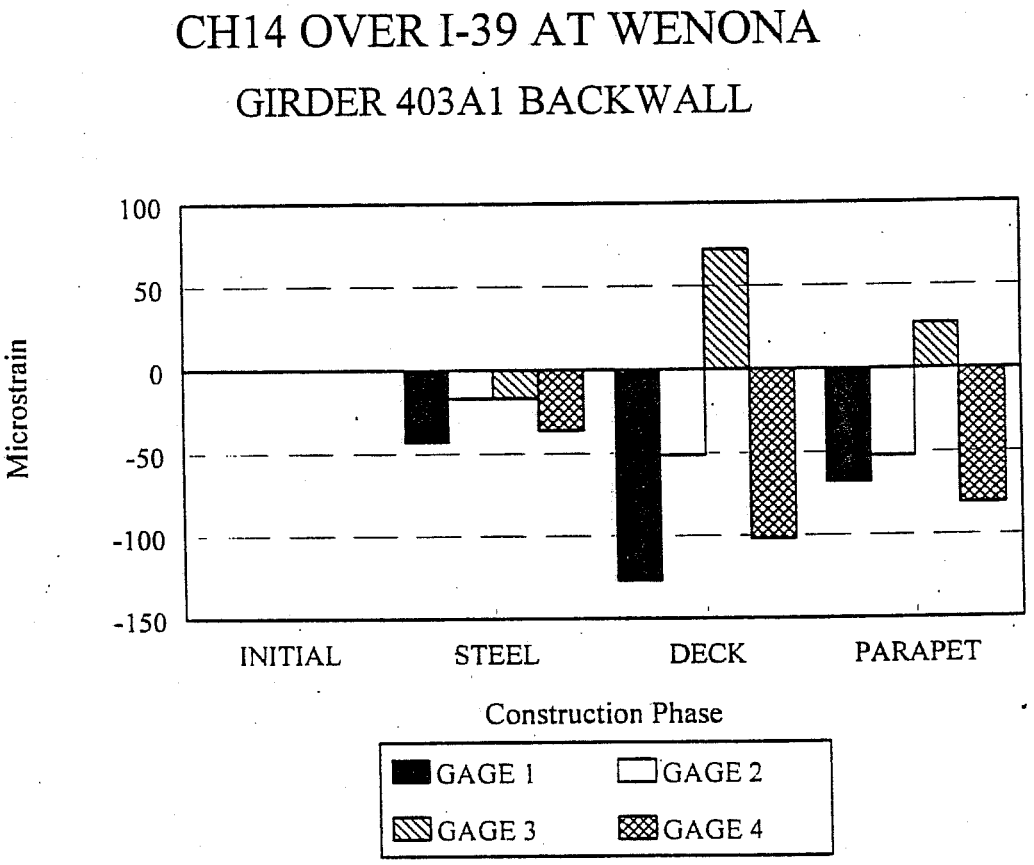

Figure 11. Strain data collected for girder 403A1 (backwall) for the construction phases of steel placement, deck placement, and parapet placement. Strain data corrected for thermal effects. Gages 1 and 4 are attached to girders; gages 2 and 3 are attached to stiffeners.

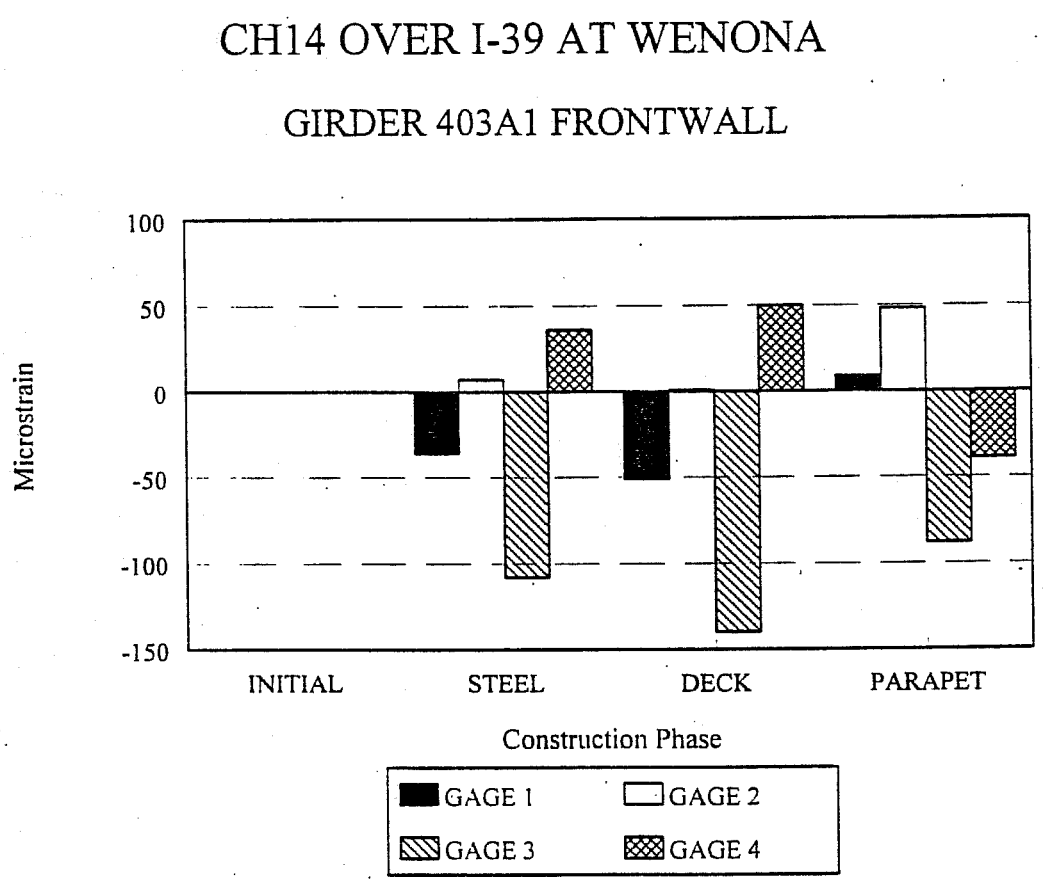

Figure 12. Strain data collected for girder 403A1 (frontwall) for the construction phases of steel placement, deck placement, and parapet placement. Strain data corrected for thermal effects. Gages 1 and 4 are attached to girders; gages 2 and 3 are attached to stiffeners.

Table 2

Strain Data For Girder 403A1 on CH14 Over I-39 at Wenona, Illinois

GAGE NUMBER	STAGE OF CONSTRUCTION* STEEL ERECTED	DECK PLACED	PARAPET PLACED
BACKWALL			
1	-43	-127	-68
2	-17	-51	-52
3	-17	72	27
4	-36	-102	-81
FRONTWALL			
1	-36	-51	9
2	7	1	48
3	-108	-140	-88
4	36	50	-39

*Strain values are given in units of microstrain (10^{-6} in/in). To convert strain data to stress in steel into MPa, multiply strain data by 0.207; for psi, multiply by 30. Positive values indicate tension; negative values indicate compression.

Table 3

Strain Data For Girder 407A3 on CH14 Over I-39 at Wenona, Illinois

GAGE NUMBER	STAGE OF CONSTRUCTION* STEEL ERECTED	DECK PLACED	PARAPET PLACED
BACKWALL			
1	-68	-128	-104
2	-43	-161	-14
3	-58	-217	-70
4	-70	-174	-76
FRONTWALL			
1	-17	148	10
2	Gage Destroyed in Transit		
3	-106	-153	-66
4	-20	-225	3

*Strain values are given in units of microstrain (10^{-6} in/in). To convert strain data to stress in steel into MPa, multiply strain data by 0.207; for psi, multiply by 30. Positive values indicate tension; negative values indicate compression.

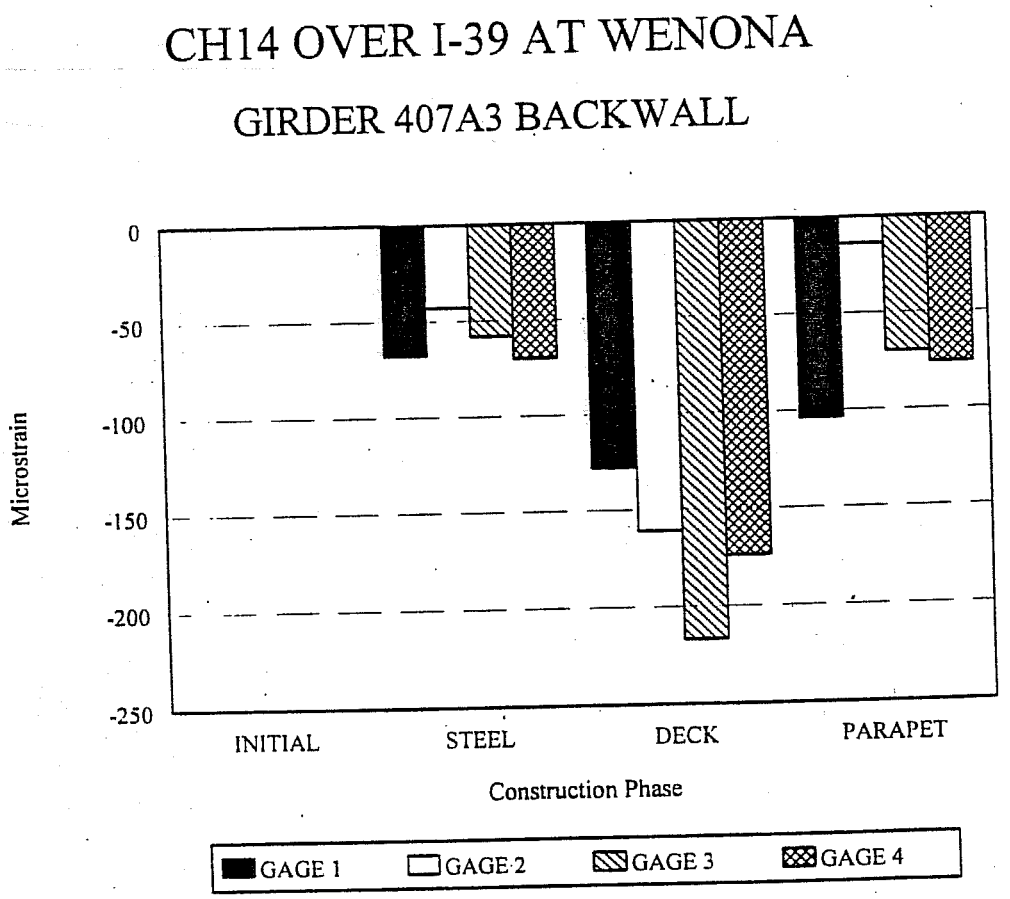

Figure 13. Strain data collected for girder 407A3 (backwall) for the construction phases of steel placement, deck placement, and parapet placement. Strain data corrected for thermal effects.

The data in ***Table 3*** are also shown graphically in ***Figures 13 and 14*** for the back and front wall, respectively. The maximum compressive built-in stress measured for the back wall detail of girder 407A3 was 3.1 ksi (22 MPa) at gage location one.

The strain data for the front wall detail of girder 407A3 is shown in ***Figure 14.*** Gage 2 was destroyed in transit. The maximum final compressive built-in stress measured for the front wall detail of girder 407A3 was 2.0 ksi (14 MPa) at Gage 3.

c. Strains Measured in Crossframes

Another detail instrumented on CH14 over I-39 at Wenona was a plate section with a circular hole cut in the center. This detail is designated as a crossframe on the fabrication plans. The circular opening provides access to the interior portion of the abutments. One of these crossframes is placed at the frontwall on each end of the bridge. Access is denied through the other frontwall spaces by use of solid plate details. The areas of interest on this detail were points on the periphery of the cutout at the 12:00 and 3:00 positions, and the upper and lower corners.

Uniaxial strain gages were used near the hole for both instrumental crossframes. Three-element rosettes were used in the corners of crossframe 411CF4-1. ***Figure 15*** provides details of the instrumented areas. Rosettes were used in the corners because this was an area where a uniaxial stress field was not a reasonable assumption. A strain gage rosette is needed to obtain maximum and minimum principal stresses, as well as orientation with respect to a reference axis. Strain gage data for crossframe 411CF4-1 is presented in ***Table 4.***

Strain data for the gages at the hole periphery are graphed in ***Figure 16*** for crossframe 411CF4-1. The highest recorded tensile stress in crossframe 411CF4-1 after the parapet was placed was 2.8 ksi (19 MPa) in Gage 2. The calculated principal stress data for Rosette 1 (upper right-hand corner) is given in ***Table 5.***

Crossframe 411CF4-2 had strain gages installed on the hole periphery only. Measured strains for this crossframe are shown in ***Table 6*** and ***Figure 17.*** The maximum final built-in stress calculated for crossframe 411CF4-2 was 1.9 ksi (13 MPa) in Gage 2.

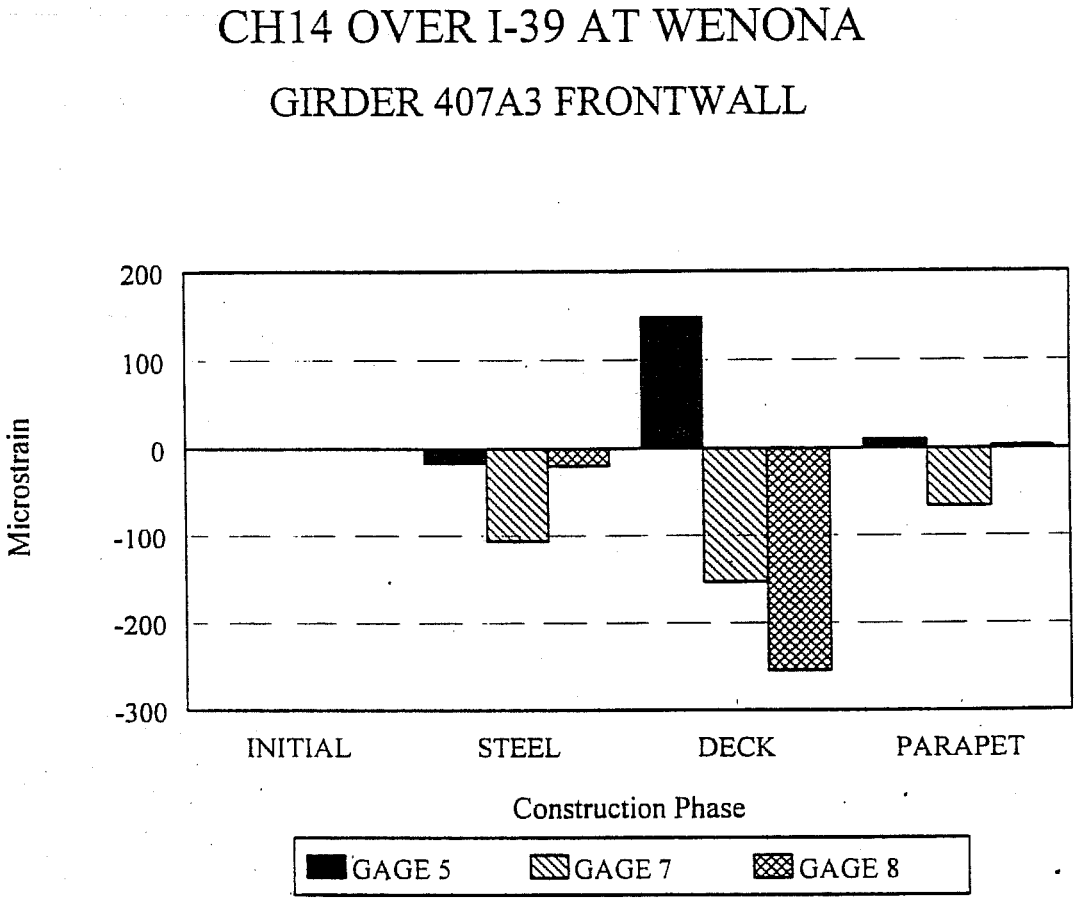

Figure 14. Strain data collected for girder 407A3 (frontwall) for the construction phases of steel placement, deck placement, and parapet placement. Strain data corrected for thermal effects.

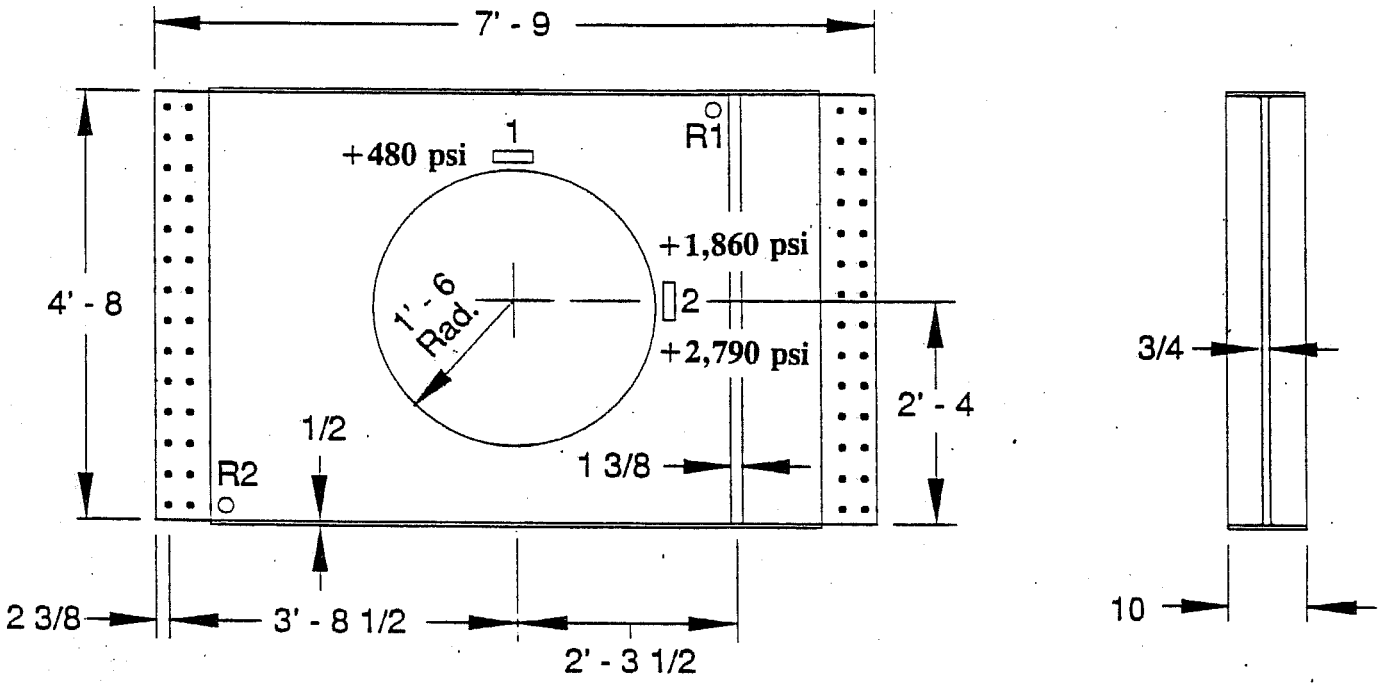

Figure 15. Detailed view of instrumented areas on crossframe components. Also shown are the final stresses for steel crossframe 411CF4-1.

Table 4

Strain Data For Crossframe 411CF4-1 / CH14 Over I-39 at Wenona

GAGE NUMBER	STAGE OF CONSTRUCTION* STEEL ERECTED	DECK PLACED	PARAPET PLACED
1	48	63	NR
2	-75	-31	93
R1-1	31	38	69
R1-2	-37	-6	18
R1-3	432	-77	28
R2-1	1962	1944	2054[B]
R2-2	Gage Destroyed During Transit**		
R2-3	328	338	366[B]

*Strain values are given in units of microstrain (10^{-6} in/in). To convert periphery strain data to stress in steel into MPa, multiply strain data by 0.207; for psi, multiply by 30. Positive values indicate tension; negative values indicate compression.
**Principal stresses cannot be resolved without all three of the gages indicating valid, discernable strains.
NR = No reading.
[B]Indicates localized yielding or other high loadings caused during truck shipment.

Table 5

Principal Stresses and Directions On Crossframe 411CF4-1*
(Upper Right-Hand Corner)

QUANTITY	STAGE OF CONSTRUCTION STEEL ERECTED	DECK PLACED	PARAPET PLACED
Maximum Principal			
Stresses, MPa	123.29	3.70	20.47*
[ksi]	[17.9]	[0.4]	[3.0]
Minimum Principal			
Stresses, MPa*	15.30	-15.37	8.59
[ksi]	[2.2]	[2.2]	[1.2]
Orientation**	-4°	-45°	-17°

*The conversion from strain to stress is not appropriate for rosette data. Instead, formulas that convert strains to principal stresses are used per Dally and Riley [Ref 1].
**Degrees clockwise from vertical.

Table 6

Strain Data For Crossframe 411CF4-2

(CH14 Over I-39 at Wenona, Illinois)

GAGE NUMBER	STAGE OF CONSTRUCTION* STEEL ERECTED	DECK ON	PARAPET ON
1	-11	27	19
2	-34	-33	62

*Strain values are given in units of microstrain (10^{-6} in/in). To convert strain data to stress in steel into MPa, multiply strain data by 0.207; for psi, multiply by 30. Positive values indicate tension; negative values indicate compression.

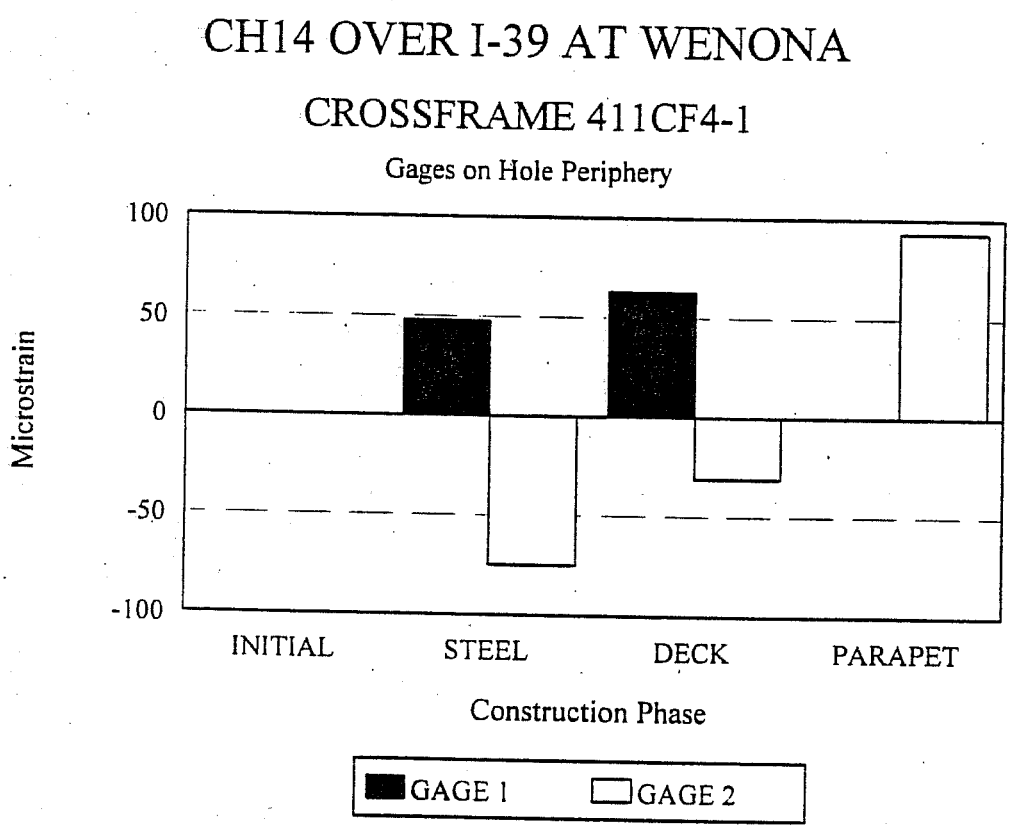

Figure 16. Strain data collected for hole periphery of crossframe 411CF4-1 for the construction phases of steel placement, deck placement, and parapet placement. Strain data corrected for thermal effects. Gage 1 is located on top and gage 2 is on the side.

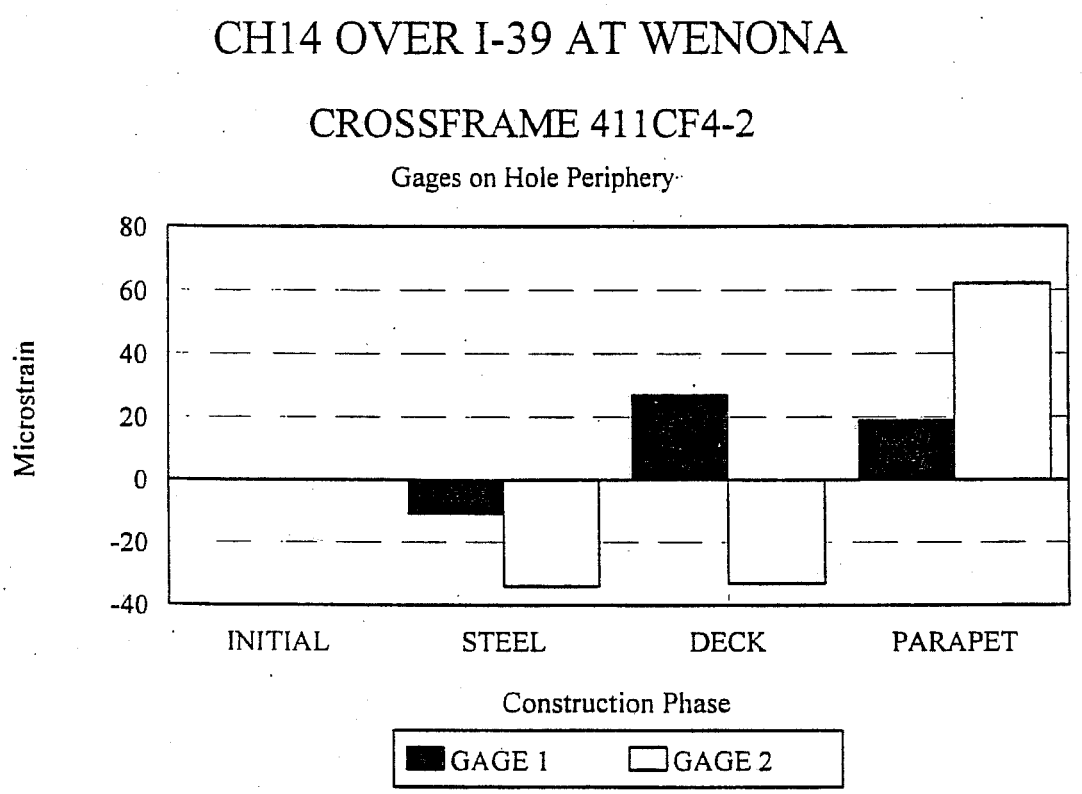

Figure 17. Strain data collected for hole periphery of crossframe 411CF4-2 for the construction phases of steel placement, deck placement, and parapet placement. Strain data corrected for thermal effects.

IL-52 Bridge over the DuPage River near Joliet

This bridge which carries IL-52 traffic over the DuPage River near Joliet is a conventional four-span, continuous, multiple-girder structure. The total span length is 449 ft (136.9 m). There are ten girder lines at 7' - 9" (2.36 m) spacings. The outer spans are 78 ft (23.8 m) long, the inner spans are 76 ft (23.2 m) long. The bridge is skewed 30° from the longitudinal centerline. The bridge superstructure was totally placed using staged construction methods. A photograph and plan layout of the steel superstructure is shown in ***Figure 18.*** The figure also shows the locations and designations of the instrumented details. The areas of interest on this bridge were points near the welded clip angles on the ends of the diaphragms. The clip angles are used to provide a surface to bolt the diaphragms in place to the stringers. ***Figure 19*** also shows a representative diaphragm which indicates individual gage locations and orientation of the diaphragm.

As shown in ***Figure 18***, six diaphragms were instrumented. Diaphragms B2-1 and B2-2 were located directly over piers. Diaphragms C2-1 and C2-2 were adjacent to a pier. Diaphragms D2-1 and D2-2 were near the center of an end span and an interior span, respectively. All diaphragms were located between the fascia beam and the next interior beam on the north side of the bridge. Data were collected for steel erection, and deck installation only. Eight strain gages were installed on each diaphragm. Gage locations and designations were shown in ***Figure 19.*** Strains measured in diaphragms B2-1 and B2-2 are presented in ***Table 7.***

Strain values for diaphragms B2-1 and B2-2 are shown in ***Figures 19, 20 and 21.*** Note that with only one exception, the largest built-in strains are due to placement of the steel. Final built-in stresses range from -17.9 ksi to -1.4 ksi (-123 MPa to -10 MPa), all compressive, for diaphragm B2-1, and from -16.7 ksi to 14.8 ksi (115 MPa to 102 MPa) for diaphragm B2-2.

Strain values for diaphragms C2-1 and C2-2 are shown in ***Table 8.*** These diaphragms are adjacent to piers. Compressive stresses are similar to stresses calculated for diaphragms B2-1 and B2-2, although tensile stresses are lower.

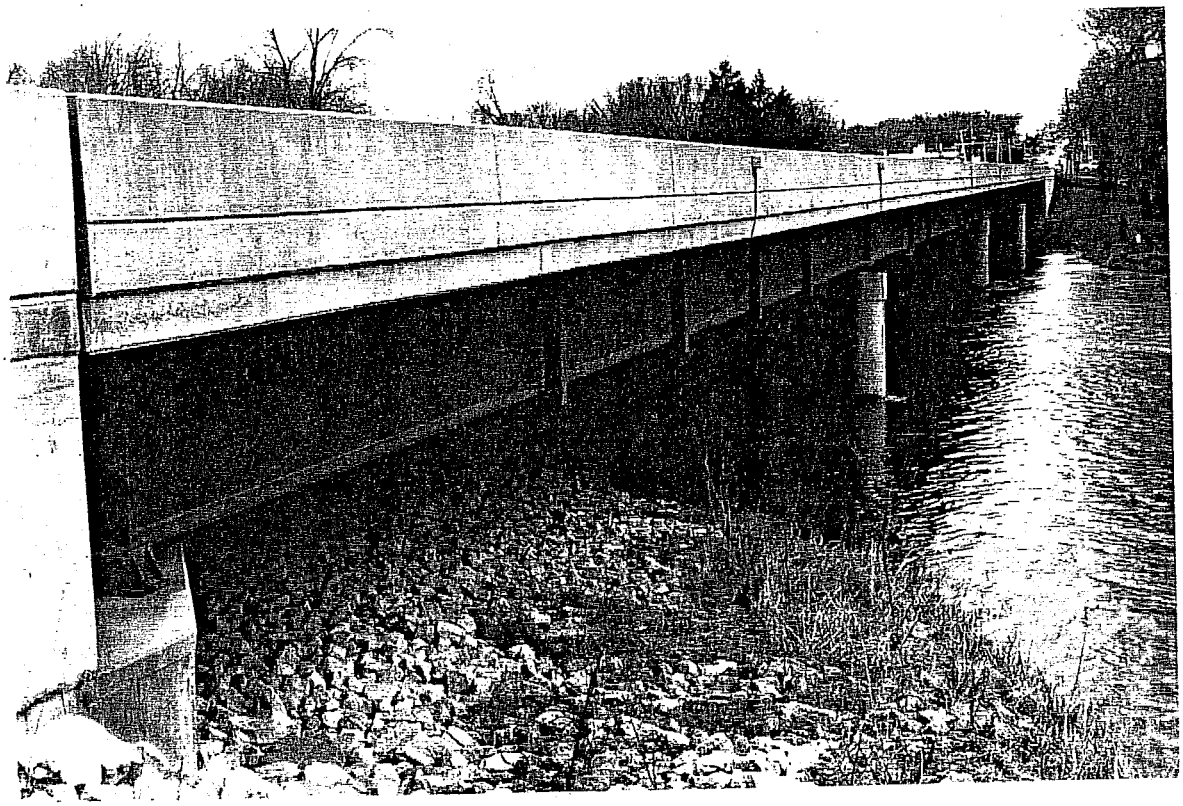

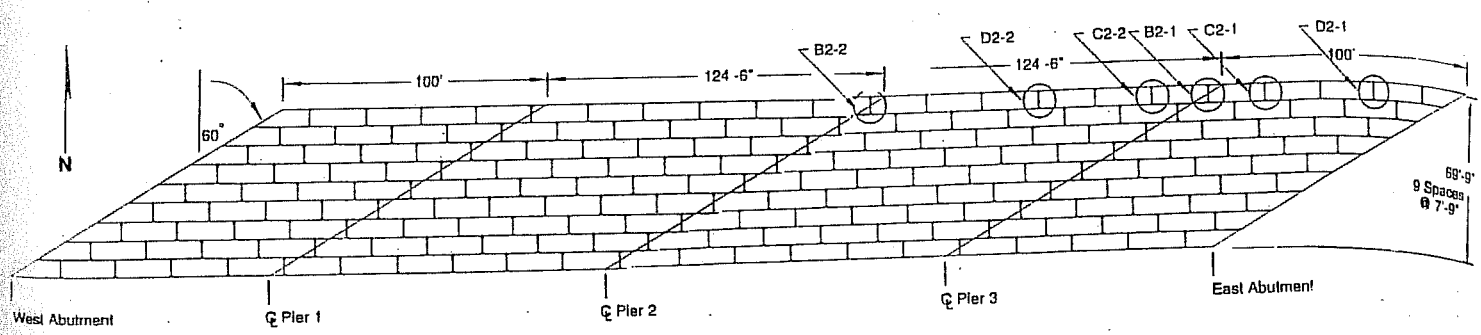

Figure 18. Photograph and plan layout of the steel superstructure of the IL-52 Bridge over the DuPage River near Joliet, Illinois showing locations and designations of instrumented diaphragms, strain gages, and orientation. The bridge has a width of 69.75 ft (21.3 m) and a total span length of 449 ft (136.9 m).

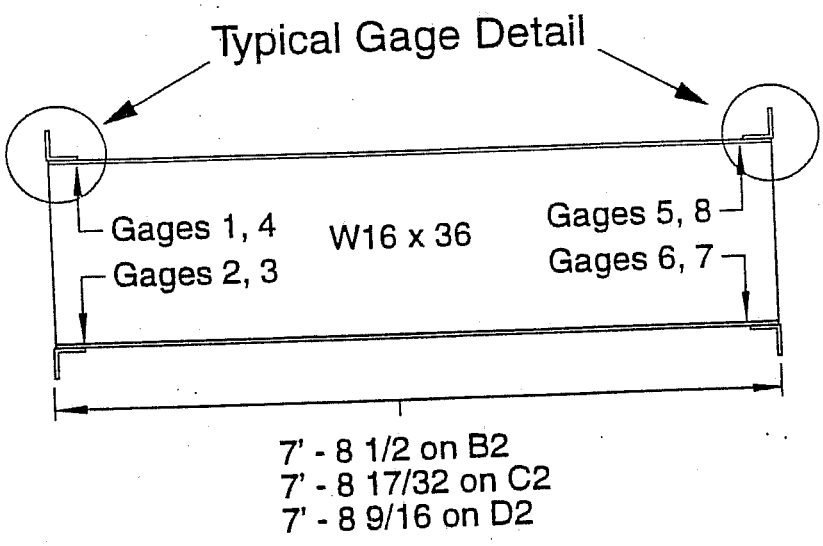

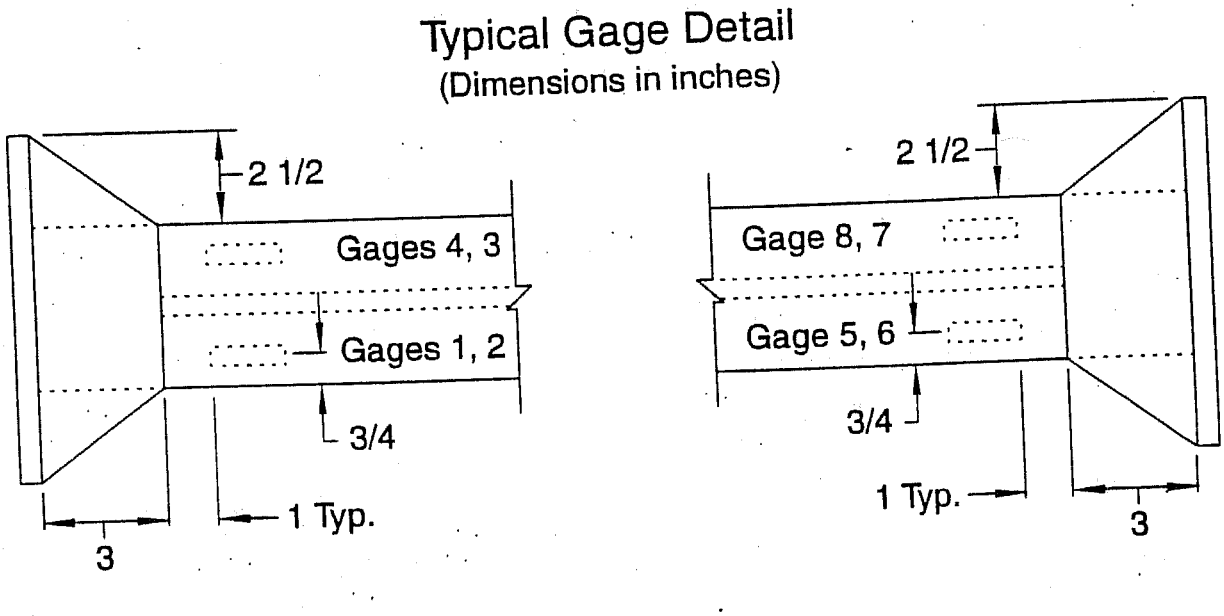

Figure 19a. Typical gage locations on diaphragms B2-1&2; C2-1&2; D2-1&2. All dimensions in inches, except as marked; 1 inch = 2.54 cm.

IL-52 OVER DUPAGE RIVER AT JOLIET

DIAPHRAGM B2-1

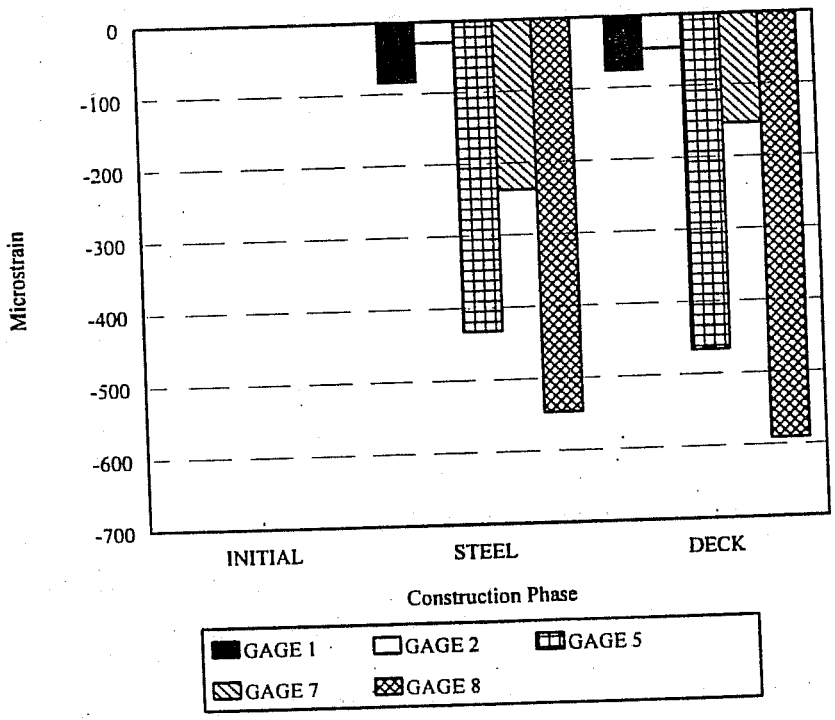

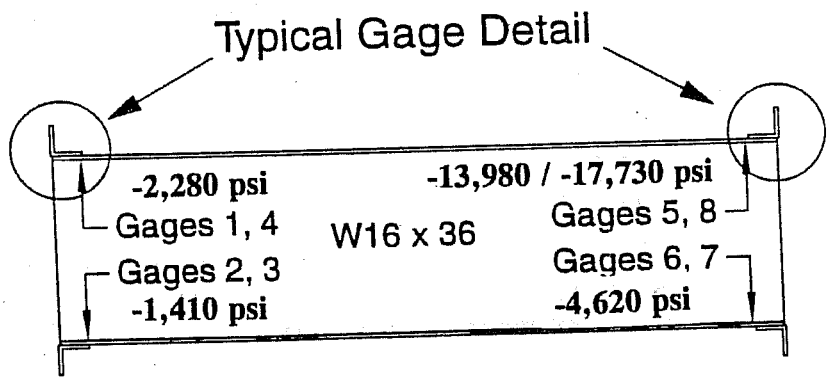

Figure 19b. Strain and stress data collected for diaphragm B2-1 for the construction phases of steel placement and deck placement. Strain data corrected for thermal effects.

Table 7

Strain Data For Diaphragms B2-1 and B2-2*

(IL-52 over DuPage River near Joliet, Illinois)

	DIAPHRAGM B2-1		DIAPHRAGM B2-2	
GAGE	STEEL ERECTED	DECK PLACED	STEEL ERECTED	DECK PLACED
1	-84	-76	-145	-556
2	-30	-47	-352	-203
3	NR	NR	409	493
4	NR	NR	-70	-93
5	-432	-466	189	228
6	NR	NR	-52	-86
7	-238	-154	NR	NR
8	-547	-591	-292	-276

*Strain values are given in units of microstrain (10^{-6} in/in). To convert strain data to stress in steel into MPa, multiply strain data by 0.207; for psi, multiply by 30. Positive values indicate tension; negative values indicate compression.

NR = No reading.

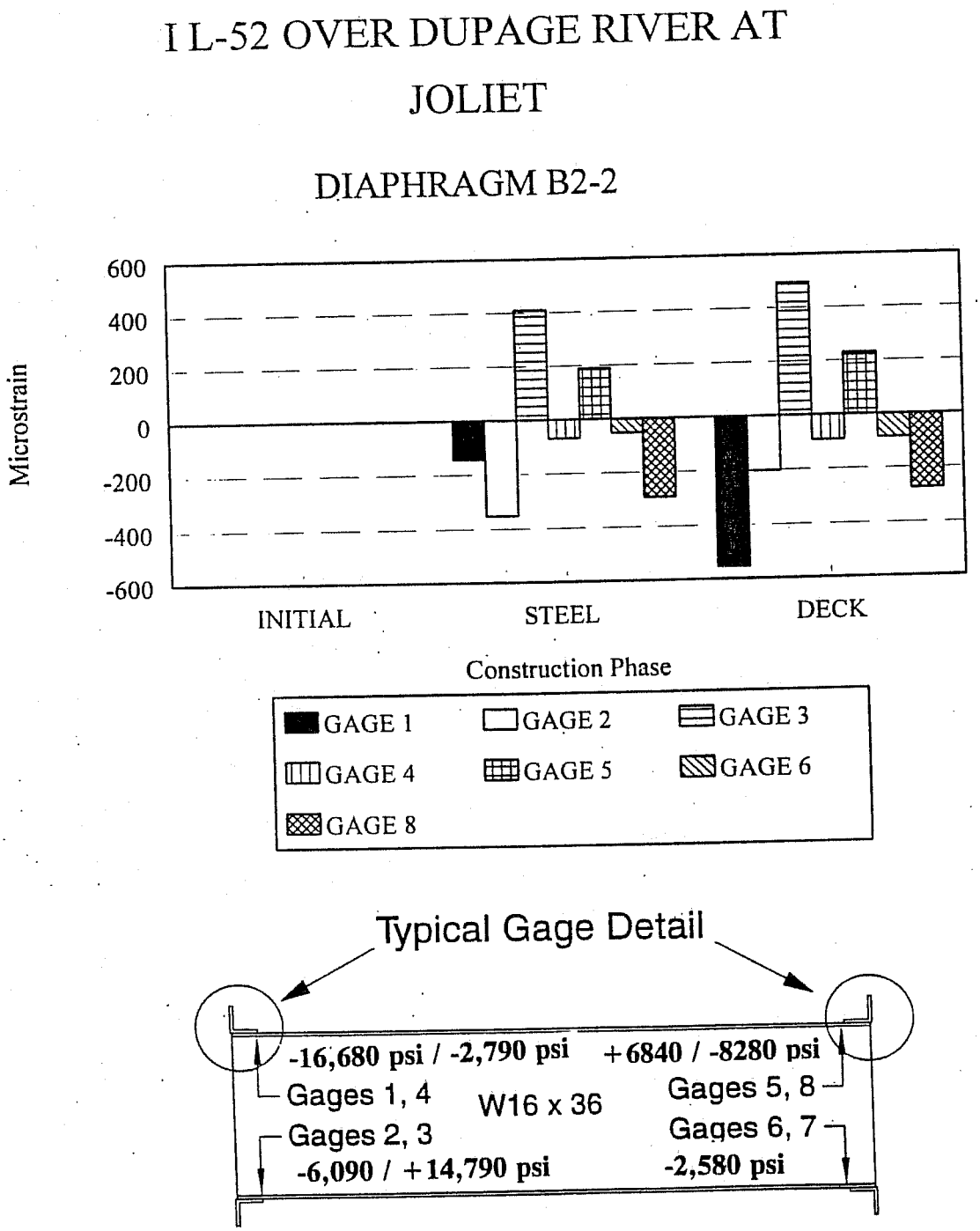

Figure 20. Strain and stress data collected for diaphragm B2-2 (gages 1-8) for the construction phases of steel placement and deck placement. Strain data corrected for thermal effects.

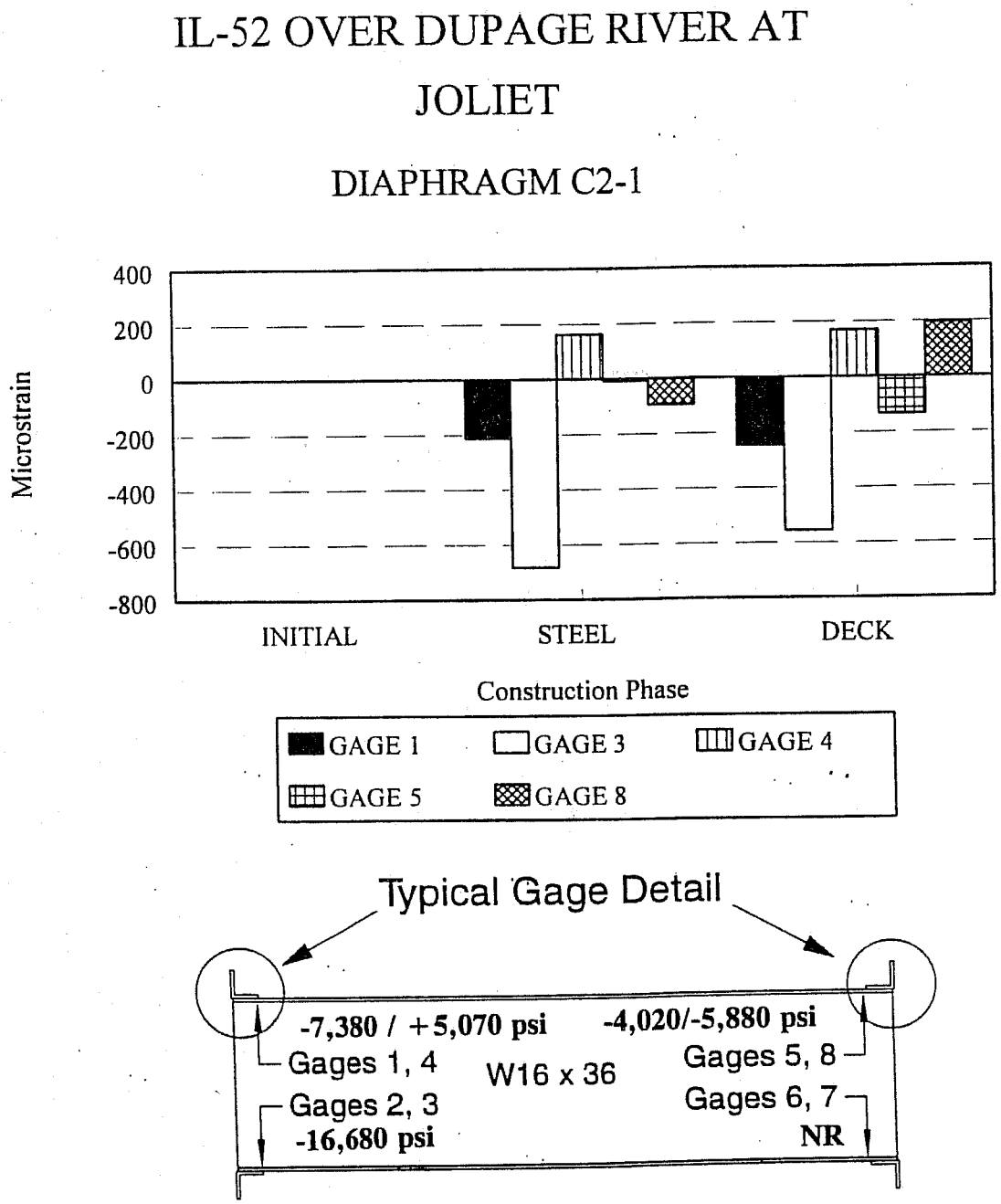

Figure 21. Strain and stress data collected for diaphragm C2-1 (gages 1-8) for the construction phases of steel placement and deck placement. Strain data corrected for thermal effects.

Table 8

Strain Data* For Diaphragms C2-1 and C2-2
(IL-52 Over DuPage River near Joliet, Illinois)

	STAGES OF CONSTRUCTION			
	DIAPHRAGM C2-1		DIAPHRAGM C2-2	
GAGE	STEEL ERECTED	DECK PLACED	STEEL ERECTED	DECK PLACED
1	-213	-246	-161	-182
2	NR**	NR	-389	-362
3	-682	-556	-507	-430
4	162	169	-491	-491
	DIAPHRAGM C2-1		DIAPHRAGM C2-2	
GAGE	STEEL ERECTED	DECK PLACED	STEEL ERECTED	DECK PLACED
5	-8	-134	-226	-225
6	NR	NR	47	33
7	NR	NR	-145	-115
8	-96	-196	-452	-446

*Strain values are given in units of microstrain (10^{-6} in/in). To convert strain data to stress in steel into MPa, multiply strain data by 0.207; for psi, multiply by 30. Positive values indicate tension; negative values indicate compression.
NR = No reading.

The strain data for diaphragms C2-1 and C2-2 are shown in ***Figures 21 and 22.*** Final built-in stresses range from -115 MPa to 35 MPa (-16.7 ksi to 5.1 ksi) in diaphragm C2-1, and from 92 MPa to 7 MPa (-13.4 ksi to 1.0 ksi) in diaphragm C2-2.

Diaphragms D2-1 and D2-2 are located at center span. Compressive stress levels are similar to previous diaphragms. No tensile strains were measured for these diaphragms. Measured strain data are presented in ***Table 9.***

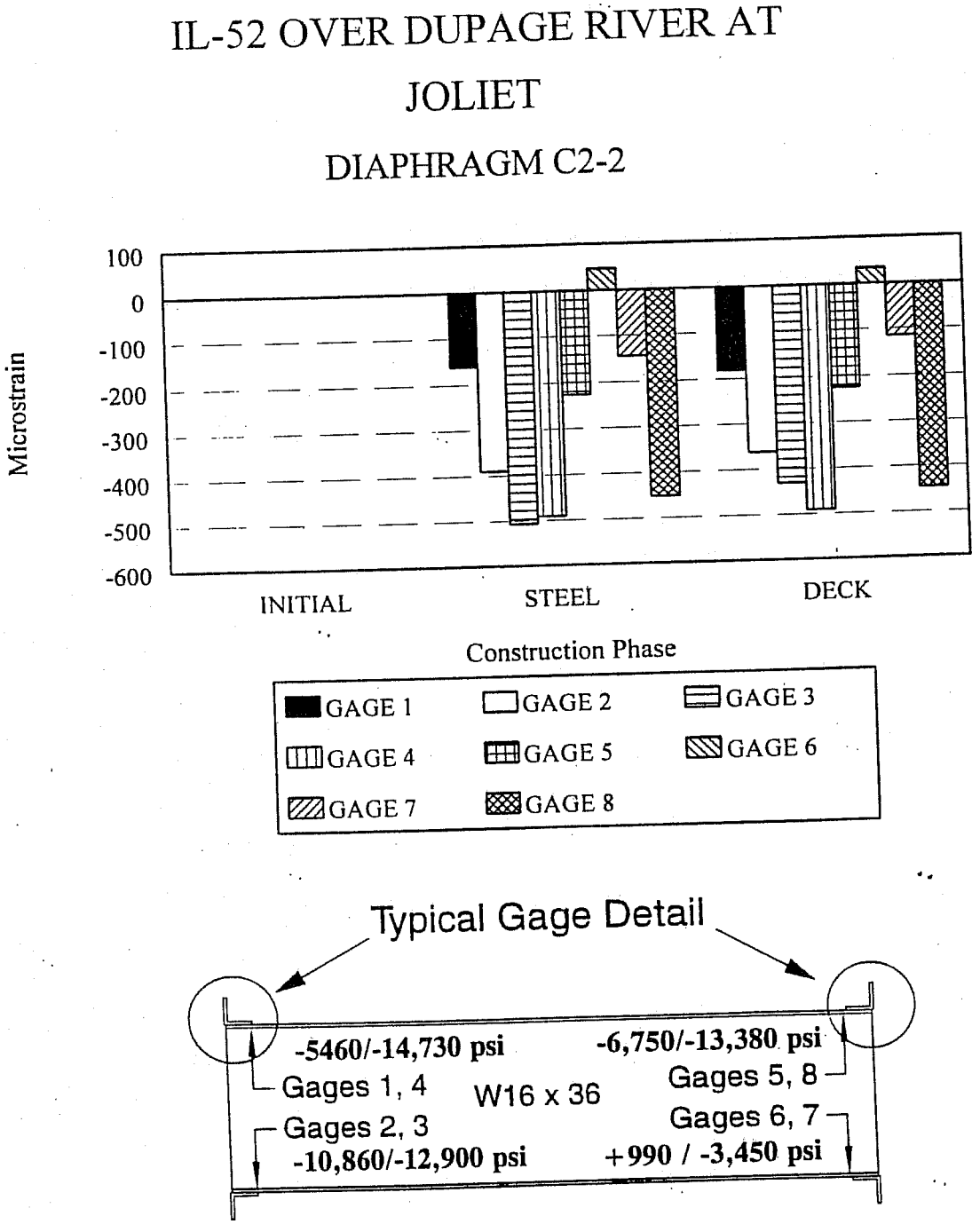

Figure 22. Strain and stress data collected for diaphragm C2-2 (gages 1-8) for the construction phases of steel placement and deck placement. Strain data corrected for thermal effects.

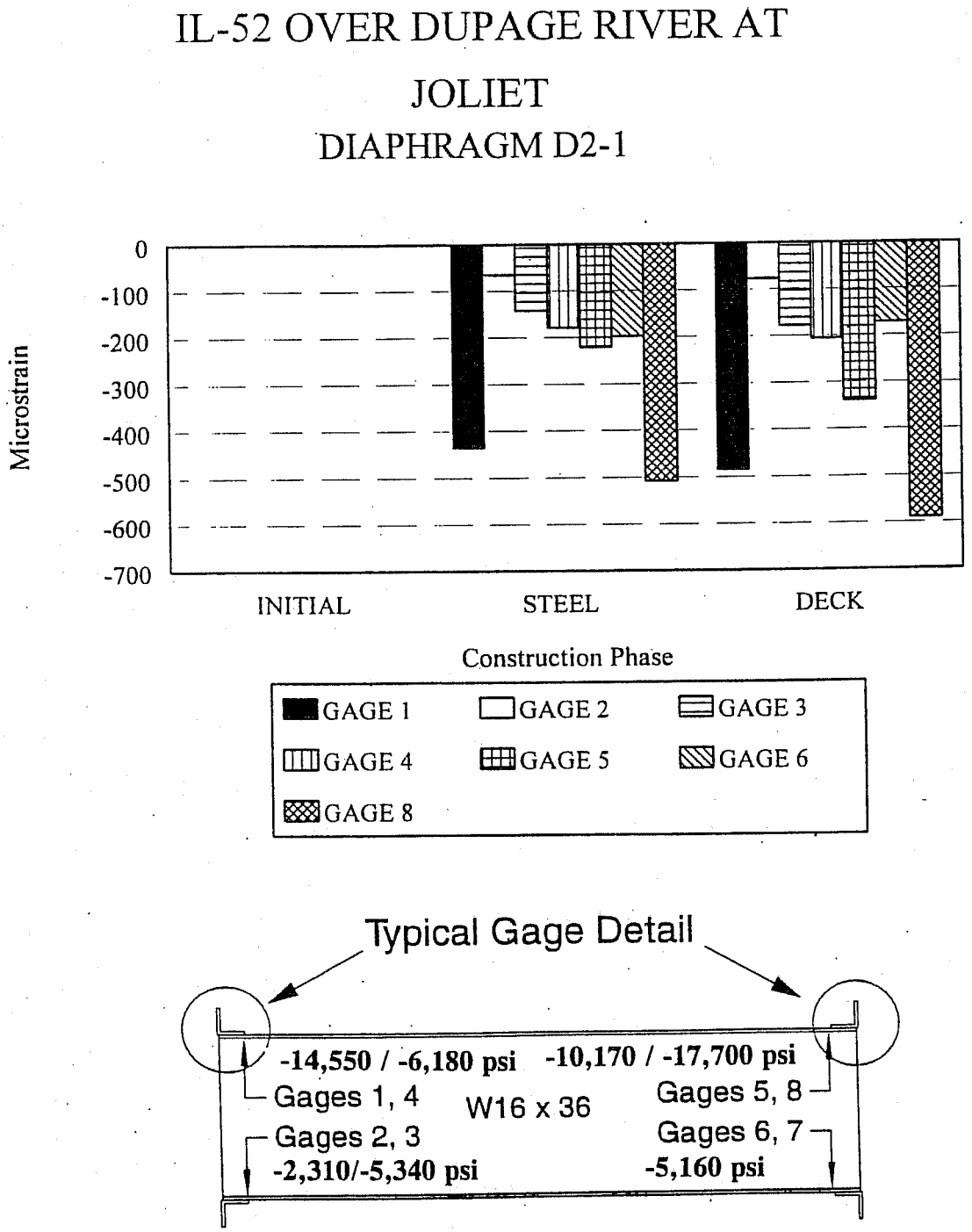

Figure 23. Strain and stress data collected for diaphragm D2-1 (gages 1-8) for the construction phases of steel placement and deck placement. Strain data corrected for thermal effects.

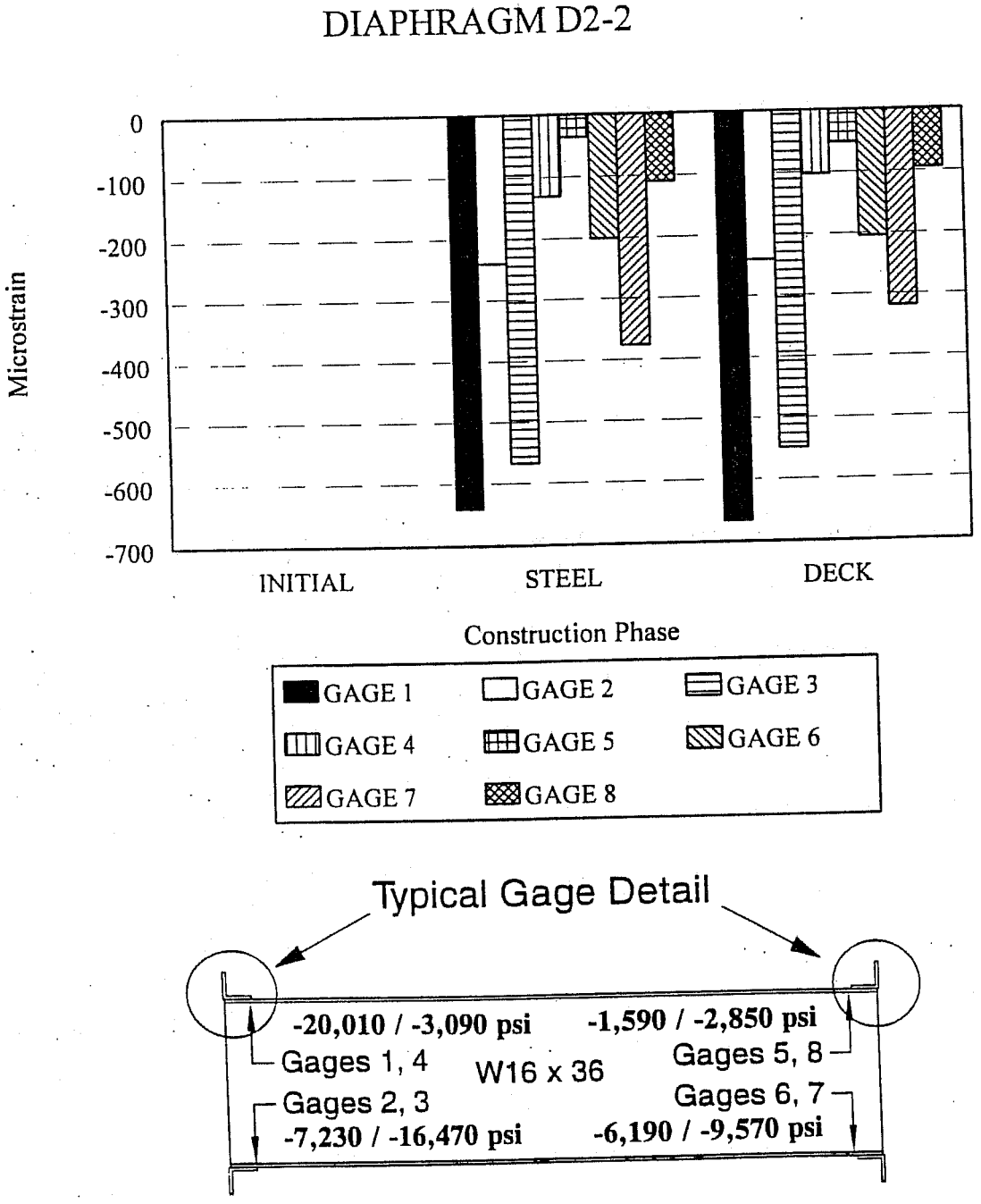

Figure 24. Strain and stress data collected for diaphragm D2-2 (gages 1-8) for the construction phases of steel placement and deck placement. Strain data corrected for thermal effects.

Table 9

Strain Data* for Diaphragms D2-1 and D2-2
(IL-52 Over DuPage River near Joliet, Illinois)

	DIAPHRAGM D2-1		DIAPHRAGM D2-2	
GAGE	STEEL ERECTED	DECK PLACED	STEEL ERECTED	DECK PLACED
1	-436	-485	-641	-667
2	-65	-77	-240	-241
3	-142	-178	-567	-549
4	-179	-206	-131	-103
5	-221	-339	-36	-53
6	-198	-172	-201	-205
7	NR**	NR	-376	-319
8	-508	-590	-110	-95

*Strain values are given in units of microstrain (10^{-6} in/in). To convert strain data to stress in steel into MPa, multiply strain values by 0.207; for psi, multiply by 30. Positive values indicate tension; negative values indicate compression.
NR = No reading.

The data in ***Table 9*** are shown in ***Figure 23*** for diaphragm D2-1, and ***Figure 24*** for diaphragm D2-2. Final built-in stresses were all compressive, and ranged from -17.7 ksi to -2.3 ksi (-122 MPa to -16 MPa) in diaphragm D2-1, and from -20.0 ksi to -1.6 ksi (-138 MPa to -11 MPa) in diaphragm D2-2.

Brandon Road over the Des Plaines River

The Brandon Road bridge over the Des Plaines River in Joliet, Illinois is a double-leaf bascule bridge, 198 ft (60.4 m) long, and 24 ft (7.3 m) wide. A plan view of the structural steel is shown in ***Figure 25.*** Locations of instrumented diaphragms and bascule leaves are also shown in ***Figure 26.*** The diaphragms were instrumented as in the other bridges. The bascule leaves were instrumented at the trunnion location. Gage locations and designations for the diaphragms and the trunnion locations are shown in ***Figure 27.*** A photograph of the bridge is shown in ***Figure 28.*** The bridge has an open steel grid deck.

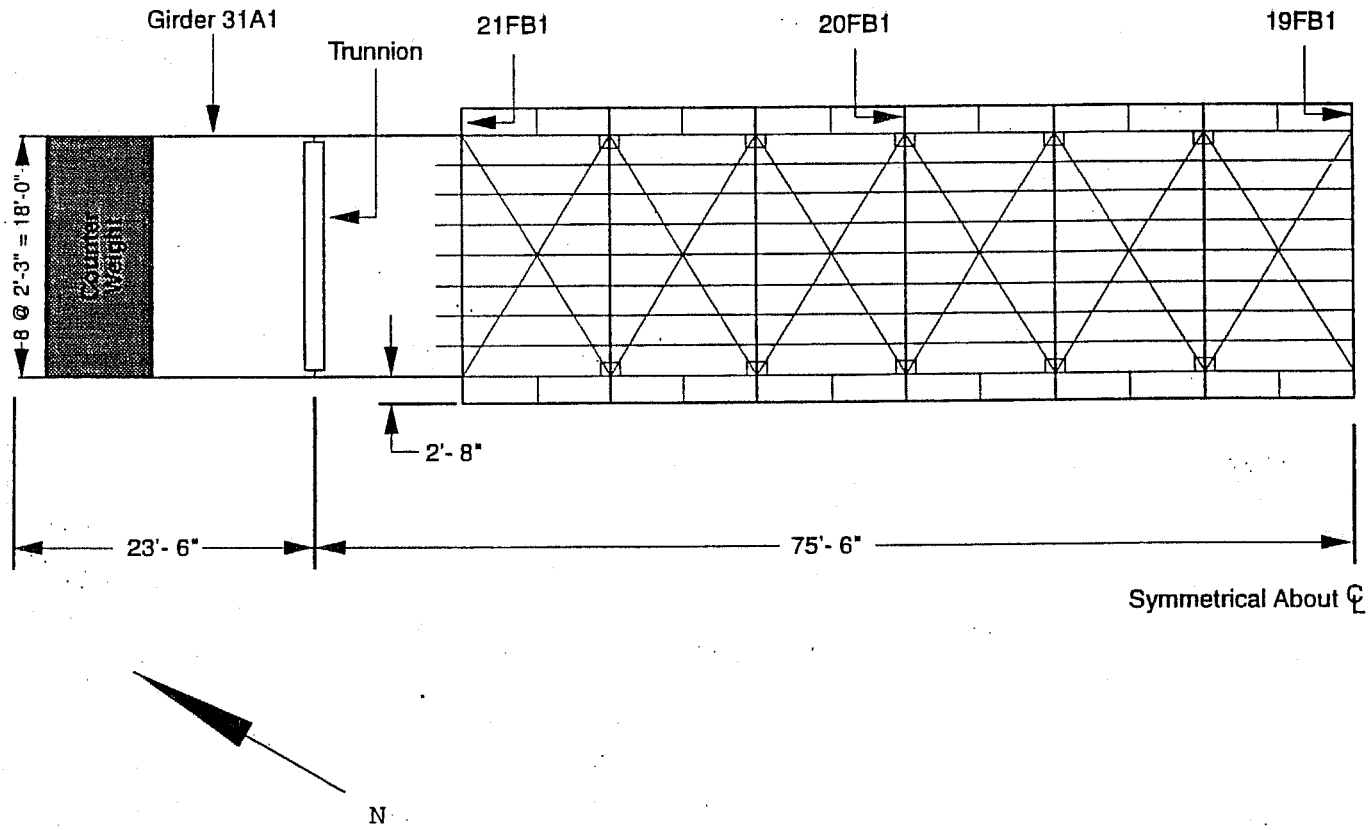

Figure 25. Plan view of structural steel framing for Brandon Road over Des Plaines River in Joliet, Illinois, showing instrumented locations.

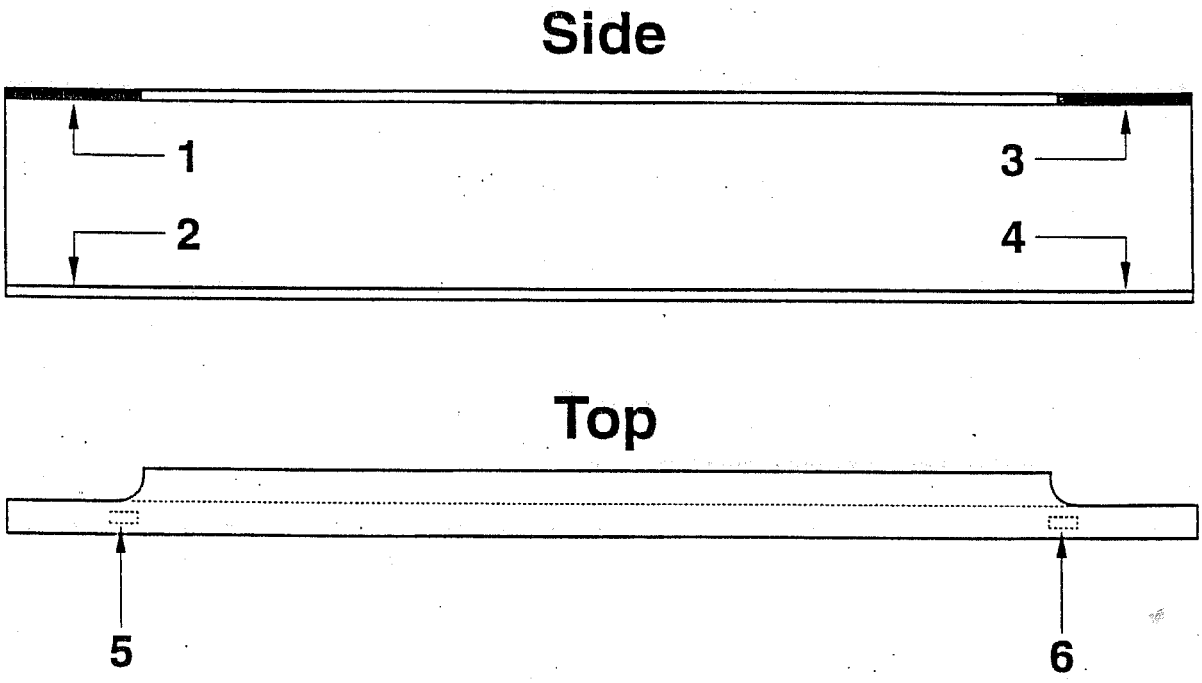

Figure 26. Strain gage locations and designations for instrumented diaphragms on the Brandon Road bascule bridge.

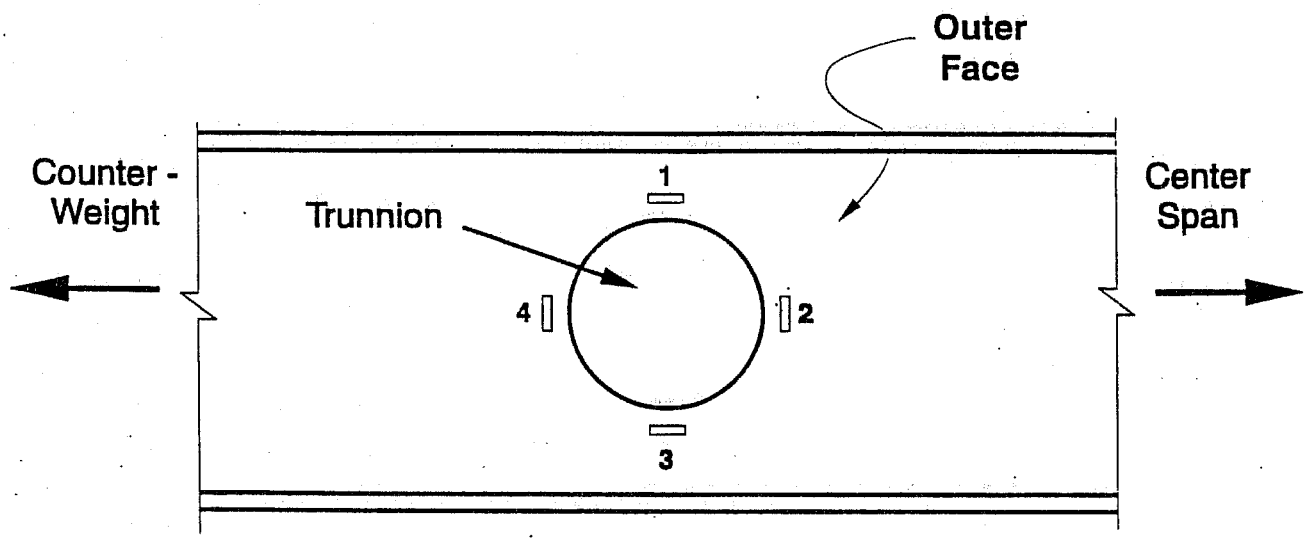

Figure 27. Strain gage locations and designations for instrumented trunnion areas on the Brandon Road bascule bridge.

Static strain readings were collected prior to installation and after the bridge was opened to traffic. Most of the data were collected when the bridge was in the down (closed) position. Strain data for the instrumented floorbeams is presented in ***Table 10***. ***Table 11*** provides strain data for the instrumented girder. Strain data for floor beams 19FB1, 20FB1, 21FB3 and girder 31Al are plotted in ***Figures 29, 30, 31*** and ***32.***

Table 10

Strain Data* for Instrumented Floorbeams
(Brandon Road Over DesPlaines River at Joliet, Illinois)

	FLOORBEAMS		
GAGE	19FB1	21FB3	20FB1
1	NR	23	88
2	NR	484	194
3	NR	10	30
4	NR	205	417
5	38	-73	14
6	15	75	70

*Strain values are given in units of microstrain (10^{-6} in/in). To convert strain data to stress in steel into MPa, multiply strain values by 0.207; for psi, multiply by 30. Positive values indicate tension; negative values indicate compression.
NR = No reading.

Table 11

Strain Data for Instrumented Girder 31A1 (Northeast Side)
(Brandon Road Over DesPlaines River in Joliet, Illinois)

GAGE	MICROSTRAIN*
1	-583
2	-151
3	NR
4	NR

*Strain values are given in units of microstrain (10^{-6} in/in). To convert strain data to stress in steel into MPa, multiply microstrain values by 0.207; for psi, multiply by 30. Positive values indicate tension; negative values indicate compression.
NR = No reading.

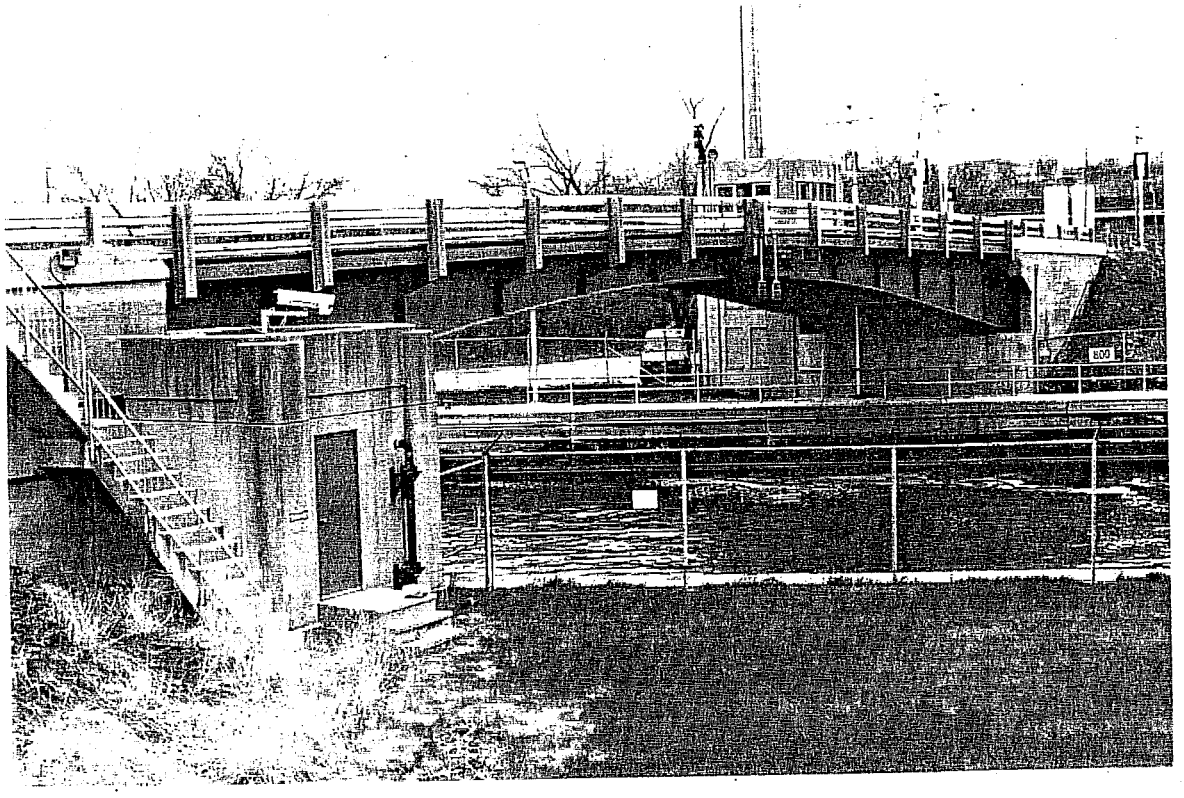

Figure 28. Photograph of the Brandon Road bascule bridge over the DesPlaines River, located at Joliet, Illinois.

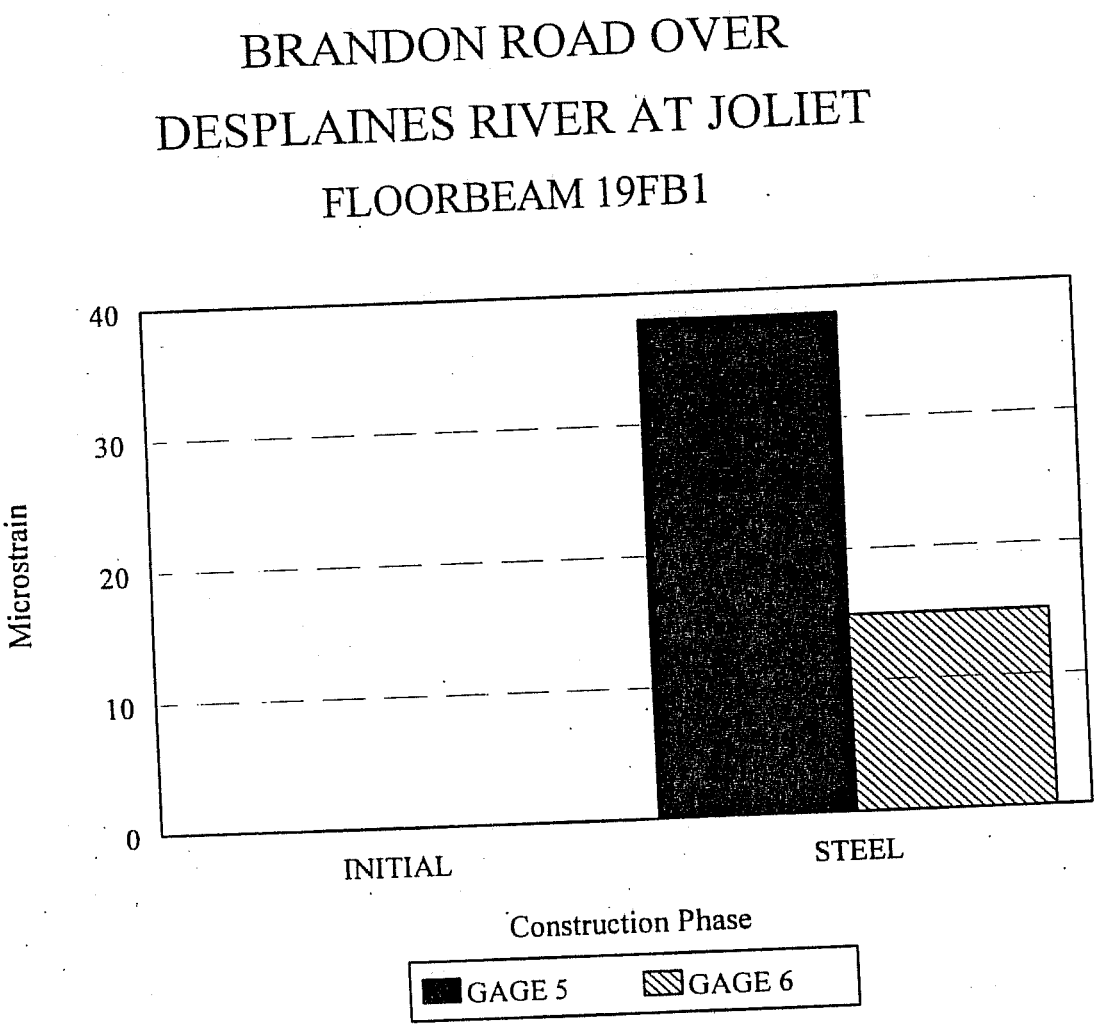

Figure 29. Strain data collected for floorbeam 19FB1 after steel and grid deck placement.

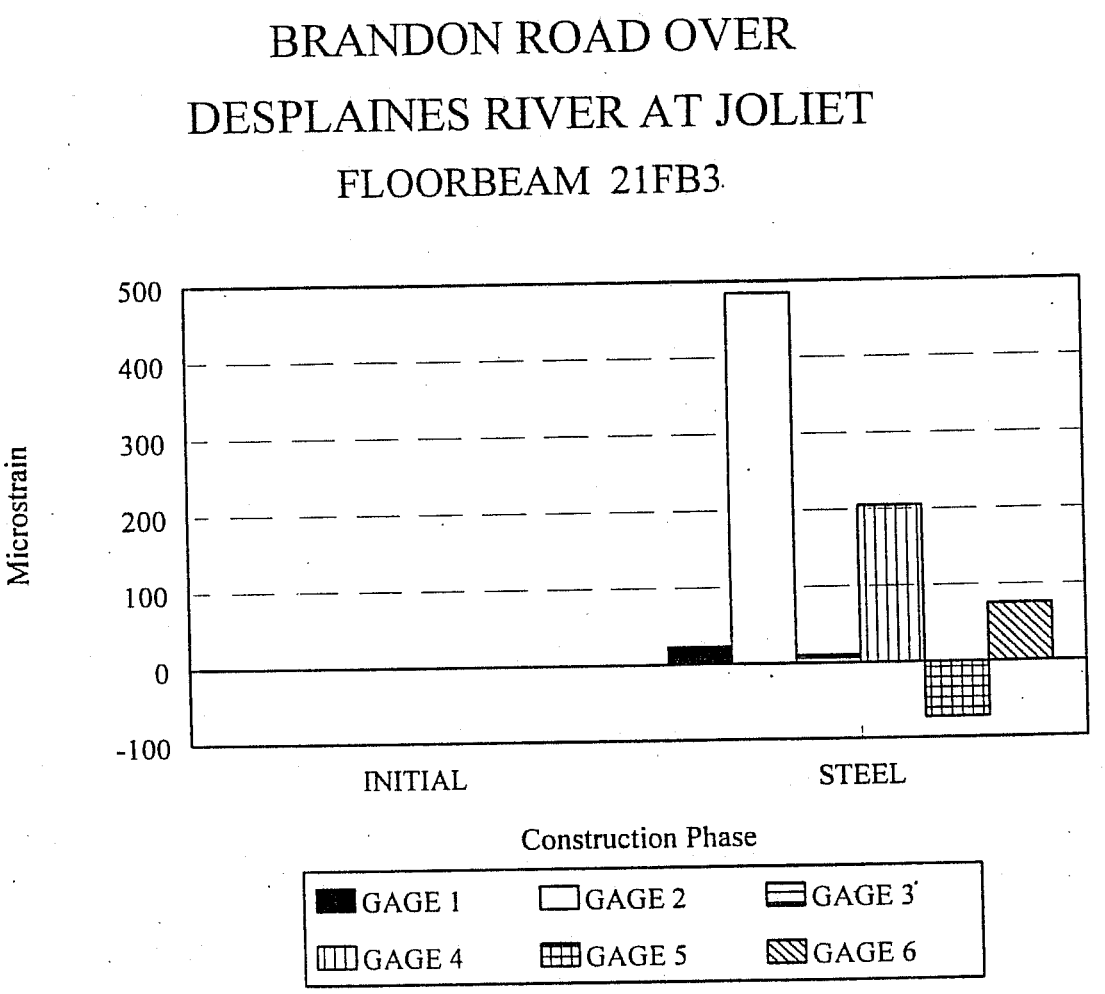

Figure 30. Strain data collected for floorbeam 21FB3 after steel and grid deck placement.

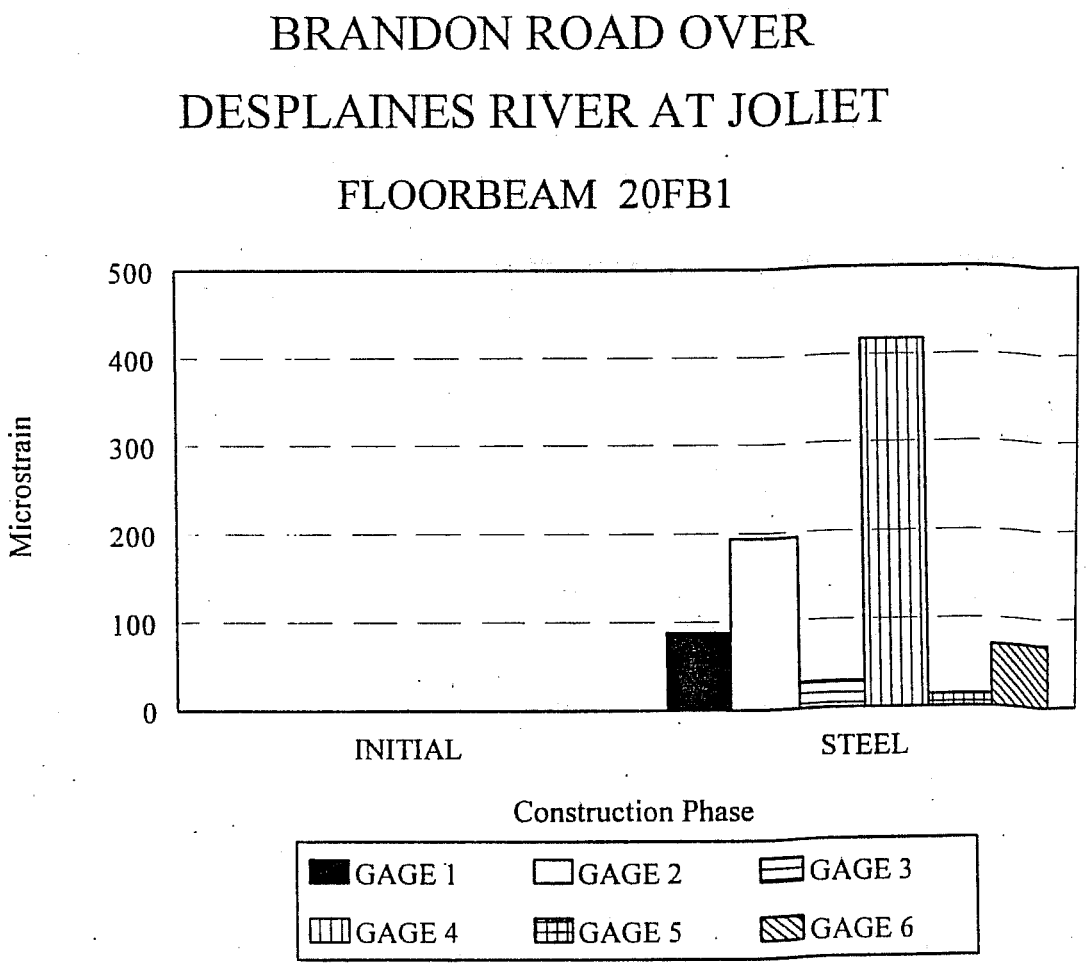

Figure 31. Strain data collected for floorbeam 20FB1 after steel and grid deck placement.

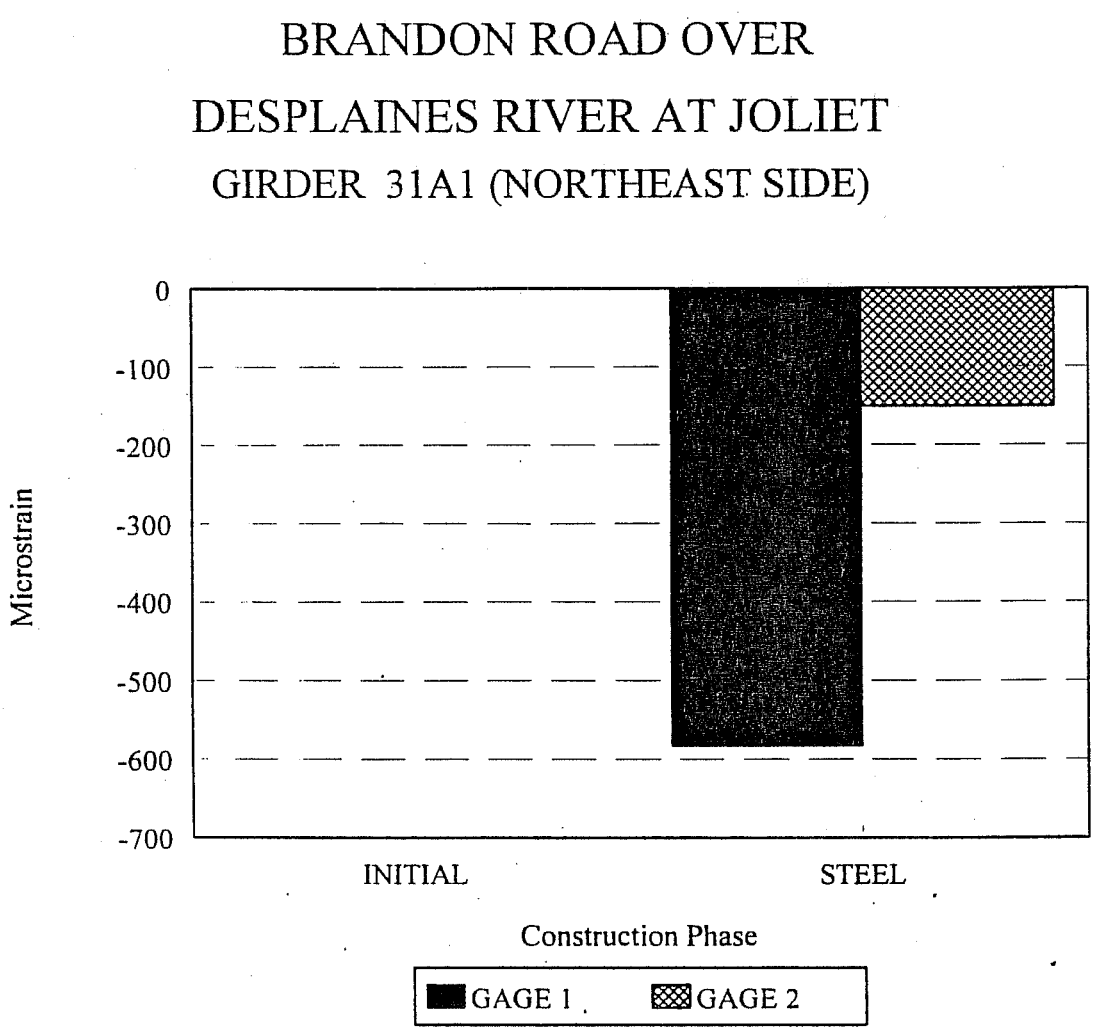

Figure 32. Strain data collected for girder 31A1 after steel and grid deck placement; gages are located near the trunnion.

Another girder was instrumented, but all four gages were destroyed before data was gathered. Data from the floorbeams indicate that mostly tensile stresses were introduced due to construction. The bottom of the floor beams indicate tension from loading of the deck through stringers attached to the floorbeams. Some compression is registered in the upper portions of the floor beams, as would be expected. The strain data from ***Table 11*** indicate compression in both gages near the trunnion. This compression results from the shrink fit of the trunnion into the girder.

Summary of Bridge Strain Data

Components from three structures were instrumented with strain gages prior to construction in order to measure the stresses in a bridge built-in during the construction process. The bridges were constructed using normal practices. Baseline data were collected at the fabrication shops. Additional static strain data were collected for different construction phases and after construction was completed. Three bridges were instrumented: (1) County Highway 14 over Interstate-39 at Wenona; (2) Illinois Route-52 over the DuPage River near Joliet; and (3) Brandon Road over the Des Plaines River in Joliet.

Inspection of the data shows that substantial tensile stresses which exceed allowable stresses for ASTM A36 structural steel can be locked into bridge components during construction. It was also apparent that the sign and magnitudes of these strain were not predictable in the design stage, and displayed wide variability. The mean tensile strain in diaphragms was 171 $\mu\varepsilon$ ±192 $\mu\varepsilon$ [std. dev.]. The mean compressive strain was -248$\mu\varepsilon$ ± -191$\mu\varepsilon$ [std. dev.]. The highest tensile stress measured in steel diaphragms was 20.8 ksi (143 MPa).

Several factors contributed to residual stresses being built-in during construction. Primary factors are: (1) the gradual loading of the bridge by its component parts, including diaphragms, girders, deck elements and parapet weights, which are all transferred through the various connections; (2) shrinkage of the concrete deck; (3) out-of-tolerance limits for bolt holes; (4) use of drift pins to forcibly connect members prior to final bolting; (5) slight dimensional displacements of main girders which requires bolts to pull the girder and diaphragm together; (6) girders and diaphragms with acceptable dimensional variations, derived from liberal construction tolerances. All of these factors complicate efforts to predict built-in stresses in the design stage of project implementation.

EFFECTS OF CYCLIC STRAIN ON FATIGUE LIFE

In this chapter, the effects of repeated, live load alternating stresses and residual mean strains on the fatigue life of bridge details are discussed. The determination of a factor of safety for many common weld details subject to fatigue is described.

Effects of Repetitive Strain on Fatigue Life of Structural Components

The fatigue life of metallic structures is controlled by the cumulative damage sustained during its service life. Structural materials can sustain a range of repetitive fatigue cycles at a certain strain amplitude before extensive cracking or failure occurs. The strain absorbed by the structural component can be either elastic or plastic, depending on (1) the material, (2) the amplitude and intensity of the applied loads, and (3) their frequency and duration.

The greatest amount of fatigue damage occurs when metallic members are subjected to continuing reversals of strain, alternating from positive to negative and back to positive. The relationship between the number of available alternating stress (or strain) cycles and the stress or strain amplitude has been extensively studied and experimentally determined by many investigators for a variety of materials [Ref 2]. The strain amplitude vs. fatigue life equation in its generalized form is as follows:

$$\frac{\Delta\varepsilon}{2} = \frac{\sigma_f'}{E}(2N_f)^b + \varepsilon_f'(2N_f)^c \qquad \text{[Equation 1]}$$

where $\Delta\varepsilon/2$= total strain amplitude = $\Delta\varepsilon_{plastic}/2 + \Delta\varepsilon_{elastic}/2$

E = modulus of elasticity

$2N_f$ = reversals to failure (2 reversals = 1 cycle)

σ_f' = fatigue strength coefficient

b = fatigue strength exponent

ε_f' = fatigue ductility coefficient

c = fatigue ductility exponent.

The coefficients ε_f' and σ_f', and the exponents b and c, are fatigue properties of a material, and are determined experimentally. The strain-life relationship for ASTM A36 steel plate is plotted in ***Figure 33,*** showing the elastic and plastic components of strain. When each component is combined, the total strain amplitude absorbed by the steel plate can be measured by compo-

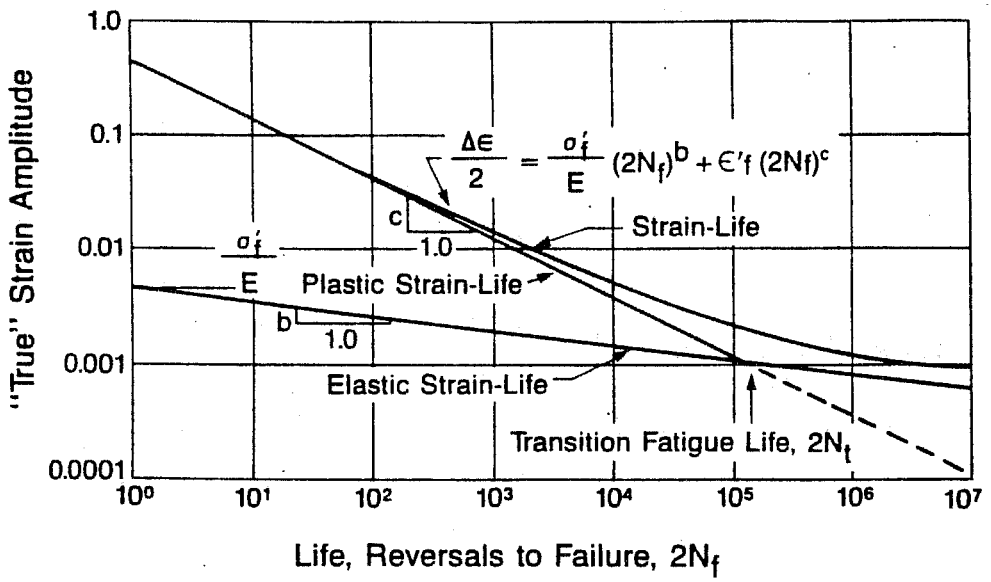

Figure 33. A plot of log [strain amplitude, $\Delta\varepsilon/2$] vs. log [reversals to failure, $2N_f$] for ASTM A36 steel. The elastic component of strain is added to the plastic component, resulting in a strain-life curve. At 10^4 reversals (which is equivalent to 5,000 cycles), the high cycle fatigue region is entered where elastic strain predominates, and the plastic component loses significance. Data source: *Fatigue Design Handbook AE-10,* Society of Automotive Engineers, 1988.

nent deflection, strain gages, photoelastic coatings, or by light interferometry. The strain-life equation for ASTM A36 structural steel plate is:

$$\Delta\varepsilon/2 = 0.00411\ [2N]^{-0.12} + 0.44\ [2N]^{-0.51} \qquad \text{[Equation 2]}$$

Similarly, the strain-life equation for 6061-T6 aluminum *extrusions* is:

$$\Delta\varepsilon/2 = 0.0086\ [2N]^{-0.093} + 5.39\ [2N]^{-1.10} \qquad \text{[Equation 3]}$$

The strain life equation for 6061-T6 aluminum *plate* is:

$$\Delta\varepsilon/2 = 0.00712\ [2N]^{-0.0728} + 1.48\ [2N]^{-0.855} \qquad \text{[Equation 4]}$$

Even for the same alloy as shown above, there are appreciable differences between the strain life equation for plate *vs.* extrusions. Plates have slightly lower yield strengths than cold-drawn extrusions, but have greater ductility.

The above strain-life equations are for smooth bars, plates and shapes which have no marked changes in section, no bolt holes, no welds and no notches subjected to numerous cyclic strain reversals. The above predictive equations are limited to rolled plate, rolled wide-flange shapes, or tubes without attachments. However, many structural members contain weld pads, attachments, bolt holes, and notches, and frequently have severe changes in section. Fortunately, most highway bridges operate with stresses in the elastic range, and their live load stresses in girders are kept between 4 to 6 ksi (28 to 41 MPa) by load limits. Occasionally, live load longitudinal stresses up to 15 ksi may be encountered with special overload truck permits. Out-of-plane bending can further magnify these nominal stresses in stiffener attachments, reducing their fatigue life. Residual stresses from welding are also significant, because they can approach 80 to 90% of the yield strength of the base metal.

Strain amplitudes in the elastic range generally result in fatigue lives greater than 1,000 cycles. Beyond about 10,000 cycles, the plastic portion of the strain-life equation is no longer significant. The elastic portion predominates, and the strain-life equation reduces to:

$$\Delta\varepsilon/2 = [\sigma_f'/E]\ [2N]^b \qquad \text{[Equation 5]}$$

To correct for mean residual stresses, a correction to the term σ_f' is sometimes made per Morrow [Ref 5] by subtracting the mean stress σ_m, resulting in:

$$\Delta\varepsilon/2 = [(\sigma_f' - \sigma_m)/E]\ [2N]^b \qquad \text{[Equation 6]}$$

Residual stresses are derived from: (a) welding and fabrication; (b) high stress concentrations from design geometry; (c) construction; and (d) dead loads. All of these residual stresses can appreciably affect the fatigue life of a bridge, depending on their magnitude.

The residual stresses of welding can cause the strain life of the structural detail to be significantly altered, depending on the direction of applied stresses and orientation of the welds. In certain weld joints where sharp changes in structural stiffness, notches, or residual stresses from severe weld restraint are present, fatigue strengths at 10^6 to 10^7 cycles can be adversely affected. Although not directly stated, the American Welding Society (AWS) weld joint fatigue categories reflect the built-in residual stresses of welds, notches and geometry. AWS Fatigue Category A represents unnotched, as-rolled plate or beams, whereas Fatigue Category E represents the worst cases. Category E weld joints are characterized by large attachments or other structural discontinuities, severe changes in section, high weld restraint, sharp notches, or have highly localized weld crack initiation sites.

Investigators at Lehigh University [Ref 6] found that web attachments are particularly vulnerable to fatigue crack initiation induced by distortion. At web stiffener gaps, cracks rapidly developed at only 50,000 to 100,000 cycles due to stress concentration factors of 3 or more [Ref 7]. Out-of-plane distortion is considered by Fisher [Ref 8] to be the largest source of fatigue cracking in bridges.

Fatigue Life as a Function of Stress Range

Fatigue literature has traditionally plotted stress or strain amplitude as a function of number of available cycles, where $\varepsilon, \sigma = f(N)$. However, fatigue data can also be represented as $N_f = f(\sigma, \varepsilon)$, which is a more logical and practical expression since cyclic stresses or strains cause fatigue failure in materials that are generally free of gross defects. Stress and strain are typically the known variables. The $N_f = f(\sigma)$ equation for an unnotched steel wide flange in bending is:

$$N_f = [5.74 \times 10^{10}]\, S^{-3.24} \qquad \text{[Equation 7]}$$

where N_f = number of available fatigue cycles

S = live load stress range

Equation 7 also represents AWS Fatigue Category A for redundant steel members. The remaining fatigue categories compared to Category A are shown in ***Table 12.*** Each successive fatigue category represents an increasing penalty due to the severity of welding and joint design, resulting in progressive decreases in fatigue life for various welded details.

Table 12

AWS Fatigue Categories for Redundant Steel Members

Fatigue Category*	Cyclic Fatigue-Life Equation	Types of Weld Joints or Connection Geometry
A	$N = 5.70 \times 10^{10} [S]^{-3.24}$	unnotched plate; rolled structural shapes
B	$N = 1.85 \times 10^{10} [S]^{-3.17}$	shapes where partial pentration or fillet welds are principally stressed in the longitudinal direction
C	$N = 1.44 \times 10^{10} [S]^{-3.46}$	shapes with stiffeners or small attachments
D	$N = 1.72 \times 10^{9} [S]^{-2.97}$	shapes with large radiused attachments or smaller attachments with sharp or notched corners; changes in section without grinding welds smooth
E	$N = 1.27 \times 10^{9} [S]^{-3.11}$	intermittent fillet welds; fillet weld terminations; sharp, notched transitions or large, notched attachments; plug or slot welds

Derived from Table 9.2 of the AWS Structural Welding Code D1.1; fatigue equations are for redundant members only; non-redundant members are more conservative per code.

Factor of Safety Determination

The magnitudes of both alternating and mean stresses in a component will influence its fatigue life. Tensile alternating stresses combined with mean tensile stresses generally reduce fatigue life. Compressive stresses have variable effects on fatigue life. It is important for a designer to know the influence of tensile mean stresses on fatigue life, since their magnitude will determine the factor of safety for details which are either main-load-carrying or fracture-critical members of the bridge. Other "secondary" details are sometimes connected to load-carrying members, and cracks from non-critical members can propagate into critical members.

Weldments without any post-weld thermal stress relief typically contain residual stresses that are near the yield strength of the base metal. However, although welds are only part of a structure, cracks originating in the weld, fusion or heat-affected zones can propagate into unwelded areas. If crack sizes are large enough, actual rupture can occur. Mean stresses from dead loads have a significant effect on the fatigue life of structural steel, and should be accounted for when determining a factor of safety.

The factor of safety in engineering design is frequently determined by use of the linear Goodman failure equation. However, the parabolic Gerber failure equation has the best fit with actual fatigue data, particularly for aluminum alloys. Both equations define a safe envelope in which no fatigue failure is expected. The Goodman and Gerber equations are as follows:

Goodman: $$N_{safety(L)} = \frac{1}{\frac{S_a}{S_e} + \frac{S_m}{S_u}}$$ [Equation 8]

Gerber: $$N_{safety(p)} = \frac{1}{\frac{S_a}{S_e} + \left[\frac{S_m}{S_u}\right]^2}$$ [Equation 9]

where N_{safety} = safety factor,

S_a = alternating stress amplitude, $(S_{max} - S_{min})/2$,

S_m = mean stress, $(S_{max} + S_{min})/2$,

S_{max} = maximum stress,

S_{min} = minimum stress,

S_e = fatigue strength at 2×10^6 or greater number of cycles

S_u = ultimate tensile strength.

Bridge design codes use a fatigue category for various weld details. Stress ranges are used instead of alternating stress amplitudes. Mean stress is a combination of live load and dead load stresses. The Gerber parabolic relationship was adapted to bridge use by Hahin, South, Mohammadi and Polepeddi [Refs 3; 4], incorporating the weld detail fatigue strength and the stress range:

$$N_{safety(p)} = \frac{1}{\frac{S_{LL}}{F_d} + \frac{[(S_{LL} + 2S_{DL})/2]^2}{(S_u)^2}} \qquad \text{[Equation 10]}$$

where $N_{safety(p)}$ = safety factor (parabolic form)

S_{LL} = live load stress range

S_{DL} = dead load stress in member

F_d = fatigue strength of detail at 2 x 10^6 or greater number of cycles

S_u = ultimate tensile strength of the weld detail.

The above fatigue safety factor relationship incorporates both the influence of dead load stresses, construction stresses, and live load stresses, but places primary emphasis on the ratio of live load stresses to the fatigue strength of the weld detail. The squared term accounts for ambient dead load and residual stresses in the detail and is a measure of the remaining strain-energy. The squared term becomes significant when ambient stresses start to approach bridge code allowable stresses. Many weld details have fatigue strengths at 10^8 cycles that are so low as to make mean stresses insignificant. These details have high residual stresses from weld joint restraint. Mean stresses become significant in welded bridges with structural details that have low fatigue strengths where live load stresses are typically 5-6 ksi (35-41 MPa) or less, but the bridges carry substantial dead loads and occasionally permit large overloads.

For example, assume a bridge with a large, unradiused gusset attachment to a plate girder with a fatigue strength of 5 ksi (34 MPa) is subjected to a stress range of 4 ksi (28 MPa) with legal loads. Also assume that the residual stress developed from deck and parapet dead loads and construction is 21 ksi (145 MPa). When combined with legal live loads, a mean stress of 23 ksi (159 MPa) results. The minimum permissible tensile strength for an ASTM A36 steel is 58 ksi (400 MPa). The safety factor for this case is $N_{safety(p)} = 1.02$.

When the safety factor N_{safety} is less than 1.00 for a welded detail, it is a danger sign of fatigue susceptibility. A calculation of safety factor $N_{safety} < 1.00$ during the design process indicates that a different detail is needed. For an existing structure with fatigue-susceptible details in place with a calculated N_{safety} factors < 1.00, inspectors should monitor those particular details more frequently.

REDUCING STRESSES BY DESIGN AND MATERIAL MODIFICATIONS

Bridges with steel girders and diaphragms sustain considerable residual stresses during construction. As documented by this investigation of various bridges, measurable strains were generated during the erection, bolting and fit-up of the steel girders and diaphragms. Construction of the bridge deck and safety parapets added even greater stresses to the diaphragms. In some cases, the stresses were compressive, and in others, tensile. The stress patterns were generally indicative of normal loadings, but also reflected evidence of twist and distortion in the various members. Fit-up stresses are largely caused by liberal construction tolerances. Peak tensile and compressive stresses ranged from 14 to 21 ksi (95 to 145 MPa) after the bridges were finally completed. The stresses found in this investigation were in consonance with similar investigations conducted by the Minnesota DOT [Ref 9] for curved bridges, and the New Mexico State Highway DOT [Ref 10] for intermediate diaphragms.

The dead load stresses of 15 ksi (100 MPa) and beyond are significantly greater than the 4-6 ksi (28-41 MPa) live load stresses that result from legal truck loadings. However, if permit loads above the 80,000 lb limit are considered, stresses can ratchet up to 12 ksi (83 MPa) or more for steel girders. The combination of live and dead loads can raise stresses to range from 23 to 33 ksi (160 to 225 MPa). If ASTM A36 steel is used for the girders and diaphragms, a stress of 33 ksi (225 MPa) would nearly exceed its minimum yield strength of 36 ksi (250 MPa). Nominal stresses at this level can result in localized yielding or pop-in cracks if a high stress-concentration zone is present. Stress concentrations in welded construction are typically caused by sharp changes in cross section or slope originating from improper design, and are compounded by welding or material defects. Weld discontinuities or design account for the majority of crack initiation sites in these connections.

The magnitudes of built-in residual stresses resulting during construction were described in previous chapters. This chapter describes the sources of construction strain and methods to reduce those stresses by better designs and material modifications.

Sources of Strain in Bridge Connections

There are multiple sources of strain in bridge connections. First, there are strains caused by loose fit-up caused by liberal tolerances, omission of tolerances, or by actual lack of known tolerances. Second, there are strains resulting from self-loading of the steel during construction, and from dead loads from deck and parapet placement. Third, there are strains

originating from concrete shrinkage. Strains from concrete shrinkage are relatively minor because the deck concrete cracks before significant strains are transferred to the steel superstructure. Fourth, significant strain results from thermal effects on the structure, such as direct solar heat, precipitation, localized freezing, or other atmospheric variations. Fifth, there are strains resulting from live load truck traffic. Studies by the University of Tennessee [Ref 11] have shown that strains in secondary members are further magnified by impact factors of 1.2 to 1.6, with magnitude depending on the speed of the truck and the location of the member.

Bridges are constructed with steel girders and diaphragms that have wide tolerances for shape, twist, and straightness. In some cases, plans have nominal dimensions stated without any indication of code or specification tolerances. Where no tolerances are directly stated or specified, selection of a tolerance can become a matter of discretion to the contractor or the inspector. Welding and fabrication tolerances are intended to be quite liberal in order to minimize fabrication and construction costs.

Rolled sections, plate girders and diaphragms all have wide tolerances that include inherent twist, camber and distortion. These deviations come from the manufacturing processes associated with plates and structural shapes. Additional deviations occur during fabrication and welding. The general production tolerances for plate and structural shapes, such as angles, channels and tees, are summarized in ***Table 13.***

In addition to the general manufacturing tolerances for structural products supplied to the fabricator, the *AWS Bridge Welding Code* also provides liberal tolerances for fabrication and fit-up of welded construction, as summarized in ***Table 14.***

As noted in both ***Table 13*** and ***Table 14***, the number of dimensional categories with wide permissible tolerances is substantial. These wide tolerances can induce high localized strains due to poor fit-up, gaps, and prying action when bolt preloads are applied. When diaphragms are bolted to webs or stiffeners, they are fastened to structural elements or components which are often not straight, or may be twisted or wavy, or that the adjacent girders are not perfectly flat, nor are they in true alignment. As noted by some of the strain gage readings in this investigation, one part of the flange may be in compression, while the other is in tension. Opposing strains can be caused by the lack of flatness or straightness either in the web or the bolted flange of the diaphragm. Rigid diaphragms bolted to stiffeners exhibiting out-of-straightness can induce stresses in the stiffener welds. Moreover, most welds in bridges, including plate girders, stiffeners and diaphragms, are not thermally stress-relieved, resulting

in high residual stresses upon cooling. These residual stresses in welded areas are typically near the yield strength.

A combined state of residual and live-load stresses exists in bridge components. The origins of these stresses are: (1) misfit of components resulting from wide tolerance limits; (2) residual stresses from fabrication, particularly from welding; (3) load sharing and out-of-plane bending caused by wheel loadings of trucks, especially trucks with gross weights above the legal limit of 80,000 lbs; and (4) residual effects of localized yielding. All of these stresses are contributors to crack formation; however, overloads by heavy trucks are typically the cause or trigger stress for crack initiation.

These distortions in service were so prominent in stiffener web-gaps that it prompted the Iowa DOT to recommend that diaphragm bolts be loosened to reduce the residual strains after the bridge was completed [Ref 12].

Table 13

Plate and Structural Shape Tolerances per ASTM A6

Type of Tolerance	*Table in A6*	*Tolerance Specification*
flatness for plates	13	for 1/4" to 3/8" plates, flatness varies from 1/2" to 1-5/8", depending on depth; *approximate formulas:* for carbon steels, flatness ≅ 0.013W for low alloy steels, flatness ≅ 0.020W
waviness	15	depends on flatness, width of plate, number of waves in 12' of length, and can vary from 1/16" to 1-1/2"
flange out-of-square	16,17,18	(a) for wide flanges and H-piles, 1/4" to 5/16"; (b) for various channels & tees, 1/32" max (c) for various angles, 1-1/2° max
straightness (s_t)	21	for S, M beams, channels, angles, tees and zees: under 3", s_t = 0.05 x [L], where L= length in ft over 3", s_t = 0.25 x [L]
camber and sweep	24	for W and HP shapes: (a) for flange widths < 6", camber & sweep = 0.025 x [L] where L = ft; (b) for flanges 6" or above, camber & sweep = 0.013 x [L]

Table 14

AWS/AASHTO Bridge Welding Code Tolerances

Category	*Section*	*Tolerance Specification*
weld alignment	3.3.3	groove welds permitted 1/8" (3 mm) longitudinal or vertical misalignment root openings ±1/16 (±1.6 mm) groove of joint angle +10°/-5°
web center line	3.5.1.8	depth from center line can vary from ±1/8" to ±5/16" (3-8 mm), depending on web depth
stiffeners	3.5.1.11, 3.5.1.12	out-of-straightness with stiffeners can vary from 1/4"-1/2" (6-13 mm), depending on web depth; intermediate stiffeners, 0.5" max; bearing stiffeners , 0.25" max
bearing joints	3.3.2.2	varies per special provisions if specified

straightness deviations (S_t)	3.5.1.1	typically varies from 1/8" to 1" depending on length, L, in ft:
		up to 30', S_t = 0.0125 [L];
		from 30' to 45', S_t = 0.375" max;
		for L > 45', S_t = 0.375 + 0.125 [(L-45)/10]

camber	3.5.1.3 (per Table 3.2)	for typical girder where: L ≥ 100 ft, C = 9/16""-1.5", depending on support distance; L < 100 ft, C = 1/4" -3/4" (see Table 3.2)
sweep variations	3.5.1.4	sweep = 0.0125 [L], where L is in ft, sweep is in inches
warpage or tilt-of-flange	3.5.1.7	0.25" or warpage = W/100, where W = flange width in inches, whichever is greater
joints & splice offset	3.5.1.14; 3.5.1.15	for main load-carrying members, 1/16" max offset, including filler plates; for secondary members, 1/8" max
flatness of webs	9.19.2	(a) intermediate stiffeners on both sides: varies from d/92 to d/130, where d = least panel dimension, in inches, which depends on D/t, where D = depth of web, inches and t = thickness, inches; (b) intermediate stiffeners on one side: varies from d/67 to d/120; (c) no stiffeners, D/150 = max.

Use of Non-Ferrous Materials to Accommodate Strain

There are several non-ferrous materials which could accommodate the strains induced by the bolting of steel components with poor fit-up or misalignment. These materials include metals, such as aluminum, zinc, and magnesium alloys; and plastics, such as nylon, polyvinyl chloride (PVC), and synthetic rubber. Common thermoplastics were not included in this study because of their sensitivity to ultraviolet (UV) radiation. When diaphragms and stiffeners are modified with slotted holes and other minor design changes, non-ferrous metals can moderate the residual and live load stresses associated with steel because of their lesser moduli of elasticity which attenuates the effects of strain. Since the typical modulus of elasticity for these materials is 1/3 of steel or less, stresses are reduced by 2/3 or more, depending on the material selected. Instead of use of rigid steel members and connections, non-ferrous alloys accommodate strain by increased elastic deformation.

a. Aluminum, zinc and magnesium alloys.

The modulus of elasticity (E) for aluminum and zinc is approximately 33% of steel, whereas E for magnesium alloys is only about 22% of steel. A strain which could be significantly damaging to steel could be a safe level within the elastic range for many commercial aluminum, zinc or magnesium alloys. Synthetic rubber, on the other hand, has such a low modulus that it essentially has no elastic behavior compared to steel. The modulus of elasticity for neoprene is approximately 700 to 1,000 psi (4.8 to 6.9 MPa), compared to 30,000,000 psi (206,700 MPa) for steel. A comparison of the engineering stress-strain characteristics of various metals is shown in ***Figure 34.***

The nominal peak *strains* read by the strain gages at various points on the steel diaphragms in this study ranged from 500 microstrain ($\mu\varepsilon$) to 700 $\mu\varepsilon$. The *stresses* generated when different alloys sustain elastic strain deformation at 100 $\mu\varepsilon$ and 700 $\mu\varepsilon$ are presented for comparison in ***Table 15.***

As shown in ***Table 15,*** a strain of 700 $\mu\varepsilon$ would result in a stress of 7,210 psi in aluminum, compared to a stress of 21,000 psi in structural steel. Non-ferrous materials can better accommodate localized strain because of their lower moduli of elasticity. A concrete deck has a much lower modulus of elasticity than the more rigid supporting steel girders. A non-ferrous diaphragm should assume a more forgiving behavior that is more in consonance with the elastic deflection characteristics of the rebar-concrete deck.

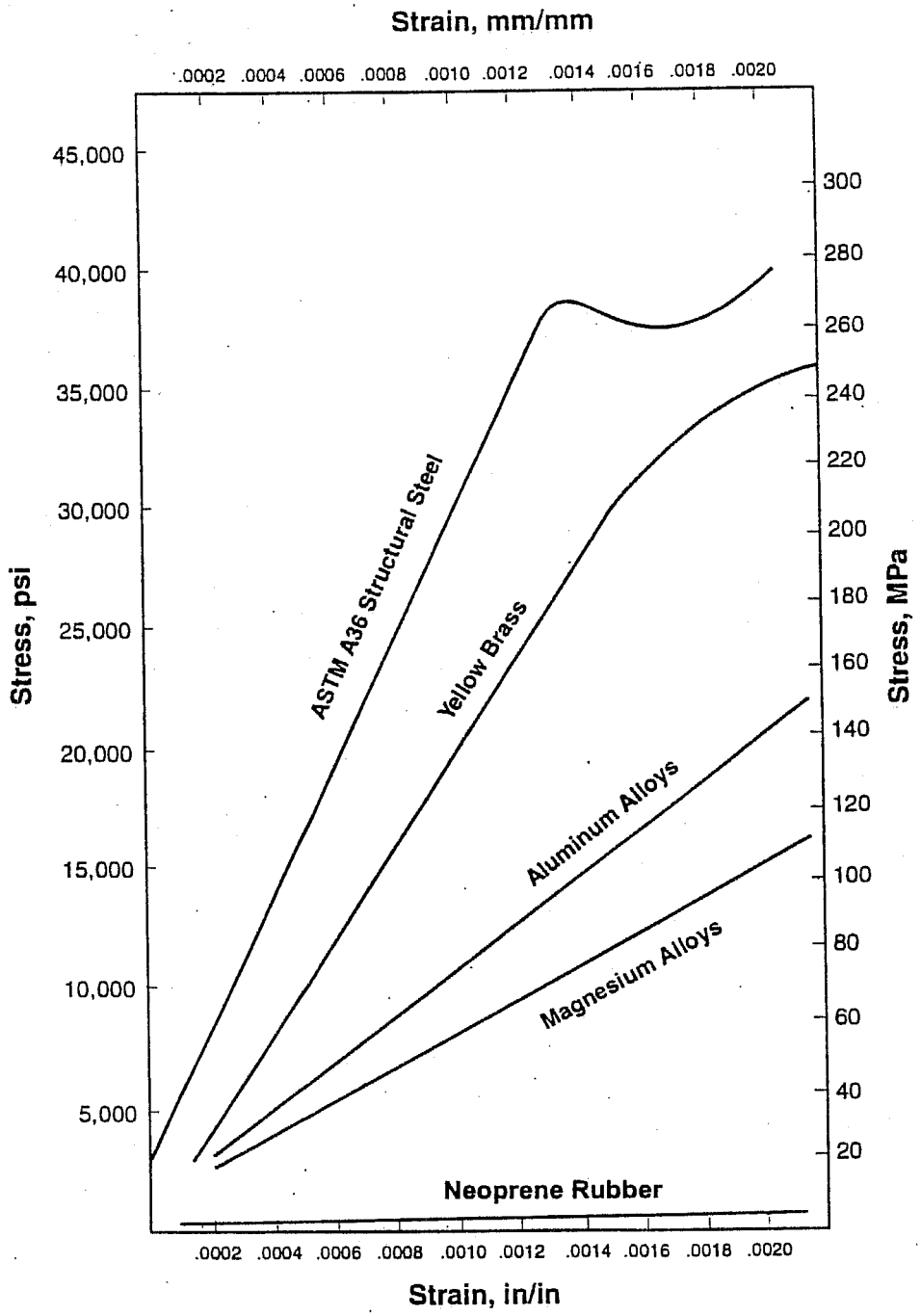

Figure 34. The comparison of the engineering stress-strain curves for ASTM A36 structural steel; ASTM B36 Alloy 260 yellow brass; ASTM B209 6061-T6 aluminum alloy; ASTM B90 AZ31B magnesium alloy; neoprene rubber. Strain values are taken out to 2200 microstrain, at which the aluminum and magnesium alloys are still behaving elastically. Neoprene rubber has such a low modulus of elasticity that the strain absorbed results in virtually negligible stress.

Table 15

Stresses Resulting from Strain in Various Materials

Material	*100 micro strain (με)*		*700 micro strain (με)*	
ASTM A36 steel	3,000 psi	20.7 MPa	21,000 psi	144.7 MPa
6061-T6 aluminum	1,030	7.1	7,210	49.7
AZ31B magnesium	650	4.5	4,550	31.3
Zn-22Al zinc	1,200	8.3	8,400	57.9

Compared with steel at the same strain level, the resulting stresses in aluminum or zinc alloys are lower. Generally their fatigue lives are also improved. Several aluminum and zinc alloys have fatigue strengths approaching those of common structural steels, such as 5083-H321 aluminum. They can accommodate almost three times the amount of strain compared to steel without yielding. The fatigue strengths of commercial aluminum, zinc and magnesium alloys are summarized and compared with those of ASTM A36 steel in ***Table 16.***

Another advantage enjoyed by aluminum and zinc alloys is their atmospheric corrosion resistance. Both aluminum and zinc alloys require no special coatings like steel does for corrosion protection. Aluminum can be anodized and decorated with many colors, or it can be clad with high purity aluminum to improve its corrosion resistance and brighten its anodizing.

Many zinc alloys have good resistance to atmospheric corrosion due to the formation of stable oxides and carbonates on the surface of the metal which form after prolonged exposure. Magnesium alloys, however, must be galvanically isolated from structural steel. The only drawback to use of certain aluminum, zinc and magnesium alloys is their impact toughness. Any non-ferrous alloys selected must have a minimum V-notch impact toughness of 15 ft-lbs at 40°F (20 J at 4°C), which eliminates most commercial magnesium and zinc alloys.

Table 16

Fatigue Strength of Various Materials in Rotating Bending[A]

Alloy Number	*Tensile Strength, ksi*	*Tensile Strength, MPa*	*Fatigue Strength, ksi*	*Fatigue Strength, MPa*
A36 steel	58 min	400	24	165
A588 steel (unpainted)[B]	70	480	16	110
5052-H32 aluminum	31	210	17	120
5083-H321 aluminum	44	300	23	160
6061-T6 aluminum	38	260	14	100
6063-T51 aluminum	35	240	10	70
Zn-22Al zinc[C]	35	240	12	85
AZ31B magnesium	37	255	10	70

Note: Original data was in ksi, and is rounded to nearest ±5 MPa. Fatigue and property data have sufficient variation to permit such rounding. Data sources: ASM Metals Handbook, Vol 2, *Non-Ferrous Alloys and Special Purpose Materials*, 10th Edition, ASM International, Metals Park, OH, 1990; *AWS Structural Welding Code--Steel,* American Welding Society, Miami, FL, 1984.

[A]Solid machined bars were subjected to pure bending and simultaneously rotated.
[B]Beams were subjected to pure bending, with no rotation.
[C]Estimated fatigue strength, based on testing of other zinc-aluminum alloys.

b. Synthetic rubber.

Both natural and synthetic rubber have very low moduli of elasticity in compression, and have an even lower moduli in shear. In addition, the amount of expansion that rubber undergoes in the lateral direction is 67% greater than steel or aluminum. The ratio of compression-to-expansion (transverse to longitudinal strain) is designated as Poisson's ratio:

$$\nu = \frac{\frac{b_f}{b_o} - 1}{\frac{L_o - L_f}{L_o}} \qquad \text{[Equation 11]}$$

where ν = Poisson's ratio

b_f = transverse width after deformation

b_o = transverse width before deformation

L_o = original length

L_f = final length after compression

Rubber has a Poisson's ratio of 0.5, compared to 0.30 for steel. Rubber has the ability to significantly expand during its compression. Coupled with its low modulus of elasticity, rubber can also absorb tremendous amounts of strain compared to steel. These properties can be significantly useful if rubber is properly applied in confined areas, and in connections where localized strain is a problem.

The mechanical properties of rubber are compared with other ferrous and non-ferrous materials in ***Table 17.*** Although rubber has a low tensile strength, it has tremendous expansion capabilities to highly localize and attenuate strain without generating stress concentrations. Rubber exhibits an elastic behavior under load that is several orders-of-magnitude greater than very stiff materials like steel or brass, which exhibit yielding if subjected to small deformations.

Table 17

Mechanical Properties of Various Ferrous and Non-Ferrous Materials

Non-ferrous material	*Tensile strength, psi*	*Yield strength, psi*	*Percent elongation*	*Modulus of elasticity, psi*	*Poisson's ratio*
ASTM A36 steel	58,000	36,000	23	30,000,000	0.30
ASTM A572 steel	65,000	50,000	18	30,000,000	0.30
6061-T6 heat treated aluminum	45,000	40,000	17	10,300,000	0.33
vulcanized rubber, firm (70H)	4,000	not measured	450	500 (tension) 700-1200 (compression)	0.50
Zn-22Al zinc	50,000	37,000	25	9,900,000	0.3*
AZ31B magnesium, annealed	37,000	22,000	21	6,500,000	0.35

Data sources: *Rubber and Rubber-like Materials,* MIL-HDBK-149A, Dept of Defense, 30 Jun 1965; ASM Handbook, Volume 2, *Non-Ferrous Alloys and Special Purpose Materials*, 10th Edition, 1990; ASTM Standards, Vol.1.04, *Steel, Structural, et. al.,* 1997.
*Estimated.

Design Modifications

a. Diaphragms

Changing the structural steel to a non-ferrous material is not the only modification available. The basic geometry of the diaphragm can also be modified to permit greater flexure and twist without concentrating stresses in the various connections and components. Concentrated stresses in stiffeners, welds, girders, bracings or chords can initiate cracks after repeated applications of cyclic strain.

The diaphragm of ***Figure 4,*** used in the grade separation carrying County Highway 14 over I-39 at Wenona, and the diaphragm of ***Figure 19,*** used in the US 52 Bridge over the DuPage River near Joliet, are both rigid designs. If the diaphragm is removed after the deck has properly cured to eliminate the residual stresses of construction, internal girders can excessively deflect under load, as reported by Canham of Syracuse University [Ref 13]. However, a rigid diaphragm design can be improved by modifying its geometry and changing material to permit greater bending and torsion to lessen the effects of stress concentrations without sacrificing its load-sharing capability.

The angles on the ends of the diaphragm of ***Figures 4 and 19*** cause unnecessary rigidity, reducing flexibility of the diaphragm after bolting it into place. Residual strain can be introduced to the diaphragm and stiffener during assembly when the girder is deflected or forced into place to conform to the dimensions of the diaphragm. Because the diaphragm is a wide flange with rigid ends, considerable end strain is induced at the connection point after bolt tightening.

b. Sources of strain in construction

There are several sources of strain in existing diaphragm designs which come into play during fit-up, including:

(a) differences in beam elevation, caused by girder deflection and camber, resulting in a slight misalignment of bolt holes;

(b) difference in positions of bolt holes, whether drilled or punched into the girder web, or attached to a welded stiffener or angle;

(c) end-attachment stiffness, caused by rigidly welded angles or welded plate attachments which do not permit any flexure, and concentrate strains in the corners, at sharp transitions, or in bolt holes.

Many of the sources of strain can be diagramatically shown by reference to ***Figure 35.*** Here the X, Y and Z axes of the diaphragm and girder connection are laid out, in addition to displacements of the adjacent girder(s). Camber, straightness and moments applied during girder flexure or deflections are also shown.

The lack of flexibility of diaphragms to permit adjustment during fit-up and final bolt tightening can be reduced by use of a new diaphragm design described in ***Figure 36.*** In ***Figure 36,*** the slotted holes on both the diaphragm and the stiffener permit easy fit-up, even if there is a significant difference in elevation between one girder and another girder. The diaphragm is also flexible in the Z-direction or longitudinal axis of the bridge. Flexibility is permitted by use of a gap D_1 between the aluminum angles which are bolted to the aluminum web plate of the diaphragm. Optional vertical stiffeners can be added to the diaphragm if the girders they attach to are particularly deep. Otherwise, the diaphragm has sufficient rigidity, and should accommodate the strains associated with steel diaphragms in the X, Y and Z directions.

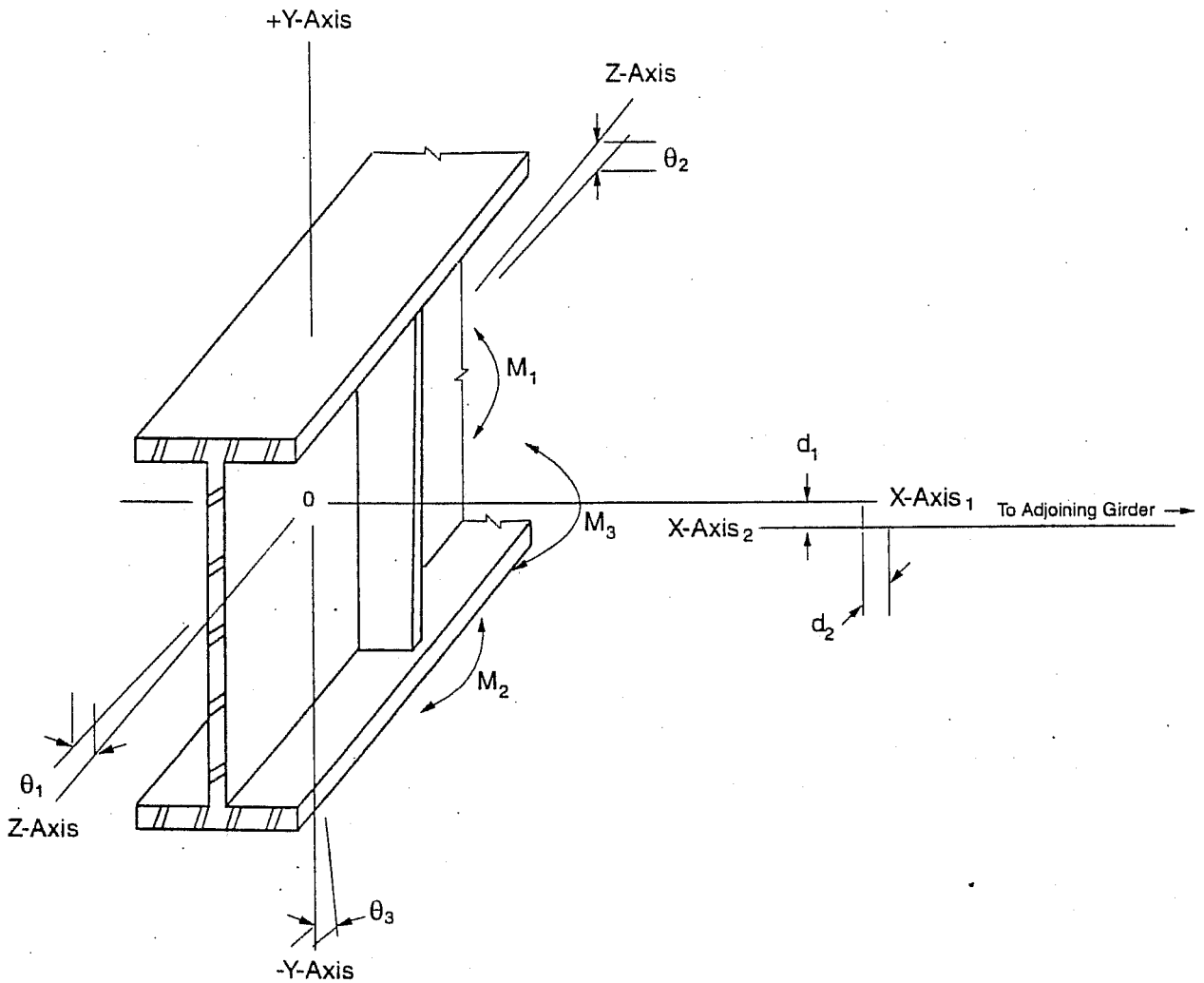

igure 35. The various axes and deviations from true alignment of a girder element. Built-in esidual stresses result from (a) welding, (b) misfit during assembly, (c) dead load deflections om deck and parapet concrete and rebar weight, and (d) overload moments applied about the -axis and Y-axis from wheel loads from trucks, resulting in yielding.

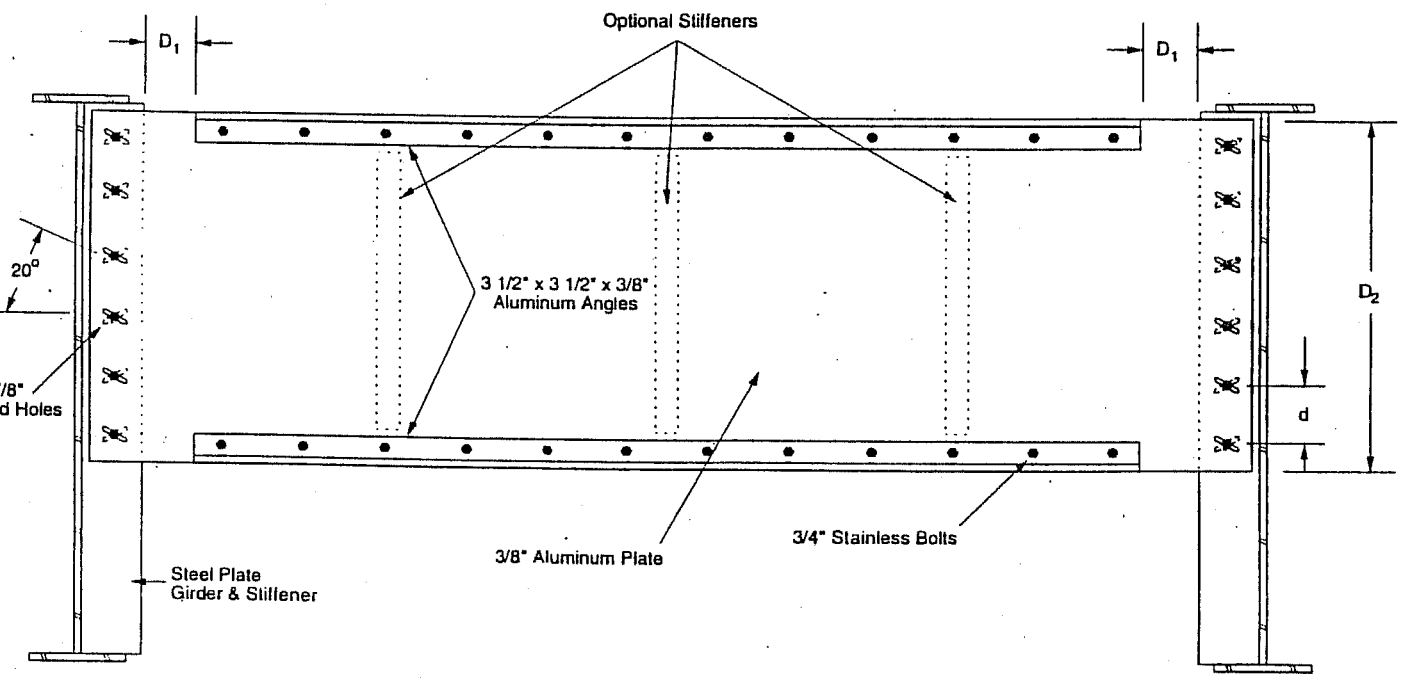

Figure 36. A diaphragm design which permits displacement in the X, Y and Z directions. The slotted holes in both the stiffeners and diaphragm web accommodate elevation differences between girders. The diaphragm has flexibility because of the lower modulus of aluminum, yet sufficient rigidity to act as a connector during assembly and afterwards in service. Bolt spacing *d* is typically 4" - 5" (10 - 13 cm) between centers.

c. Stiffener connections.

Compared to bolting a stiffener angle to the girder, welding stiffeners to girders is efficient from a fabrication and labor standpoint, particularly if automatic dual electrode flux core or submerged arc welding is employed. However, if the end of a welded stiffener is subject to considerable localized strains, this can lead to cracking, which can extend into the main load-carrying girder.

Keating [Ref 14] has proposed to eliminate this problem by welding stiffeners to a base plate bolted to the lower flange. His proposal is shown in ***Figure 37***, and imposes only minor costs of drilling and welding. An alternate method is to use a stiffener angle bolted to the web with holes drilled by precision fixtures. A copper-composite gasketing material or metal powder-filled epoxy filling irregularities between the web and stiffener angle would decrease localized bolting stresses.

d. X-web and K-web braces.

The X-shaped and K-shaped braces have been used as semi-rigid diaphragms in deep-girder bridges for many years. Their advantage is that they have limited stiffness in the Z-axis (longitudinal) of the bridge, and generally accommodate the displacement of the stiffeners along the Z-axis. They have lesser accommodation of differences in elevation of the girders or bolt hole locations in the stiffeners. Frequently they are forced into position with drift pins, or the holes are expanded by the use of reamers to accept out-of-position bolts.

A commonly used X-shaped brace diaphragm is shown in ***Figure 38***. Here equal-leg angles form an X-shaped cross, which is attached to stiffeners by bolting 3/8" or 10 mm plate gussets. Although this diaphragm is economically welded and is an efficient use of material, the welded connection between the 3.5" x 3.5" angle and the gusset plate has low fatigue strength in tension. Munse *et al* at the University of Illinois [Ref 15] found that this connection in direct axial tension has a fatigue strength of 4.4 ksi (30 MPa) at 10^8 cycles. This same connection is rated by the AWS *Structural Welding Code D1.1* as 5 ksi for redundant structures. Fortunately, this connection has a fatigue strength in bending of 13.1 ksi (90 MPa) at 10^8 cycles per Munse *et al* [Ref 15]. In an actual bridge however, tension and bending stresses may be simultaneously exerted on this connection.

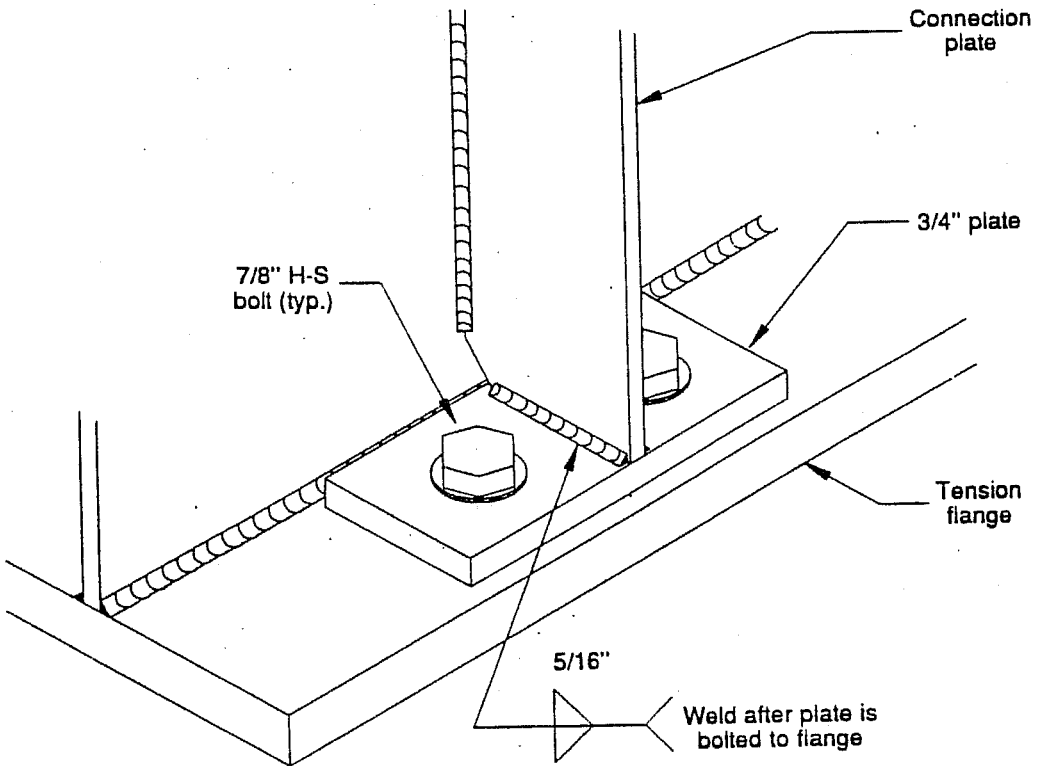

Figure 37. Bolted base plate design of Keating [Ref 14] which addresses the sharp notch problem at the end of a stiffener. The stiffener connection plate shares its moment application by transferring forces via shear to a bolted base plate, rather than by prying action on the stiffener. Data source: ASCE, *Civil Engineering,* November 1994.

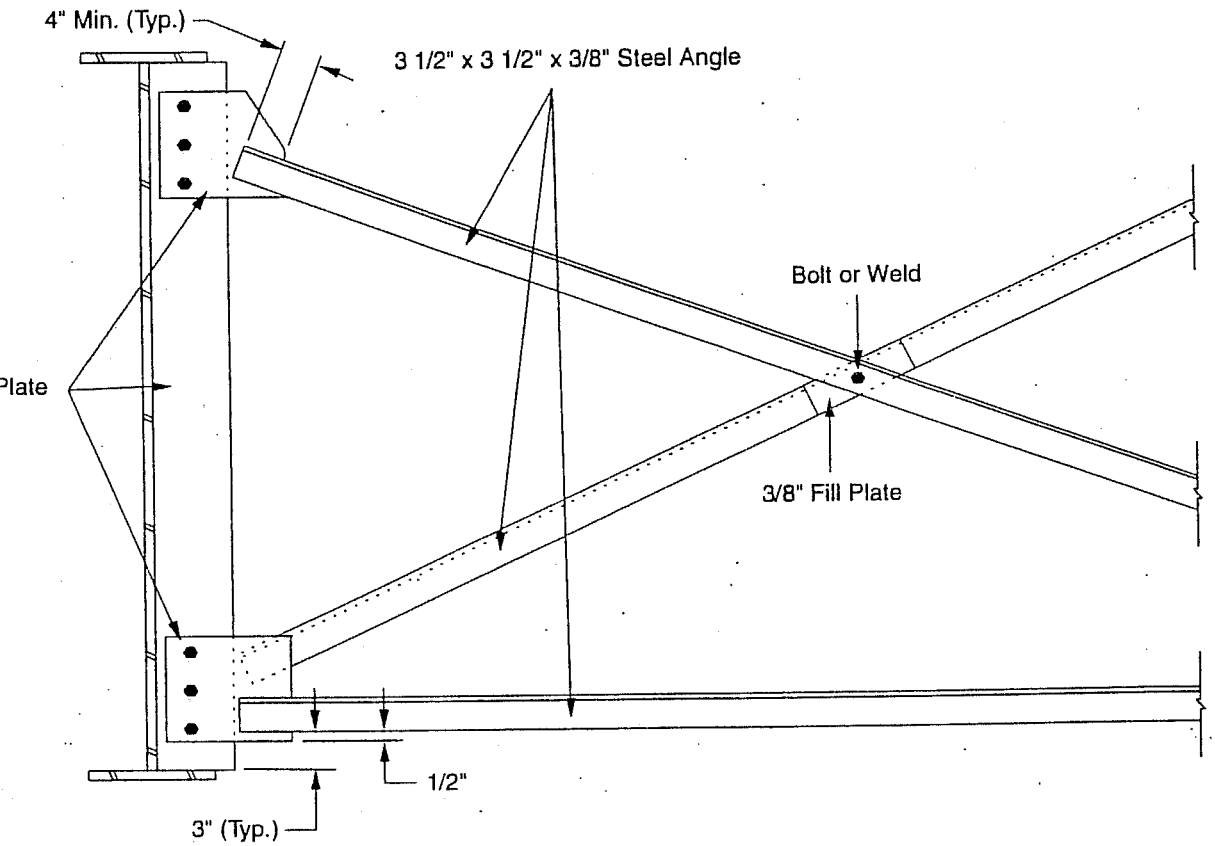

gure 38. Typical semi-rigid X-brace steel diaphragm used in deep girder bridges, with achments points at the most vulnerable locations of the stiffener. Other problematic areas e the fillet-weld attachments to the gussets. These weld joints in tension have some of the west fatigue strengths, and are rated as Category E by the AWS *Structural Welding Code .1.* Diaphragm has the advantage of being flexible in the Z-direction. Data source: AISC *odern Steel Construction*, August 1997.

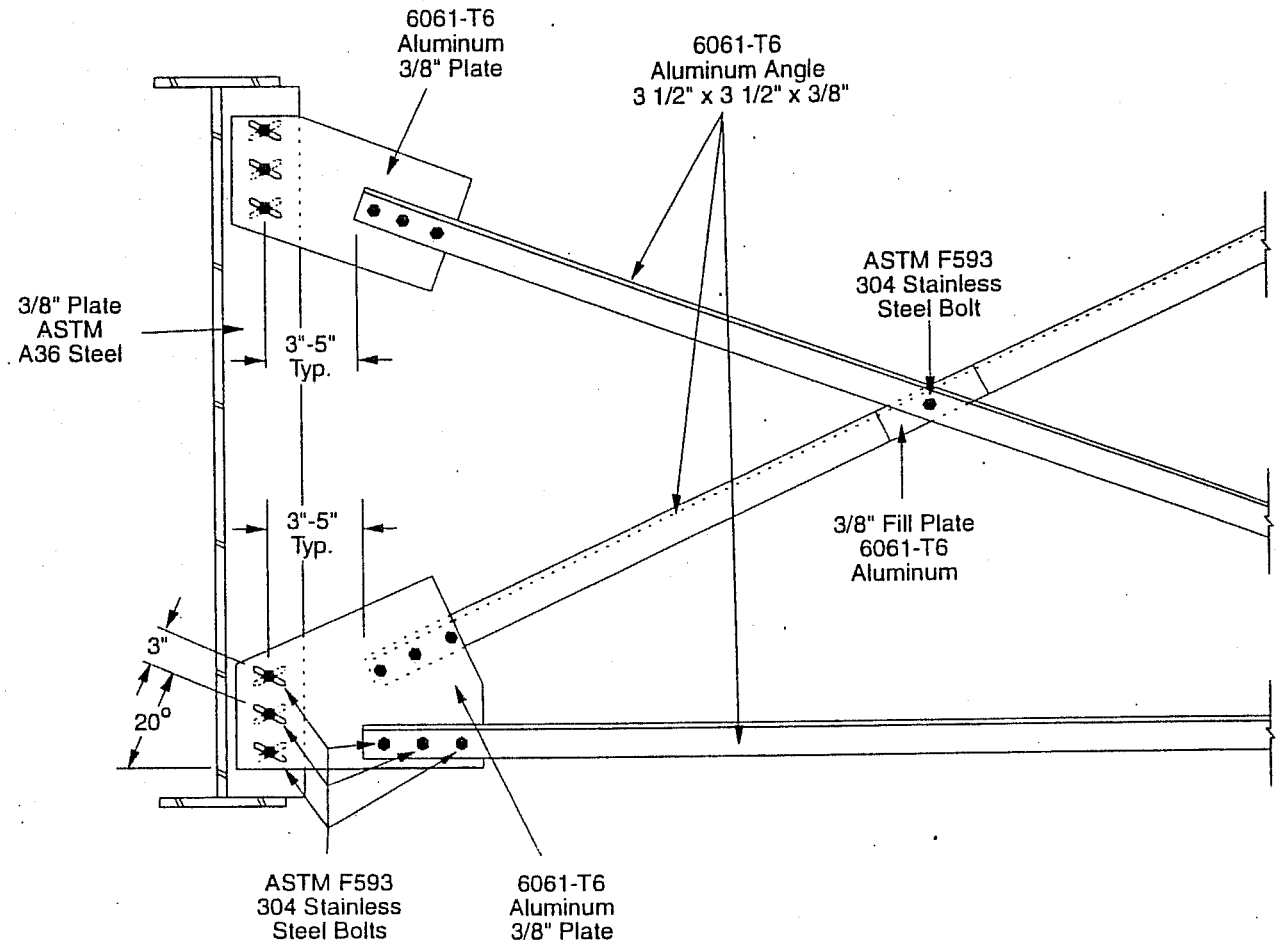

Figure 39. An X-brace diaphragm design with significantly greater flexibility due to substitution of 6061-T6 aluminum for steel, and the use of slotted holes tilted off-horizon for improved accommodation of differences in girder elevation. This diaphragm can also be adapted for retrofit of existing steel diaphragms using only aluminum gusset plates if out-of-plane bending is not severe.

The fatigue strength of a welded stiffener-to-web connection in tension can be significantly improved by bolting the connection, which raises its fatigue rating to 16 ksi (110 MPa) at 10^8 cycles. The rigidity of this connection can be diminished by replacing the steel gusset with 6061-T6 or other aluminum alloy plates, as shown in ***Figure 39.***

Stainless steel bolts are used in this new diaphragm to minimize galvanic corrosion. The tilted slotted holes virtually negate the effects of any minor geometric distortion of the X-brace, or any small differences in elevation between adjoining girders. Moreover, the aluminum angle eliminates the need for painting. Aluminum angles are widely available in either 6061-T6 (higher fatigue strength) or 6063-T52 (higher corrosion resistance) aluminum alloys.

In order to retrofit an existing X-brace or K-brace diaphragm where severe distortion is involved, two alternate splice connectors using neoprene rubber for strain relief are proposed. Installation of these strain-relief connectors is shown in ***Figure 40.*** The existing steel is cut at X-cross angles and chords near the gussets, and the strain-relief connectors are bolted into place.

In the slotted splice connector of ***Figure 41***, the neoprene rubber sustains shear strain during deformation. Bolts are tightened sufficiently to provide a semi-rigid connection, which permits the splice to accept both high shear strain and bending. As shown in ***Figure 42***, the shear modulus of rubber is very low compared to steel. The modes of deformation that the splice can handle include torsion, compression, tilt and axial shear, as shown in ***Figure 43.***

An alternate connector, using welding and bolting, is shown in ***Figure 44***. Although such a connection in welded steel construction would have a low fatigue strength, stress concentrations are mitigated by the non-rigid neoprene rubber which has a modulus of elasticity of 500 - 700 psi (3.4 - 4.8 MPa), compared to 30,000,000 psi (206 GPa) for steel. The splice is able to sustain high strains under which a comparable steel connection would either severely bend or rupture by fatigue action. The resistance of neoprene, silicone, or fluorocarbon synthetic rubbers to oils and ozone is well documented [Ref 16]. The connectors are situated below the bridge deck, and the rubber is covered by steel plates. The rubber is generally shielded from direct sunlight, and is not subject to continuous exposure of high surface temperatures and degrading ultraviolet (UV) and infrared (IR) radiation.

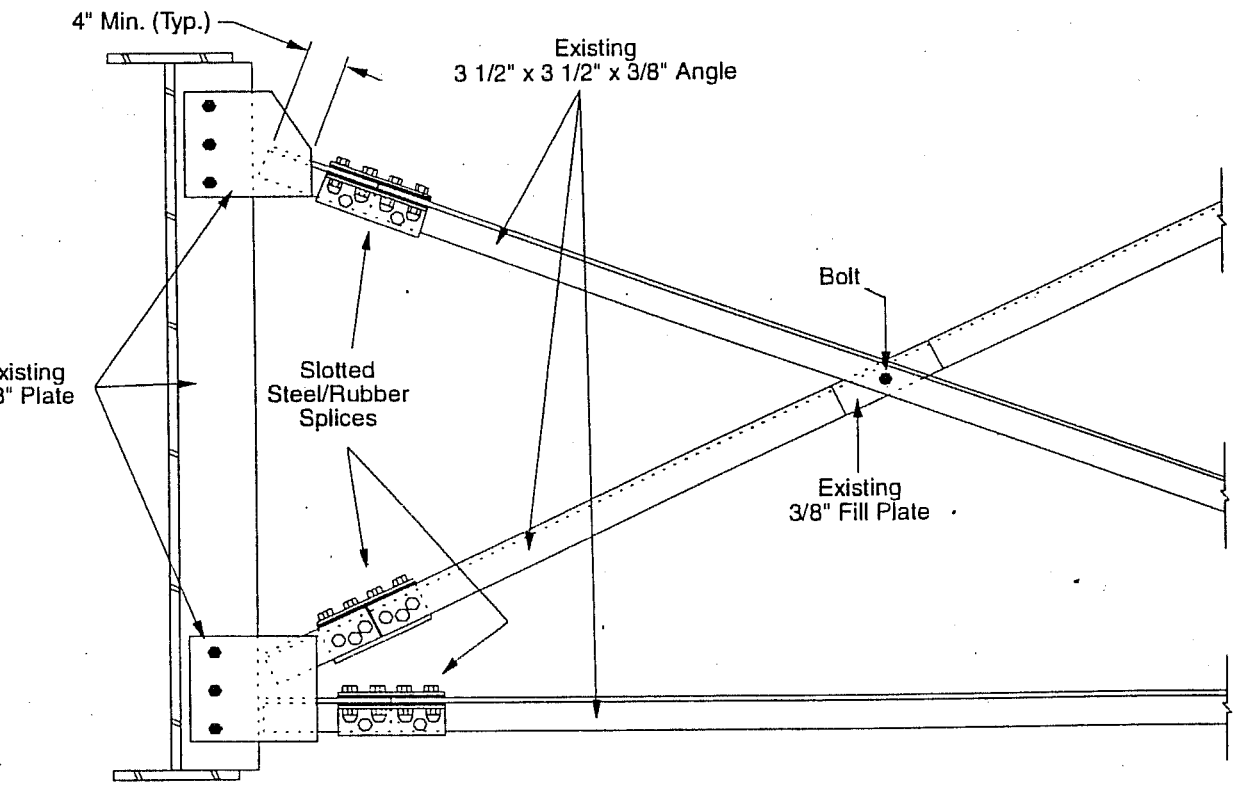

Figure 40. Installation of slotted steel-rubber splice plates for relief of severe strain. These solation devices can absorb high strains without significant effect on stress levels in the rubber solators.

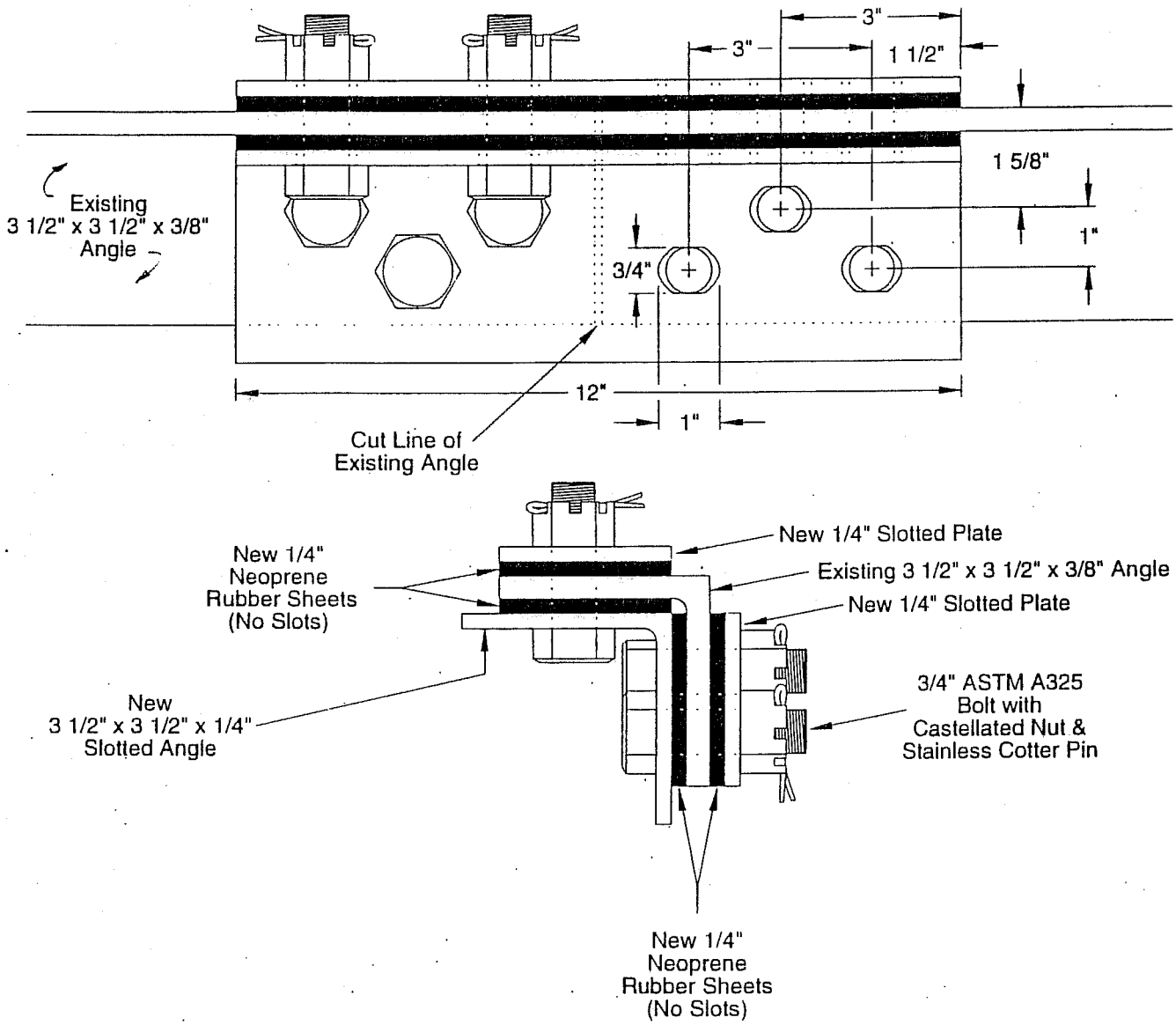

Figure 41. Detail of slotted steel-rubber sandwich splice connector, showing top and cross-sectional views. The rubber sheets are not slotted to absorb strain.

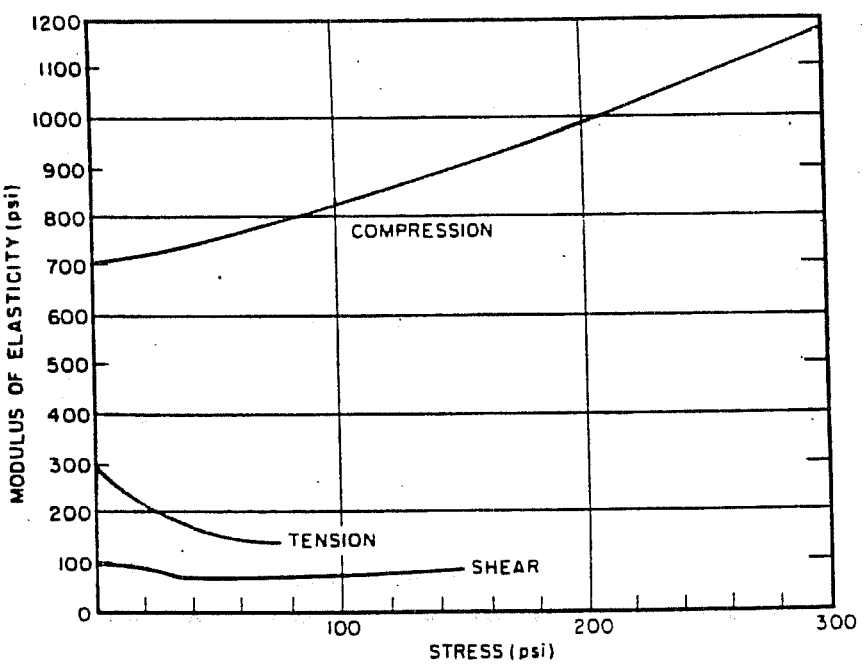

Figure 42. The relationship between modulus of elasticity in psi vs. stress in psi for rubber in compression, tension and shear. Note the very low modulus in shear, which is how the splice connector can absorb such a marked amount of strain. Data source: MIL-HDBK-149A, *Rubber and Rubber-like Materials*, Dept of Defense, 1965.

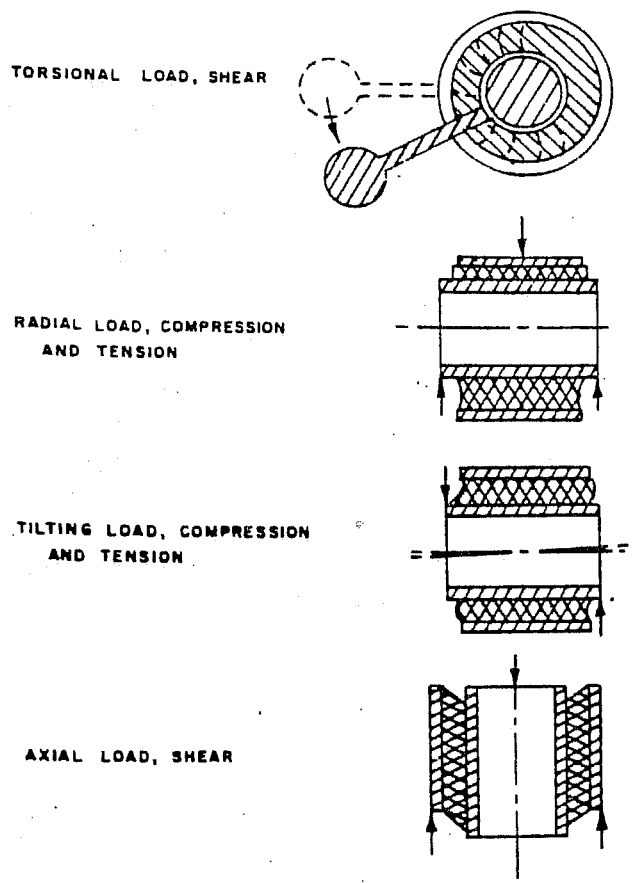

Figure 43. Diagrams showing the ability of rubber confined by steel sandwich plates to accept strain in torsional, radial compression and tension, tilting, and axial shear modes. Data source: MIL-HDBK-149A, *Rubber and Rubber-like Materials*, Dept of Defense, 1965.

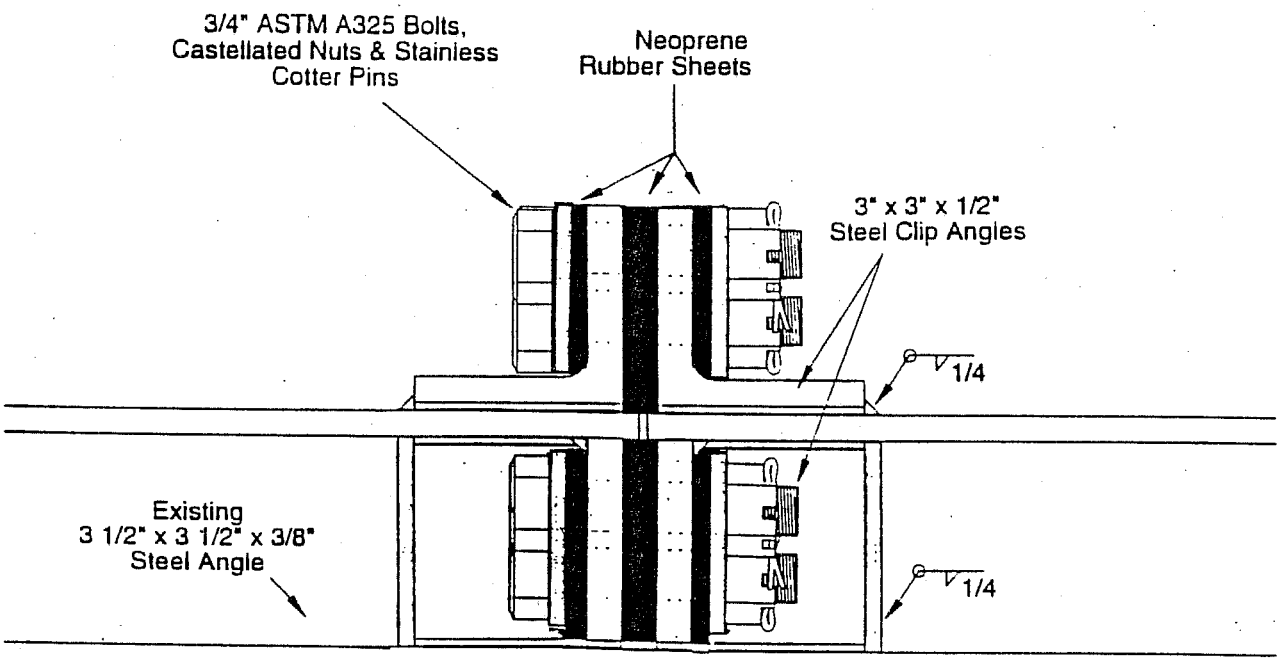

Figure 44. Alternate rubber sandwich connector, using clip angles and small plates. Clip angles may be bolted or welded onto the existing X-brace or lower chord angles of the existing steel diaphragm.

d. Safety factors for bridges with residual stresses.

e anticipated safety factors for these new designs can be compared with the maximum rmissible stress ranges associated with the same welded or bolted connections in existing el bridges. Alternating stresses in steel connections are limited to 5 ksi per AASHTO; wever, the diagonals may experience considerably higher stresses during live and dead ds. Average maximum live load stress as measured by strain gages mounted on 15 urban, burban and rural bridges in Illinois was 5.5 ksi (38 MPa) for legal loads, and 10 to 12 ksi (69 83 MPa) for permit loads, per work of Hahin and South [Ref 4]. The Minnesota DOT and the iversity of Minnesota completed a very comprehensive study of construction and live load esses in curved steel bridges [Ref 6]. Typical stresses in cross-frame diagonals were 4 to 6 (28 to 41 MPa), with peak stresses reaching 12 ksi (83 MPa). Stresses in curved bridges re slightly greater than stresses in bridges without curvature or skew. Peak strains proached 600 με to 700 με in this investigation of rigid diaphragms in Illinois bridges. This ain range translates to stresses of 18 to 21 ksi (124 to 145 MPa) in steel. These were the al stresses which resulted after the New Jersey-style parapets were constructed.

Strains at the 700 με level in aluminum, however, would only result in a stress of proximately 7 ksi (48 MPa). Alternating stresses for aluminum cross frames are estimated at ksi (21-28 MPa). These reductions in stress are due to the modulus of elasticity of minum, which is only 1/3 of the elastic modulus of steel.

The Gerber parabolic equation is the most accurate relationship for the calculation of ety factor in fatigue, and is described in [Equation 9]. Using the high cycle (10^8) fatigue ngth for 6061-T6, a reliable safety factor can be calculated for typical conditions of dead d and live load stresses in bridges. The short-form Gerber parabolic equation for safety tor adapted to bridges and its pertinent variables are:

$$N_{safety(p)} = \frac{1}{\frac{S_{LL}}{Fd} + \frac{[(S_{LL} + 2S_{DL})/2]^2}{(S_u)^2}} \qquad \text{[Equation 10]}$$

re $N_{safety(p)}$ = parabolic safety factor, which must be > 1.0, and is typically 1.5-1.8

S_{LL}/F_S = ratio of alternating or live load stresses to fatigue strength

$[(S_{LL} + 2S_{DL})/2]/S_u$ = ratio of mean stresses to tensile strength

As an example calculation, using realistic quantitites found in this and other similar investigations in the literature:

S_{LL} = live load stress range; assumed to be 12 ksi (83 MPa) for steel;
4 ksi (28 MPa) for aluminum or zinc
S_{DL} = dead load stress; assumed to be 21 ksi (145 MPa) for steel;
7 ksi (48 MPa) max for aluminum or zinc

F_S = fatigue strength at 10^8 cycles; for steel, 24 ksi (165 MPa);
for 6061-T6 aluminum, 14 ksi (96 MPa);
for Zn-22Al zinc, 12 ksi (83 MPa)

T_S = tensile strength; for steel, 58 ksi (400 MPa);
for 6061-T6 aluminum, 45 ksi (310 MPa);
for Zn-22Al, 50 ksi (345 MPa).

A steel bridge diaphragm with a 12 ksi (83 MPa) live load stress and a 21 ksi (145 MPa) dead load residual stress has a fairly low safety factor, even when the residual stresses of welding are not included. Residual stresses of welding approach the yield strength, and can be of the order of 30 - 35 ksi (207-241 MPa) in the weld toe or throat of the weld joint. Neglecting the stresses of welding and using only the dead load stresses found by strain gages alone, the safety factor for the steel bridges in this study were determined to be $N_{safety} = 1.41$.

When aluminum is substituted for steel, the strains induced are not as influential on stress because of the change in modulus of elasticity. Calculating with assigned values for aluminum to the above variables, the resulting safety factor $N_{safety} = 3.06$, which is a very wide margin of safety. For the Zn-22Al zinc alloy, $N_{safety} = 1.88$.

The more conservative Goodman safety factor equation places greater emphasis on mean stress by not squaring the mean term. Even if the linear Goodman equation is used for the 6016-T6 aluminum connection, the result is still favorable, where $N_{safety(L)} = 2.06$.

SUMMARY

The objectives of this research project were to: (a) measure strains and stresses built into bridge components during construction; (b) consider the effects of residual stresses on fatigue life; and (c) recommend various construction methods or designs which minimize the buildup of residual stresses.

Built-in stresses were measured in three different bridges: (1) a multi-girder grade separation without a center pier, where the girders are anchored at the abutments; (2) a 4-span continuous multi-girder bridge with piers; and (3) a movable, double-leaf bascule bridge.

Substantial strains are introduced into bridge griders, stiffeners and diaphragms during construction. The resulting stresses range from compression to tension, and are not easily predicted by classical stress analysis. The mean tensile strain in diaphragms was 171±192 με, and the mean compressive strain was -248 ± -191με. The highest tensile stress measured in steel diaphragms was 20.8 ksi (143 MPa).

There are multiple contributors to strain during construction. These include: (1) dead loads from deck and parapet placement; (2) shrinkage of the concrete in the deck during curing; (3) thermal variations of the atmosphere; (4) fit-up stresses, resulting from liberal tolerances for plates and structural shapes as permitted in ASTM A6, and tolerances of the AWS/AASHTO Bridge Welding Code for alignment, web centerlines, straightness deviations, camber, sweep, warpage and flatness of various fabricated structural shapes. The use of drift pins and other undocumented field modifications to force-fit structural components together are also sources of residual strain.

Several methods to attenuate built-in strain effects were proposed, including the use of non-ferrous materials to accommodate strain, with primary reliance on aluminum and zinc alloys. Synthetic rubbers in the form of shear connectors can also be used for areas requiring high strain relief. New designs were developed which accommodate misalignment, distortion and deflections which can severely affect the fatigue life of steel diaphragms and stiffeners. Aluminum X-brace and K-brace diaphragms, along with retrofit attachments, were proposed.

The effects of tensile strains built into bridge components and connections on fatigue life were analyzed by the use of parabolic and linear safety factor equations. Safety factors of 1.00 or less indicate severe susceptibility to fatigue failure, whereas values of 1.5 or greater are good indicators of a fatigue-resistant component or connection.

CONCLUSIONS

1. Normal bridge construction practices can result in built-in stresses. The phases of steel bridge construction, including fabrication, assembly, deck and parapet placement, result in the development of various detrimental stresses, distortion and twist.

2. Built-in stresses can be either tensile or compressive. Stresses in steel diaphragms varied widely in magnitude. Mean tensile stress was 5.1 ksi (35 MPa) with a standard deviation of 5.8 ksi (40 MPa). The mean compressive stress was -7.4 ksi (-51 MPa), with a standard deviation of -5.7 ksi (39 MPa). The highest tensile stress measured was nearly 21 ksi (146 MPa).

3. The effect of built-in stresses on fatigue life can be potentially significant, depending on whether the residual stress is compressive or tensile. Residual or built-in tensile stresses approaching AASHTO allowable stresses can affect component fatigue life by aiding in the formation of cracks in vulnerable details. After the cracks form, live load stresses from truck traffic will continue the development of crack length.

4. Use of parabolic or straight-line fatigue safety factor equations can indicate to bridge engineers the potential danger that live load, dead load, built-in or other residual stresses can have on the fatigue life of a bridge.

RECOMMENDATIONS

1. The effect of high mean stresses on the fatigue life of common bridge weld details should be physicially tested, and compared with published AASHTO fatigue strengths.

2. The proposed diaphragm designs intended to attenuate built-in stresses should be tested as experimental features on new and existing bridges exhibiting out-of plane bending or experiencing significant distortion.

3. The proposed strain-relief connectors and modified diaphragm designs using aluminum cross frames or retrofit gussets should be applied to existing bridges experiencing localized cracking at diaphragms or stiffeners in Illinois or its neighboring states. The X-brace or K-brace diaphragms should be instrumented with strain gages at the gusset plates and connection points to note if stress levels are as predicted, or if relaxation occurs.

4. Similarly, the behavior of new bridges using the new all-aluminum plate or X-brace diaphragm designs of ***Figures 36 and 39*** should be considered for new or retrofit construction. These proposed diaphragm designs should be preferably compared on bridges using rigid or semi-rigid steel diaphragms.

5. Bridges with the proposed non-ferrous diaphragms should be monitored after several years of sustained traffic, and compared with steel bridges of the same geometry and location. Superstructure and deck deflections and general bridge condition should be noted. Other aspects to be monitored should include localized yielding, corrosion or fatigue cracking at holes in the aluminum diaphragms or gussets, or any other abnormal changes in the behavior of the bridge deck. A general assessment should be made whether the material substitution was either beneficial or deterimental to bridge performance.

REFERENCES

[1] J. Dally and W. Riley, *Experimental Stress Analysis, Second Edition*, McGraw-Hill, New York, 1978, p. 327.

[2] SAE Standard J1099, "Technical Report on Fatigue Properties", *SAE Handbook*, Society of Automotive Engineers, Warrensburg, PA, 1983.

[3] C. Hahin and J. South, *Accurate and Rapid Determination of Fatigue Damage in Bridge Superstructures,* FHWA / IL Physical Research Report No. 106, Illinois Department of Transportation, 1992.

[4] C. Hahin, J. South, J. Mohammedi and R. Polepeddi, "Accurate and Rapid Determination of Fatigue Damage in Steel Bridges", *ASCE J. of Structural Engineering*, Vol. 119, No. 1, January, 1993.

[5] J. Bannantine, J. Comer and J. Handrock, *Fundamentals of Metal Fatigue Analysis*, Prentice Hall, Englewood Cliffs, NJ, 1990, pp. 68 - 69.

[6] J. Fisher, J. Jin, D. Wagner and B. Yen, *Distortion-Induced Cracking in Steel Bridges,* NCHRP Report 336, Transportation Research Board, Washington, DC, December 1990.

[7] J. Fisher, A. Nussbaumer, P. Keating and B. Yen, *Resistance of Welded Details Under Variable Amplitude Long-Life Fatigue Loading,* NCHRP Report 354, Transportation Research Board, Washington, DC, 1993.

[8] J. Fisher, "Evolution of Fatigue Resistant Bridges", *1997 TRB Distinguished Lecture (Part 1); Structures (Part 2),* Transportation Research Record 1594, National Research Council, Washington, DC, 1997.

[9] T. Galambos, J. Hajjar, R. Leon, W. Huang, B. Pulver and B. Rudie, *Stress in Steel Curved Girder Bridges,* Minnesota DOT Technical Report 96-28, August 1996.

[10] T. Ross, H. Sorenson, S. Donald, S. Pringle, K. Riddick and R. Thompson, *Investigation of Intermediate Diaphragm Loads on Steel Bridges,* New Mexico State Highway and Transportation Dept. Report FHWA-HPR-NM-91-02, June 1994.

[11] S. Clarke, J. Detherage, D. Goodpasture and E. Burdette, "Influence of Bridge Approach, Surface Condition and Velocvity on Impact Factors for Fatigue-Prone Details", *Structural Analysis and Design: Bridge Culverts and Pipes,* Transportation Research Record 1624, National Research Council, Washington, DC, 1998.

[12] T. Wipf, L. Greimann, A. Khalil and D. Wood, *Preventing Cracking at Diaphragm/Plate Girder Connections in Steel Bridges,* Iowa State University, Iowa DOT Project HR-393, June 1998.

[13] R. Canham, "Analysis and Evaluation of Diaphragms and Cross Bracings in Slab Girder Bridges", M.S. Thesis, Syracuse University, August 1990.

[14]. P. Keating, "Focusing on Fatigue", *Civil Engineering*, November 1994, pp 54-57.

[15]. W. Munse, T. Wilbur, M. Tellalian, K. Nicoll and K. Wilson, *Fatigue Characterization of Fabricated Ship Details for Design,* University of Illinois, Ship Structure Committee Project SR-1257, US Coast Guard, August, 1982.

[16]. Military Handbook 149A, *Rubber and Rubber-like Materials,* Department of Defense, Washington, DC, 1965.